Plan revision number: 2
Plan revision date: December 2024

AREA OF REVIEW AND CORRECTIVE ACTION PLAN
40 CFR 146.84(b)

Kern River Eastridge CCS

Facility Information

Facility name:	Kern River Eastridge CCS MC19001INJ, ANO9004INJ, MC19002INJ, ANO9005INJ
Facility contact:	David Wessels – Project Manager 9525 Camino Media, Bakersfield, CA 93311 David.wessels@chevron.com / 661-412-6039
Well location:	Bakersfield, Kern County, CA 93308 35.4404°/-118.9983°; 35.4465°/-119.0012°; 35.4401°/-118.9981°; 35.4462°/-119.0010°

Computational Modeling Approach

Model Background

An industry consortium has leveraged years of experience, research, development, and best practices to develop INTERSECT®, a software for high-fidelity compositional reservoir simulation. Chevron U.S.A., Inc. (Chevron) uses INTERSECT® for CO_2 sequestration simulation to understand CO_2 plume and pressure front migration through time, delineate the Area of Review (AoR), and optimize development scenarios. INTERSECT®, a trademark of SLB, allows for robust simulation forecasts that account for the following processes:

- Multiphase fluid flow, including supercritical, gaseous, and dissolved phase CO_2
- Relative permeability hysteresis trapping (non-wetting phase trapping)
- Structural and stratigraphic trapping
- Capillarity effects
- Fault seal analysis to model sealing capacity of faults
- Pore volume compressibility (dilation and compaction)

Chevron expects these processes to be the most impactful for AoR evolution through time.

Chevron has been successfully using INTERSECT® reservoir simulator for other Chevron projects. Chevron has leveraged static and dynamic modeling best practices to support the permit for Kern River Eastridge CCS (Project).

The INTERSECT® model considers temperature, pressure, and salinity dependent fluid properties and solubility of CO_2 in brine. Carbon dioxide solubility table and subsequent mixture property changes due to dissolution were also modeled through a Chevron in-house propriety tool and imported into INTERSECT®. In these models, CO_2 solubility in brine is calculated following the method of Ziabakhsh-Ganji & Kooi (2012). The impacts of dissolved CO_2 on the density of brines were modeled using the workflow demonstrated by McBride-Wright (2015) and Calabrese et al. (2019) using the mixture density model of Wagner (2002). The impact of dissolved CO_2 on the viscosity of brines was benchmarked & modeled by Calabrese et al. (2019).

Hysteresis effects are included in the model. The term hysteresis refers to irreversibility, or path dependence. In multiphase flow, hysteresis manifests itself through the dependence of the relative permeability (and optionally capillary pressure) on the saturation path and the saturation history. The trapped critical saturation is calculated using Land's method (1968) which was adapted by Jerauld (1997a and 1997b). Gas trapping is then modeled by using Killough (1976).

The Project model was developed by Chevron for the purposes of testing the storage capacity of the Vedder Sand, predicting lateral and vertical extents of the CO_2 plume and pressure front during the operational and post-injection periods, and to model injection operations throughout the life of the project. The geocellular model characterizes the geology, structure, faults, and properties pertinent to modeling fluid flow through porous media (e.g., porosity and permeability). Unless otherwise stated, the geocellular model presented is the best technical case (most likely scenario) for the CO_2 sequestration opportunity in the Vedder Sand. The 3D model includes lateral and vertical variations to facies and petrophysical properties.

The site-specific INTERSECT® model constructed for the Project accounts for CO_2 and H_2O as modeled fluids. The equation of state (EOS) was developed outside of INTERSECT® using Chevron's internal phase behavior software, Chevron Phase Calculation Program (CPCP), and the modified Peng-Robinson equation of state (PR-EOS) model and imported to INTERSECT®. During the PVT (pressure, volume, and temperature) modeling process, calculated CO_2 viscosity and density values were matched to those from National Institute of Standards and Technology (NIST).

The properties of both CO_2 and H_2O are modeled using experimental data for the conditions within the Vedder Sand. Key assumptions used in the INTERSECT® model are:

- Simulation model is isothermal and uses the modified PR-EOS for CO_2 phase properties, and
- CO_2 is soluble in brine.

In addition, Chevron worked with Lawrence Berkley National Laboratory (LBNL) to quantify the geochemical reactions between CO_2, reservoir brine, and the mineralogy of the Vedder Sand and Freeman-Jewett Silt. The study showed little to no significant reaction between the rock formations, the injected CO_2, injected impurities, and the in-situ brine in the injection zone and caprock seal. This work was completed using the TOUGHReact & TReactMech simulation

models and is documented in the Project Narrative. For more information on the site-specific geochemistry, see the Geochemistry Section of the Project Narrative.

Through the life of Project, Chevron will collect monitoring data which will be used to compare against forecasts and, if needed, calibrate static and dynamic models.

Site Geology and Hydrology

An extensive review of the geological and hydrological context is provided in the Hydrologic and Hydrogeologic section of the Project Narrative. This section summarizes conclusions that are relevant to the AoR modeling effort.

The AoR, which is contained within the administrative boundary of the Kern River Oil Field, Area of Interest (KRF, AoI), is located within the southeastern San Joaquin Basin of California (**Figure 1**).

Cenozoic sedimentation in the San Joaquin Basin records a shift from predominantly forearc-basin sedimentation to a complicated array of transpressional and transtensional basins associated with the development of the San Andreas fault system during Neogene time (Bartow and Nilsen, 1990; Miller and Graham, 2018). The Project AoI is near the crest of the Bakersfield arch, a broad southwest-plunging anticlinal feature on the eastern side of the southern San Joaquin Basin (e.g., Sheehan, 1986). The Bakersfield arch plunges about 20 miles to the west, where it separates the southern San Joaquin Basin into a northern Tulare sub-basin and a southern Maricopa sub-basin (e.g., Saleeby and Saleeby, 2019). The southwest-plunge of the Bakersfield arch forms a 3-6 degree southwest-dipping homocline, interrupted by high-angle normal faults active since Miocene time (Saleeby et al., 2013a and 2013b). These faults have been the primary trapping mechanism for Vedder oil accumulations in the eastern San Joaquin basin. These faults are important in the AoR for arresting CO_2 plume migration. Within the AoI, apparent-normal faults with both easterly and westerly dip are well-documented and have been the primary trapping mechanism for light oil accumulations within the AoI.

During Paleogene time, erosion along the western flank of the ancestral Sierra Nevada delivered clastic detritus to the eastern flank of the southern San Joaquin Basin, forming deltaic adepositional systems within the region and the AoR, namely the Oligocene Vedder Sand, the injection interval in the AoR.

Based on well-log correlations and seismic interpretations within the AoI, the Vedder Sand has been subdivided into five distinct parasequences that represent progradational episodes of a fluvially dominated delta, each of which are bounded vertically by laterally continuous shaley zones that define marine transgressions. Multiple environments of deposition (EODs) are interpreted in the Vedder Sand, including shallow-marine, deltaic/coastal plain, and fluvial settings that include incised valleys, amalgamated fluvial channel-belts associated with braided river systems, tidally influenced distributary channels and distributary mouthbars, and shoreface and marine sediments. **Figure 2** and **Figure 3** show the top Vedder structure and a cross section through the Apollo Fault System. **Figure 4** and **Figure 5** show dip and strike cross sections through the AoI.

Within the AoI, reservoir properties were determined from standard and special logging suites, whole-core, and sidewall-core data from 70 penetrations. Within the AoR the Vedder Sand has an average thickness of ~1,050 ft occurs at an average elevation of -3,910 ft True Vertical Depth Sub-Sea (TVDSS), ranging from -3,470 to -4,300 ft TVDSS.

After the deposition of the Vedder Sand, rapid subsidence of the AoI in late Oligocene-early Miocene time led to the widespread deposition of the Freeman-Jewett Silt, the primary confining layer in the AoR. The Freeman–Jewett Silt is the primary caprock seal for the Vedder Sand. The Freeman–Jewett Silt is laterally continuous across the region and has a mean gross thickness of 1,140 ft across the AoI. Thickness variations along fault trends are due to structural juxtapositions that locally decrease apparent thickness across normal faults. Faults mapped in the underlying Vedder have maximum throws of 380 ft, which are approximately one third of the average thickness of the caprock seal. Therefore, the Freeman–Jewett Silt is expected to continuously seal across the AoI.

Within the Project AoI, characteristics of the Freeman–Jewett Silt were derived from 70 well penetrations and mapping from 3D seismic data. The elevation of the Top of the Freeman-Jewett Silt ranges from -2,610 to -4,590 ft TVDSS across the AoI. The Freeman–Jewett Silt confining zone is laterally continuous across the Project AoI, ranging between approximately 580 and 1,420 ft thick within the Project AoI. At the proposed Project injection sites, the Freeman–Jewett Silt is at an elevation of -2,950 and -2,990 ft TVDSS, and a thickness of approximately 1,287 ft and 1,243 ft at ANO9004INJ and MC19001INJ, respectively.

By late Miocene time, the southern San Joaquin Basin underwent rapid structural changes, with flanking uplifts shedding clastic detritus into the basin as deep-marine turbidite channel-and-lobe systems interfingered with siliceous (diatomaceous) shale of the Monterey Formation and correlative units. During this time, sediments eroded from the Sierra Nevada were laid down as marine deposits of the Santa Margarita Sandstone (deepest Underground Source of Drinking Water (USDW) in the AoR), marginal-marine and fluvial deposits of the Chanac Formation, and fluvial deposits of the Kern River Formation within the AoI.

Coburn and Gillespie, 2002 summarized the hydrogeologic characteristics of the AoI in the Santa Margarita Sand, Chanac Formation, And Kern River formations, using hydrological pressure data from (1) open-hole formation pressure tests, (2) nuclear logs combined with temperature surveys, and (3) static fluid levels.

The Santa Margarita sandstone conformably overlies the Round Mountain formation and represents the lowermost USDW within the AoI and the AoR. The Santa Margarita sandstone is an upper Miocene marine interval consisting of gray to white, fine-grained to coarse-grained sandstone that thins eastward (Kodl et al., 1990). The Santa Margarita sandstone consists of a lower main zone and an upper transition zone across most of the AoI and is conformably overlain by the Chanac Formation. In the eastern part of the AoI, the transition zone and the Chanac Formation are progressively eroded, resulting in an unconformable contact between the Santa Margarita and the Chanac or Kern River formations (Kodl et al., 1990). Within the AoI, the thickness of the Santa Margarita Sandstone ranges between approximately 125 and 650 ft, the average porosity is 31 percent, and the average permeability is 400 mD (Coburn and Gillespie, 2002). It occurs at a depth of 760’-1,185’ below ground surface in the AoI, and dips southwest (California Division of Oil and Gas, 1981, p. B-5).

The reservoir model was conditioned using sixty-four (64) wells, and six (6) sidetracks that penetrate the Vedder Sand within the Kern River Oil Field administrative boundary, which is the Project AoI (**Figure 1, Table 3)**. The associated logs and core comprise a rich source of petrophysical and routine core analysis (RCA) and special core analysis (SCAL) data to characterize the Vedder Sand and underlying units. The overall quality of borehole geophysical logs varies with vintage and is a result of historical development objectives; thus, wells may have different types of logs across the AoI**.** Numerous types of borehole geophysical logs were used to interpret the reservoir framework and reservoir properties. Triple-combination (neutron porosity, density, gamma ray, and resistivity) log suites are the most common modern log suites used to describe borehole conditions and reservoir properties. These logs were supplemented with spontaneous potential, dielectric, borehole-image, nuclear magnetic resonance (NMR), sonic, and formation-pressure logs.

Reservoir properties calculated from triple combo borehole geophysical logs and core data using Chevron petrophysical standard for sandstones include volume of shale (Vshale), total and effective porosity (PHIT and PHIE, respectively), total water saturation (Swt), and effective shale-corrected water saturation (Swe). Permeability transforms are based on regressions among PHIT, PHIE and Vshale. Rock quality was assessed using the Rock Quality Index (RQI) of Amaefule et al. (1993). Special core analysis (SCAL) was conducted on legacy wells, including mineralogy (e.g., XRD). CO2-specific analyses (i.e., CO2-brine interfacial tension and contact angle analysis) were conducted on core samples from the Vedder Sand and were incorporated into the reservoir model. Additional information on this topic can be found in the Fault Seal Capacity section of the Narrative Document. Additional Vedder data collection is planned for the Pre-Operational phase of the project. Please refer to the Pre-Operational Logging and Testing Plan for more details.

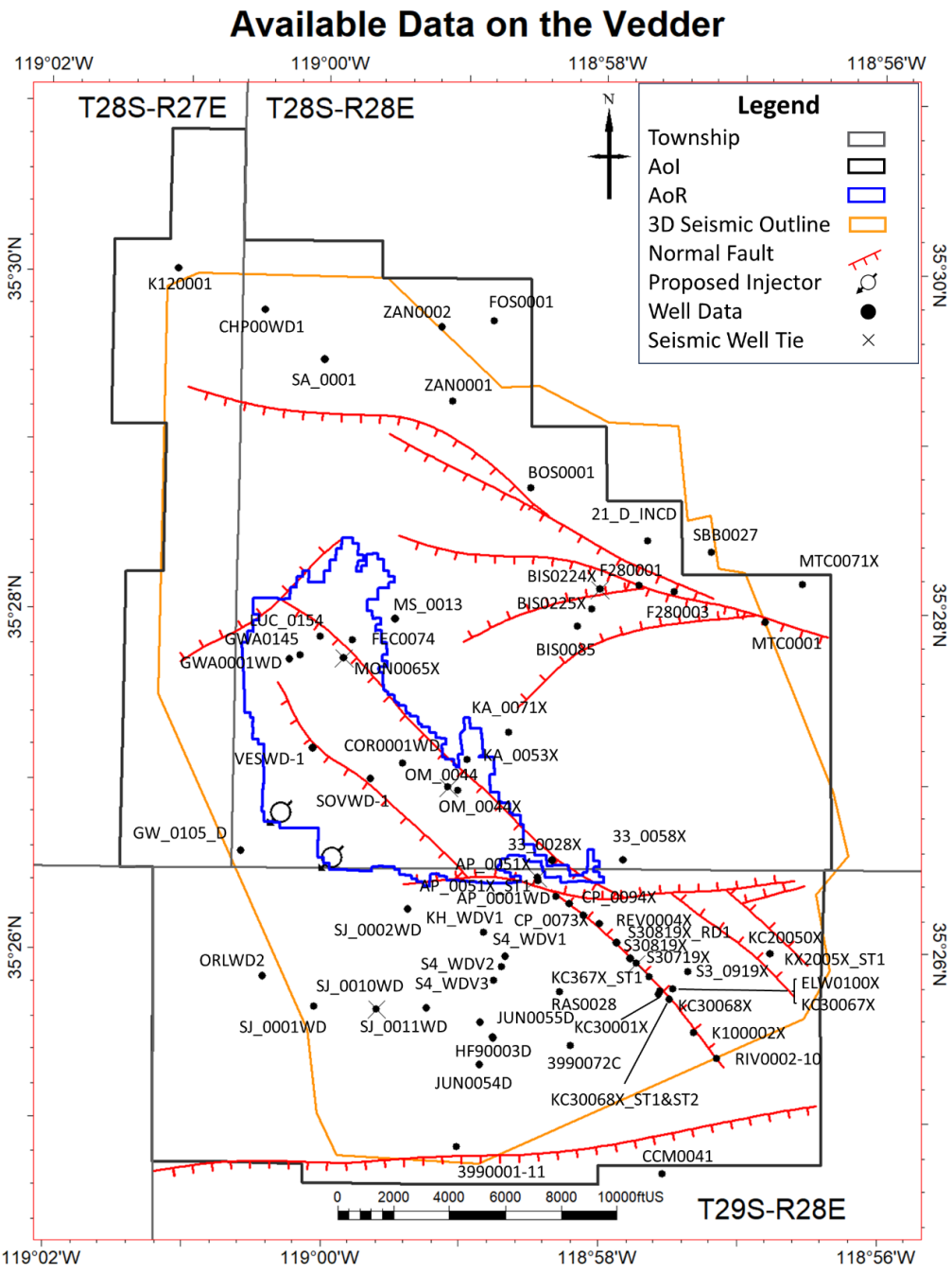

Figure 1. Location map for data sources for the Vedder Sand in the AoI.

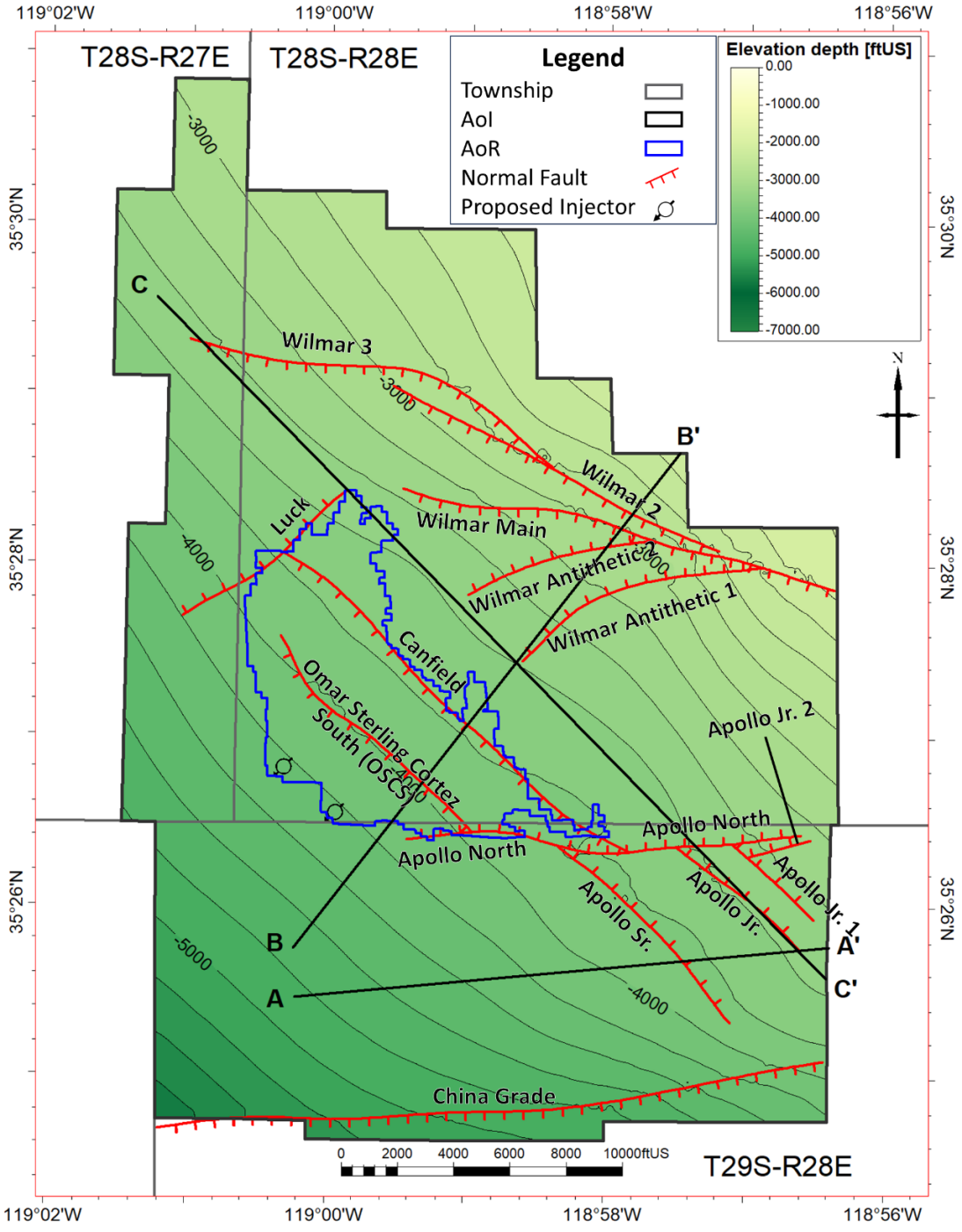

Figure 2. Structural surface map depicting mapped faults that intersect the top of the Vedder Sand. Structure contour interval is 100 ft. Hachures mark the downthrown side of fault traces. Cross section line A-A' shown on **Figure 3**. Cross section line B-B' shown on **Figure 4**. Cross section line C-C' shown on **Figure 5.**

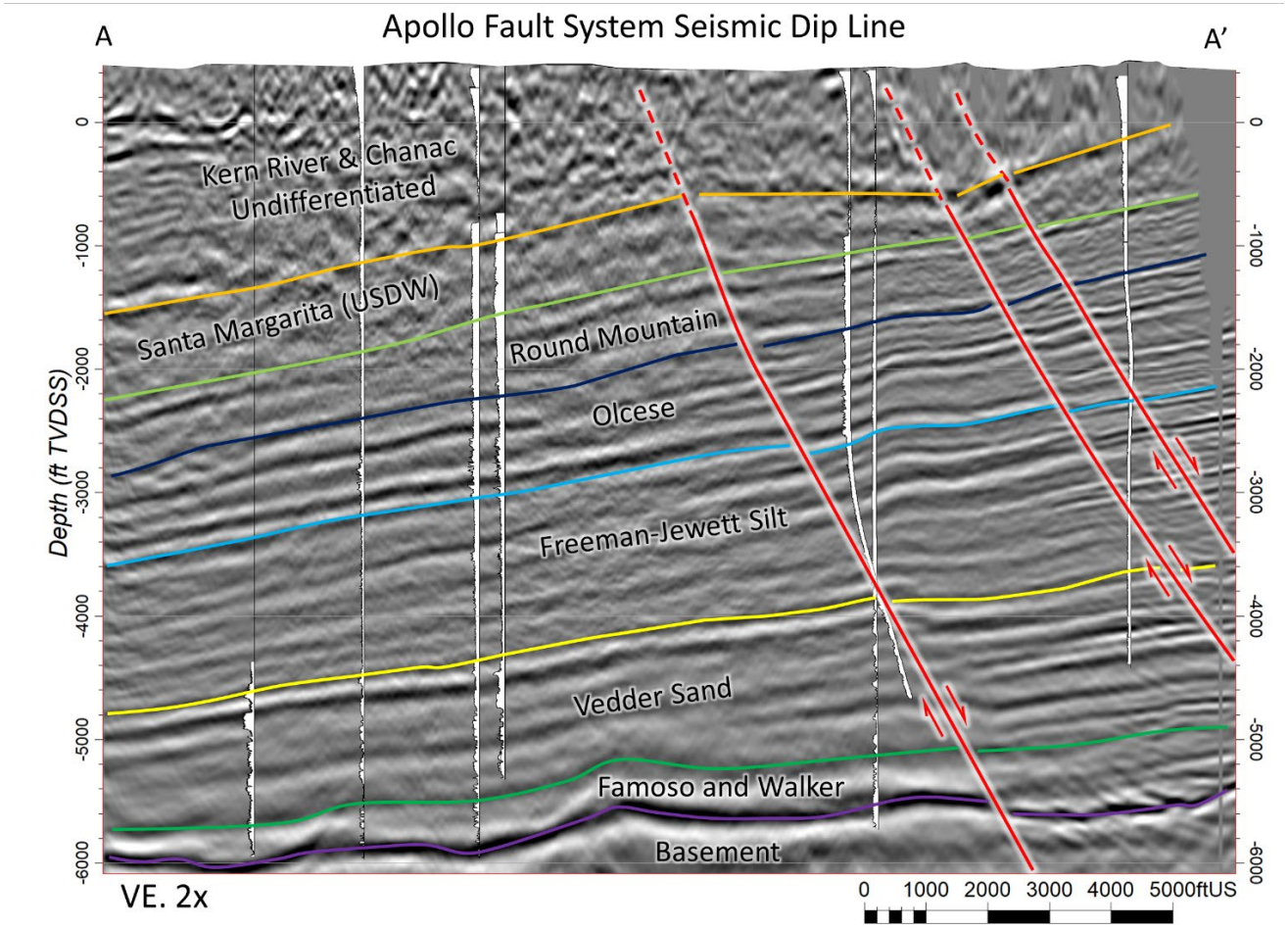

Figure 3. Geologic cross section across the southeastern portion of the AoI, showing depth-converted seismic (in ft True Vertical Depth Sub-Sea (TVDSS)) and interpreted reservoir horizons, faults, and projections of nearby wells with normalized spontaneous potential (SP) logs that penetrate the Vedder Sand. Cross section is vertically exaggerated by a factor of two (VE:2x).

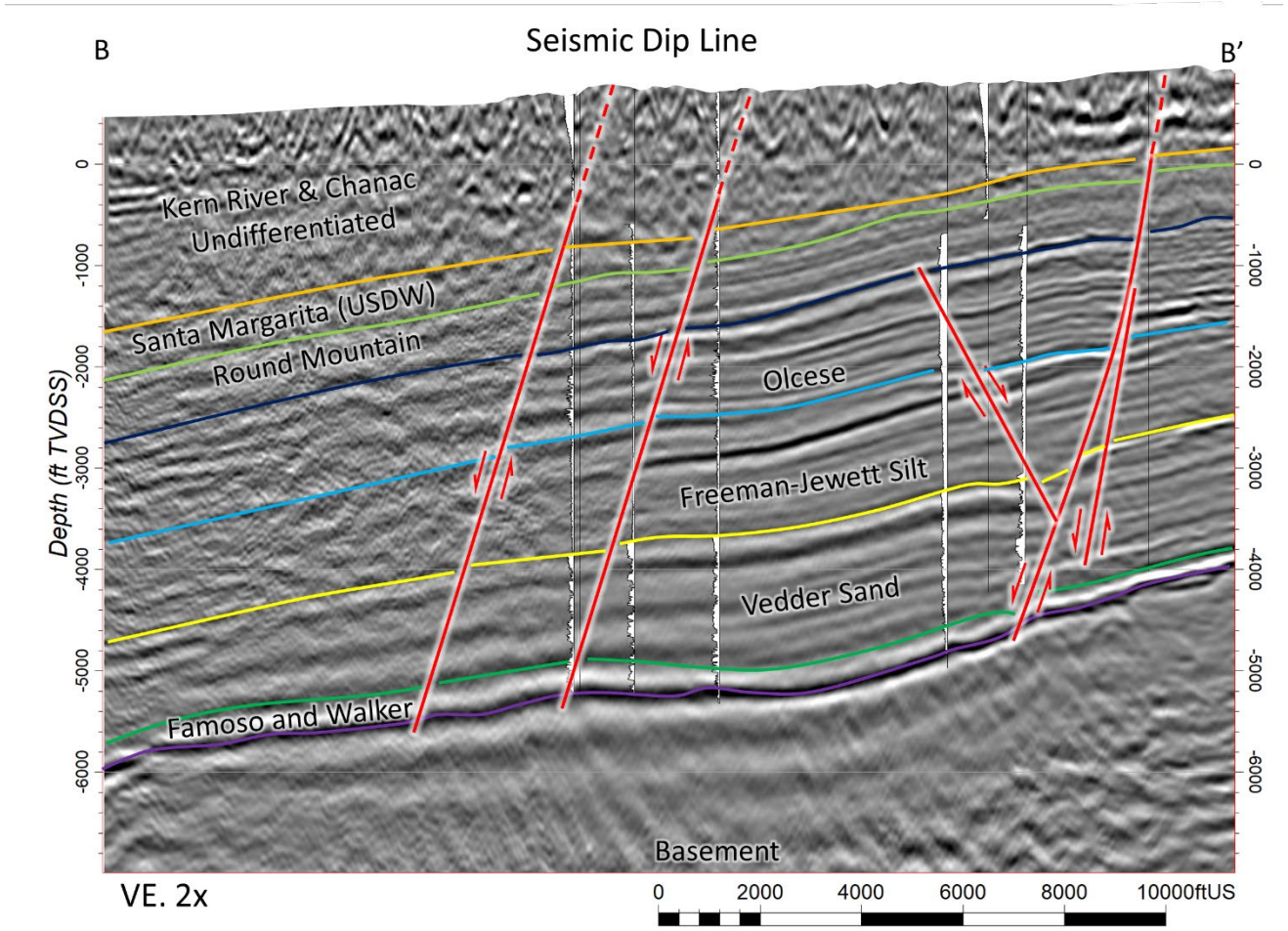

Figure 4. Geologic dip cross section across the AoR, showing depth-converted seismic (in ft TVDSS) and interpreted reservoir horizons, faults, and projections of nearby wells with normalized SP logs that penetrate the Vedder Sand. Cross section is vertically exaggerated by a factor of two (VE:2x).

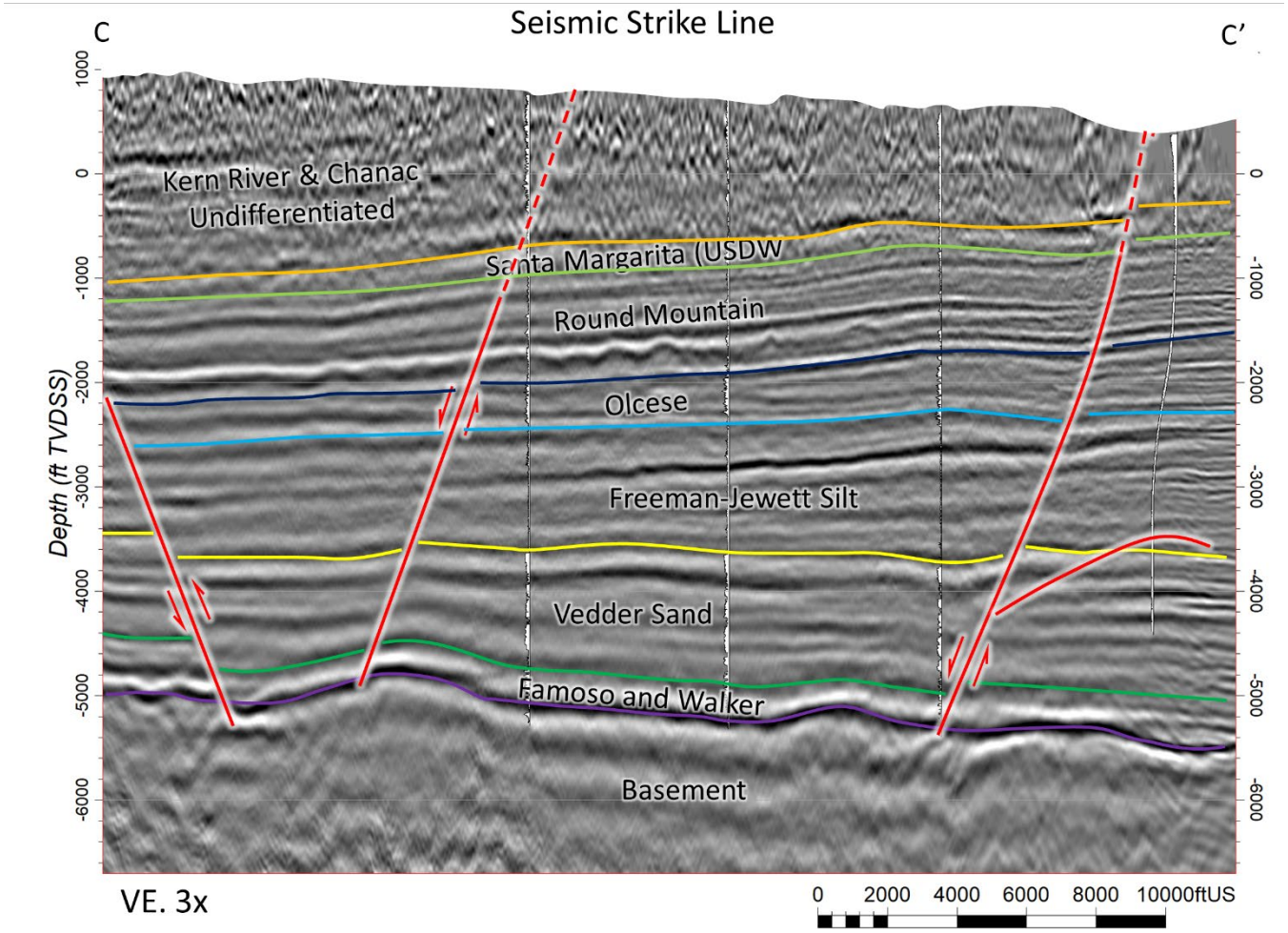

Figure 5. Geologic strike cross section across the AoR, showing depth-converted seismic (in ft TVDSS) and interpreted reservoir horizons, faults, and projections of nearby wells with normalized SP logs that penetrate the Vedder Sand. Cross section is vertically exaggerated by a factor of two (VE:3x).

Model Domain

The simulation model encompasses the administrative field boundary of the Kern River Oil Field, the Project's AoI. This area is ~7 miles in the North-South direction and ~5 miles in the East-West direction as shown in **Figure 6**, totaling approximately 16,500 acres.

A cartesian variable grid (X, Y, Z) resolution is utilized with an aerial resolution of approximately 200ft x 200ft x 4ft within and near the AoR and approximately 400ft x 400ft x 4ft outside the AoR. This variable grid resolution is implemented with a local grid refinement (LGR) using the Petrel software package. Finer spatial resolution of properties is maintained within the LGR, and a coarser scale resolution is used outside the LGR using flow-based upscaling. The application of the LGR in the area swept by CO_2 allows for faster simulation run times that accurately capture the impact of fine-scale heterogeneities in the CO_2 swept regions. The coarse scale resolution is 60 gridblocks in the I direction (E-W), 94 gridblocks in the J direction (N-S), and 342 gridblocks in the K direction (Depth). The LGR area, within the AoR, has a resolution of 76 gridblocks in the I direction (E-W), 74 gridblocks in the J direction (N-S), and 342 gridblocks in the K direction (Depth). The injector locations are contained within the LGR region. The model contains a total of 2.08 million cells. A plan view of the numerical grid is shown in **Figure 6**. Cross sections through the grid are shown in **Figure 7** and **Figure 8**. **Table 1** and **Table 2** provide summaries of model domain and vertical resolution.

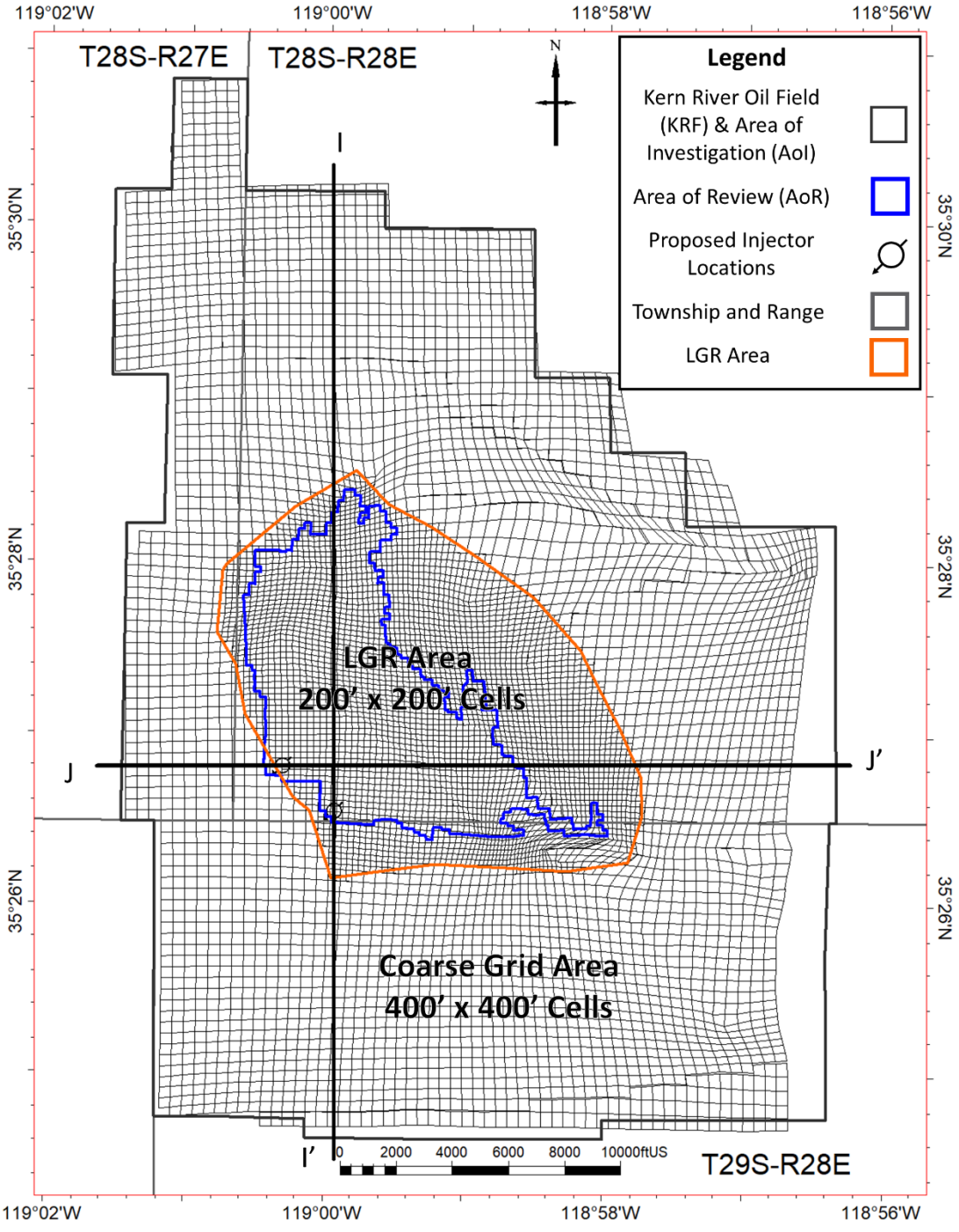

Figure 6. Plan view of the numerical grid illustrating injector locations relative to the area with fine grid resolution within the LGR (200ft x 200ft x ~4ft) and coarser resolution outside the LGR (400ft x 400ft x ~4ft).

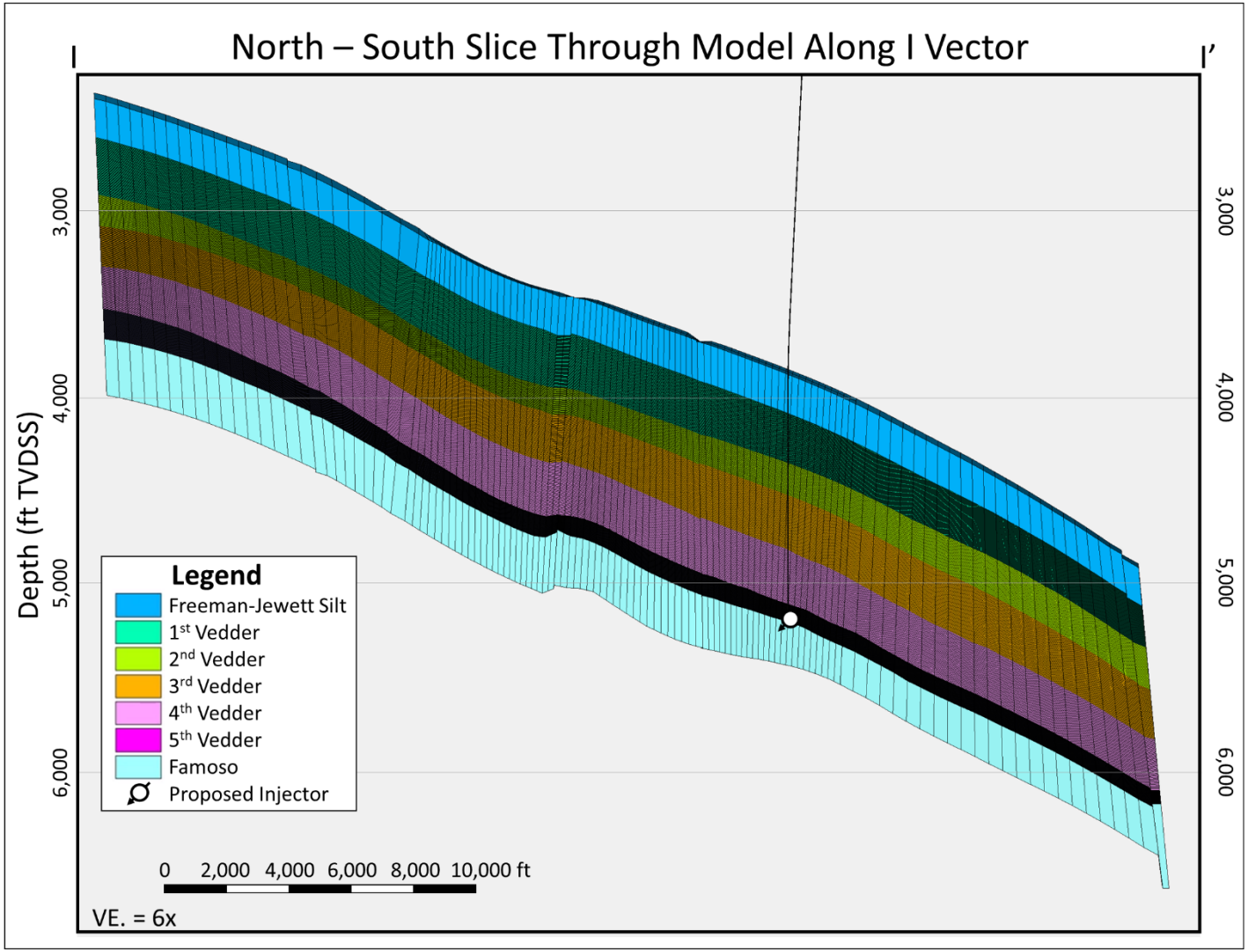

Figure 7. North to south cross section I-I' through the model along the J vector. Injector location is projected onto the section. See **Figure 6** location.

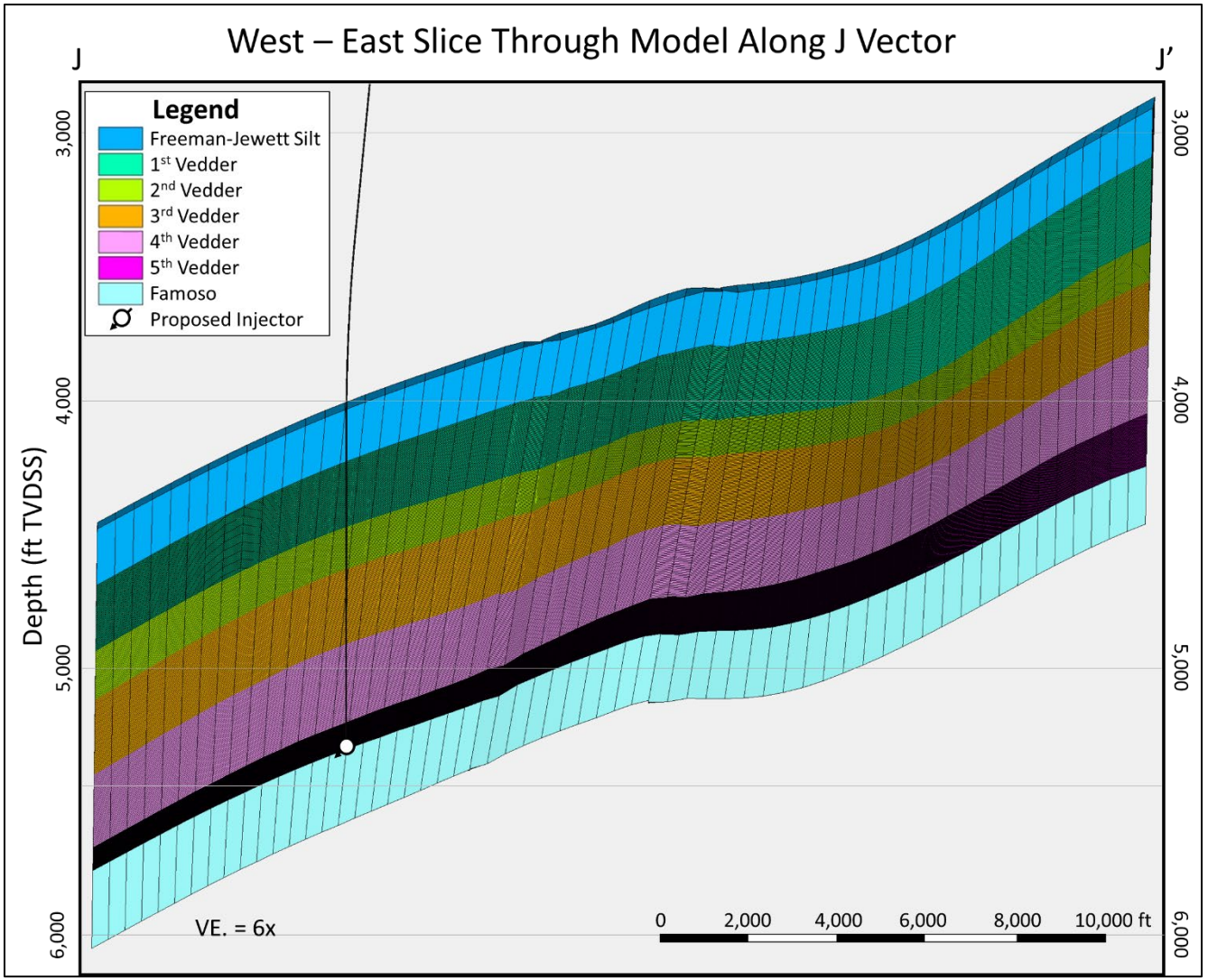

Figure 8. West-east cross section J-J' through the model along the J vector. Injector location is projected onto the section. See **Figure 6** location.

Table 1. Model domain information.

Coordinate System	USA NAD27 SPCS CA 5 USFT Chevron,720669		
Horizontal Datum	NAD27		
Coordinate System Units	ftUS		
Zone	SPCS CA 5 USFT		
FIPSZONE	06029		
Coordinate of X min	1,694,672	**Coordinate of X max**	1,719,410
Coordinate of Y min	696,327	**Coordinate of Y max**	734,174
Coordinate of Z min	-7,031	**Coordinate of Z max**	-1,872

Table 2. Illustrates the vertical scale resolution of the simulation model broken down by the Vedder Sands. Average thickness of ~4ft over the AoI.

Formation	Number of Layers	Average Layer Thickness (ft)
Freeman-Jewett Silt	1	200
1st Vedder	90	3.1
2nd Vedder	40	3.8
3rd Vedder	60	4.4
4th Vedder	60	4.6
5th Vedder	90	1.5
Famoso	1	180

Porosity and Permeability

Within the AoI, 30 wells have reliable electric log data for calculating volume of shale (Vsh), porosity, permeability, and saturation within the Vedder Sand. Additionally, there are 7 wells with quantitative whole-core data and logs, yielding a total of 260 individual routine core analysis (RCA) data points to enable robust calibration. As detailed in the Pre-Operational Logging and Testing Plan, Chevron has collected an additional whole core in the Vedder sand from KC20050X_ST1 and plans to incorporate the results from these data during the Pre-Operational phase of the Project. Quantitative RCA core analysis consisted mainly of porosity, permeability, and water saturation measurements. Additional legacy core data predominantly comes from percussion sidewall cores. Percussion sidewall coring can induce physical damage to the sample, mostly from disaggregation and fracturing during the sampling process (e.g., Bajsarowicz, 1992), and is interpreted to be less representative of the reservoir properties than the whole core data.

These wells and associated logs and core comprise a rich source of petrophysical and routine and special core analysis data (RCA and SCAL) to characterize the Vedder Sand and underlying

units. **Table 3** summarizes the legacy well evaluation, well logs, and special core analysis that support the geological interpretations and reservoir description of the Vedder Sand in the AoI.

Table 3. Summary of borehole datasets for wells that penetrate the Vedder Sand.

Well Info		Core & Mineralogy Data				Well Log Data									Derived Logs				
API12	Well Name	Vedder Whole core	Vedder Sidewall	Freeman–Jewett Sidewall	Vedder XRD	SP	SRES	DRES	GR	RHOB	DPHI	NPHI	NMR	FMI	RQI	PHIE	PHIT	VSH	PERM
040292497300	3990001-11					X	X	X								X	X	X	X
040296721700	AP_0051X	X			X		X	X	X	X	X	X			X	X	X	X	X
040294479200	BIS0085					X	X	X		X									
040296771100	CP_0073X		X				X	X	X	X	X	X			X	X	X	X	X
040292631600	F280001					X	X	X											
040292411200	FEC0074					X	X	X											
040296110500	GWA0001WD		X			X	X	X											
040292697300	GWA0145					X	X												
040294934300	JUN0055D		X			X	X	X	X	X	X								
040296990300	KA_0053X		X	X		X	X	X	X	X	X	X			X	X	X	X	X
040290031800	KA_0071X					X	X	X											
040296989800	KC30001X		X	X		X	X	X	X	X	X	X			X	X	X	X	X
040292803800	LUC0154		X			X	X												
040292273800	MS_0113					X	X	X											
040290009800	OM_0044		X			X	X	X											
040296655800	OM_0044X	X	X		X	X	X	X	X	X	X	X			X	X	X	X	X
040292403700	SA_0001					X	X	X											
040295391100	SJ_0001WD		X			X	X	X											
040296110600	SJ_0002WD		X			X	X	X											
040301418200	SJ_0010WD					X	X	X	X	X	X	X	X		X	X	X	X	X
040301621700	SJ_0011WD					X	X	X	X	X	X	X			X	X	X	X	X
040296641100	33_0028X	X	X		X		X	X	X	X	X	X			X	X	X	X	X
040292887200	33_0058X					X	X	X											
040294423200	3990072C					X	X	X											
040296441200	AP_0001WD		X			X	X	X	X	X	X	X			X	X	X	X	X
040298942100	CHP00WD1					X	X	X	X	X									
040295678200	COR0001WD	X				X	X	X											
040306065200	KH_WDV1		X			X	X	X	X	X	X	X	X		X	X	X	X	X
040296758700	MON0065X		X			X	X	X	X	X	X	X			X	X	X	X	X
040306215900	ORLWD2		X	X		X	X	X	X	X	X	X			X	X	X	X	X
040296194100	S4_WDV1		X			X	X	X	X	X	X	X			X	X	X	X	X
040298201900	S4_WDV2	X	X			X	X	X	X	X	X	X			X	X	X	X	X
040305241300	S4_WDV3					X	X	X	X	X	X	X			X	X	X	X	X
040297837600	SOVWD-1	X	X			X	X	X	X	X	X	X			X	X	X	X	X
040297837500	VESWD-1		X					X		X	X	X			X	X	X	X	X
040296905500	BIS0224X					X	X	X	X	X	X	X			X	X	X	X	X
040297107500	BIS0225X					X	X	X	X	X	X	X			X	X	X	X	X
040297559102	KC30068XSTD					X	X	X	X	X	X	X							

Well Info		Core & Mineralogy Data				Well Log Data									Derived Logs				
API12	Well Name	Vedder Whole core	Vedder Sidewall	Freeman–Jewett Sidewall	Vedder XRD	SP	SRES	DRES	GR	RHOB	DPHI	NPHI	NMR	FMI	RQI	PHIE	PHIT	VSH	PERM
040298795500	S3_0919X		X				X	X	X	X	X	X			X	X	X	X	X
040294247600	JUN0054D		X			X	X	X											
040304573400	CP_0094X					X	X	X	X	X	X	X			X	X	X	X	X
040297301700	ELW0100X					X	X	X	X	X	X	X			X	X	X	X	X
040294937400	HF90001D					X	X	X	X	X	X	X			X	X	X	X	X
040296906900	HF90003D					X	X	X											
040297205000	K100002X					X	X	X											
040304874500	KC20050X		X			X	X	X	X	X	X	X		X	X	X	X	X	X
040304874501	KC20050X_ST1	X			X	X	X	X	X	X	X	X	X	X					
040297396900	KC30067X		X	X		X	X	X	X	X	X	X			X	X	X	X	X
040297396901	KC30067X_ST1					X	X	X	X	X	X	X							
040297393700	RIV0002-10					X	X	X											
040297135800	S3_0719X		X			X	X	X	X	X	X	X			X	X	X	X	X
040297371201	S3_0819XRD1		X			X	X	X	X	X	X	X			X	X	X	X	X
040296721701	AP_0051X_ST1					X	X	X	X	X	X	X							
040290026100	GW_0105-D		X	X		X	X	X											
40292215100	RAS0028																		
040296976200	REV0004X	X				X	X	X	X	X	X	X			X	X	X	X	X
040297371200	S3_0819X		X	X		X	X	X	X	X	X	X			X	X	X	X	X
040292404700	MTC0001					X	X	X											
040294034800	MTC0071X					X	X	X											
040292200100	BOS0001																		
040293200900	CCM0041					X	X												
040292404800	F280003					X	X	X											
040292689700	FOS0001					X	X	X											
040294615600	K120001					X		X											
040297559100	KC30068X		X	X		X	X	X	X	X	X	X			X	X	X	X	X
040297559101	KC30068XST					X	X	X	X	X	X	X							
040291846200	SBB0027					X	X												
040292620100	SEC21-D																		
040292402900	ZAN0001					X	X	X											
040292673800	ZAN0002					X	X												

Sequential Gaussian Simulation was used to populate porosity away from the wells using the sand quality facies. Inputs used to determine effective porosity were: PHIE logs, histograms from the wells, variograms, and depth trend (0.92 per 100-ft of thickness). The porosity has a normal distribution in the Vedder Sand, with an average of 28% in the AoR.

Variability in permeability away from wells was characterized based on modeled porosity as second variable, cloud transforms by RQI-based facies, and variograms. Like the porosity model, Sequential Gaussian Simulation was used to populate permeability and the range of variability in permeability is set by porosity and permeability variability using multipliers for the simulation models. The permeability has a log normal distribution in the Vedder Sand, with average of 2,900 (range: 260-8,540) mD in the AoR. **Table 4** provides additional geologic statistics within the AoI and AoR. **Figure 9, Figure 10, Figure 11, Figure 12, and Figure 13** provide net porosity and net permeability maps for each Vedder subunit.

Table 4. Summary of depth, thickness, porosity, and permeability ranges for the Freeman–Jewett Silt, Vedder Sand, and Famoso sand.

Within AoI	Elev. (ft)			Thickness (ft)			PHIE Porosity (%)			Permeability (mD)		
Unit	Mean	Min.	Max.	Mean	Min.	Max.	Mean	Min.	Max.	Mean	Min.	Max.
Freeman–Jewett Silt	-2,610	-4,590	-1,100	1,140	580	1,420	---	---	---	---	---	---
1st Vedder (Vd1)	-3,750	-1,980	-5,760	270	180	360	0.29	0.20	0.34	3,580	510	17,470
2nd Vedder (Vd2)	-4,020	-2,270	-5,980	150	100	220	0.27	0.23	0.32	2,900	660	8,820
3rd Vedder (Vd3)	-4,170	-2,450	-6,200	250	140	300	0.28	0.23	0.33	470	150	940
4th Vedder (Vd4)	-4,420	-2,630	-6,450	260	170	300	0.29	0.23	0.33	4,550	1,480	9,090
5th Vedder (Vd5)	-4,680	-2,850	-6,700	140	80	220	---	---	---	---	---	---
Famoso sand	-4,820	-3,070	-6,760	---	---	---	---	---	---	---	---	---

Within AoR	Elev. (ft)			Thickness (ft)			PHIE Porosity (%)			Permeability (mD)		
Unit	Mean	Min.	Max.	Mean	Min.	Max.	Mean	Min.	Max.	Mean	Min.	Max.
Freeman–Jewett Silt	-2,720	-3,020	-2,310	1,180	1,060	1,340	---	---	---	---	---	---
1st Vedder (Vd1)	-3,910	-3,470	-4,300	270	240	300	0.29	0.27	0.32	3,580	1,810	7,000
2nd Vedder (Vd2)	-4,180	-3,760	-4,540	140	130	160	0.27	0.24	0.31	3,120	1,370	6,380
3rd Vedder (Vd3)	-4,320	-3,880	-4,700	260	230	290	0.28	0.23	0.31	470	260	730
4th Vedder (Vd4)	-4,580	-4,130	-4,980	270	250	300	0.29	0.25	0.31	4,990	2,450	8,540
5th Vedder (Vd5)	-4,860	-4,410	-5,270	110	90	170	---	---	---	---	---	---
Famoso sand	-4,970	-4,530	-5,360	---	---	---	---	---	---	---	---	---

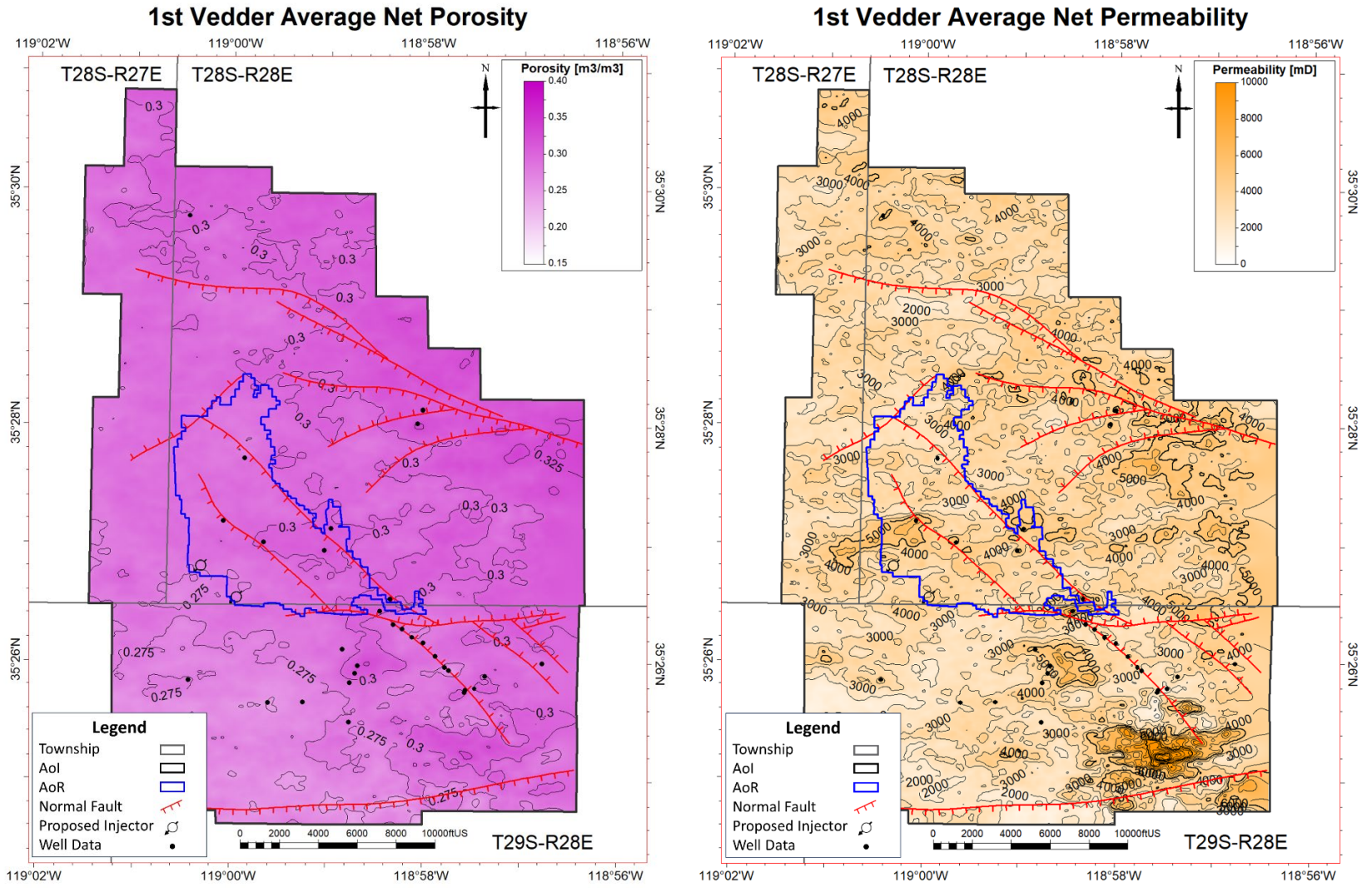

Figure 9. Maps of average sand porosity (left) and sand permeability (right) for the 1st Vedder Sand (Vd1). Red hachured lines denote faults.

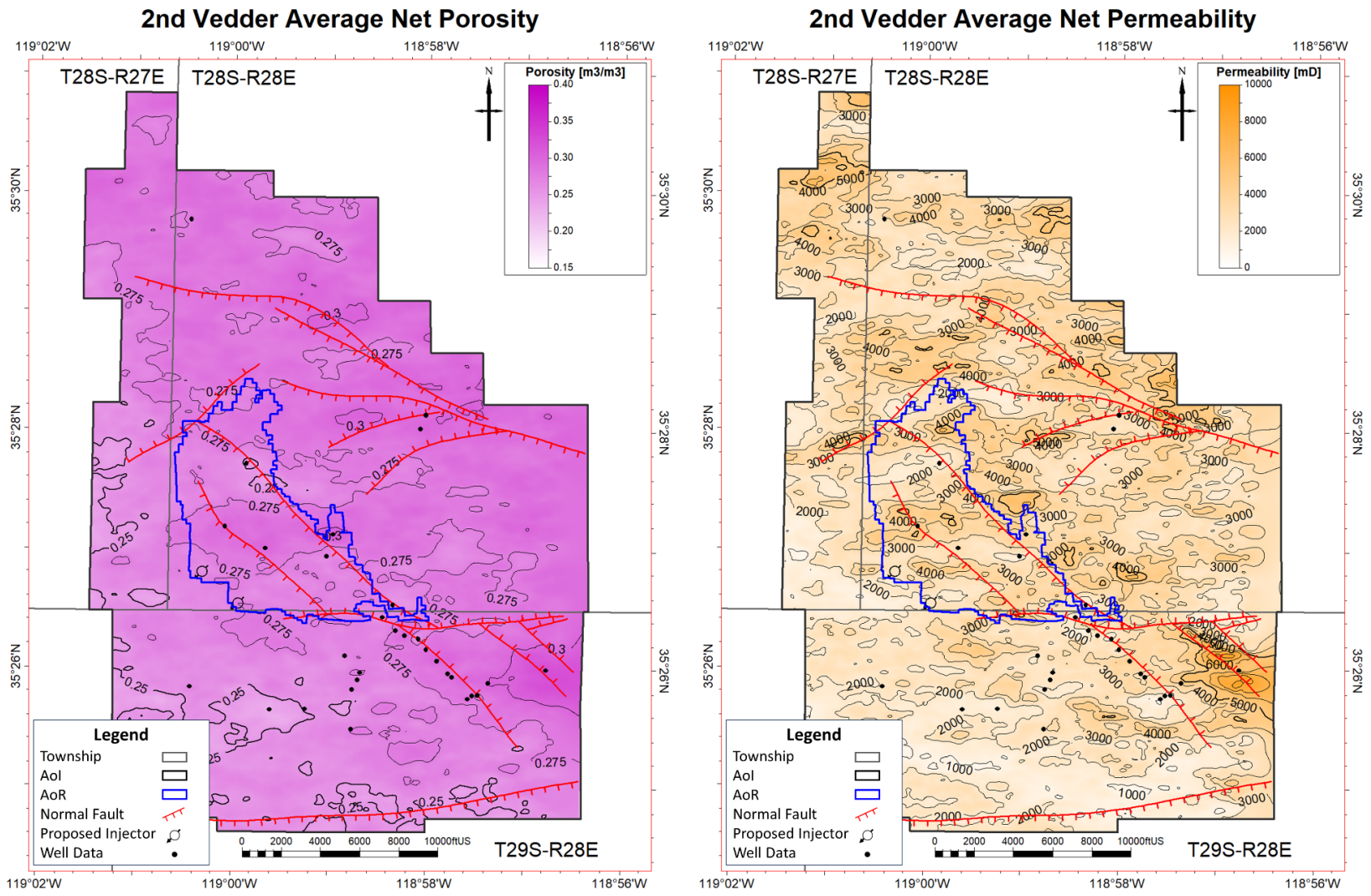

Figure 10. Maps of average sand porosity (left) and sand permeability (right) for the 2nd Vedder Sand (Vd2). Red hachured lines denote faults.

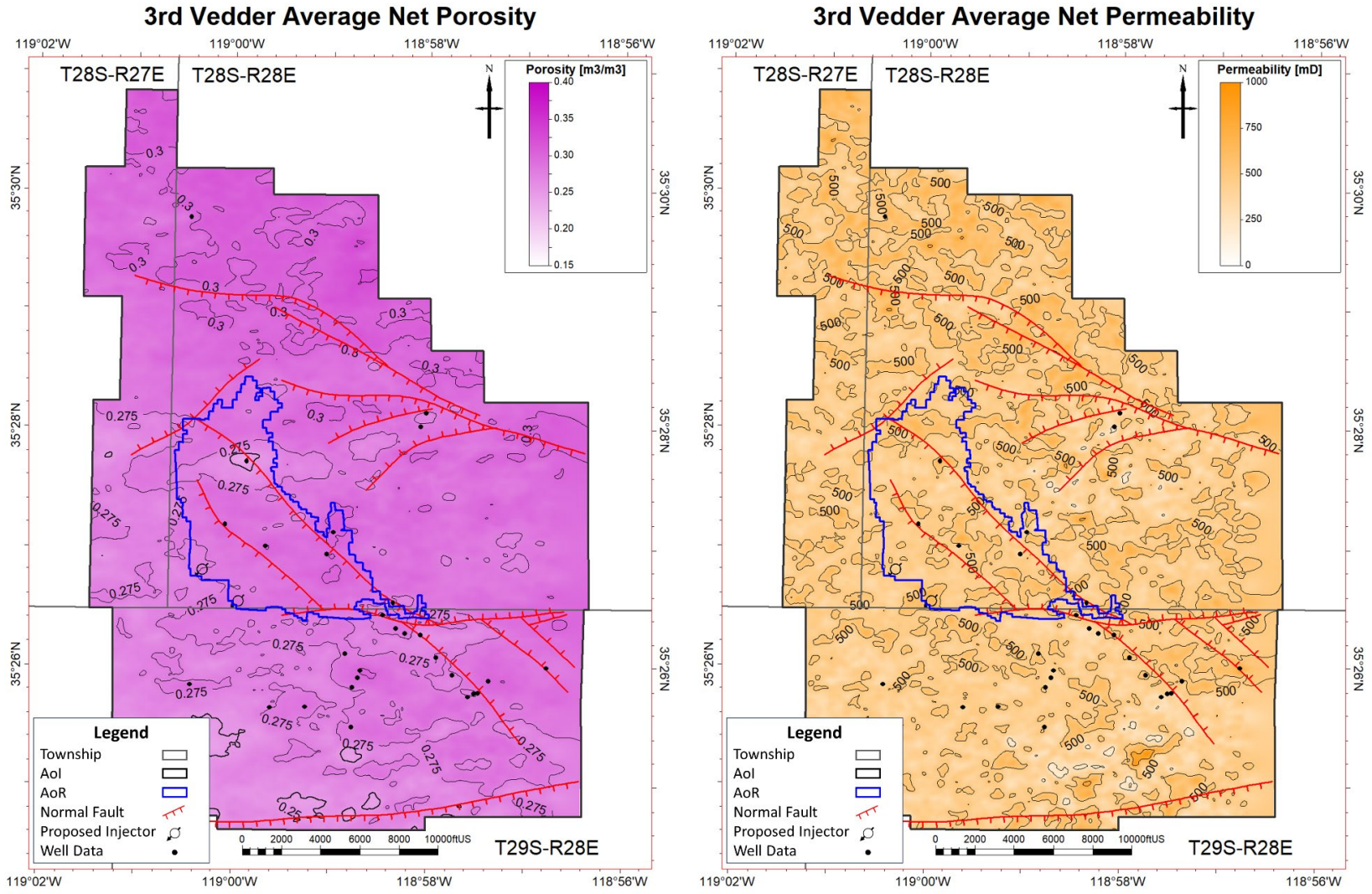

Figure 11. Maps of average sand porosity (left) and sand permeability (right) for the 3rd Vedder Sand (Vd3). Red hachured lines denote faults.

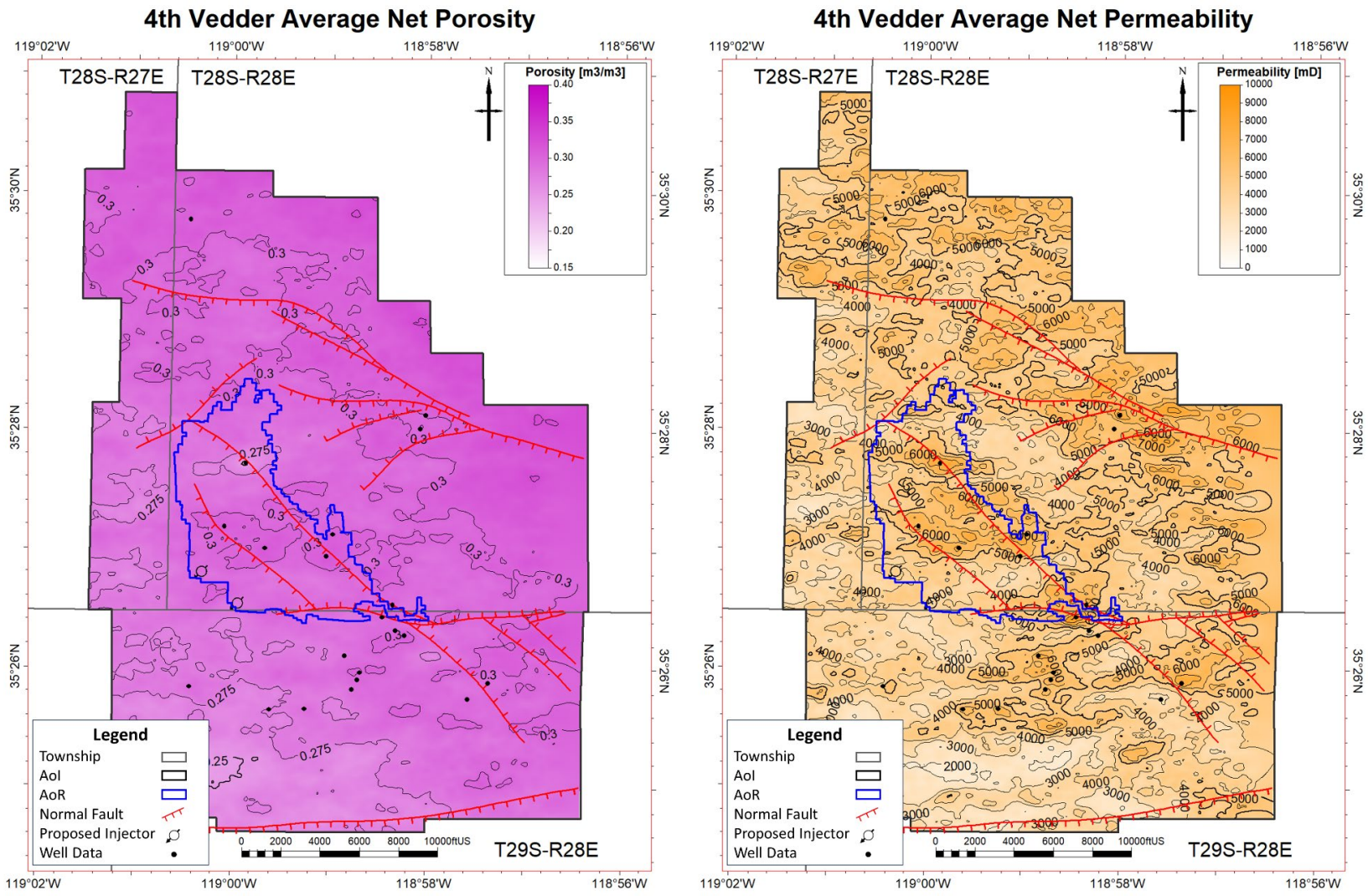

Figure 12. Maps of average sand porosity (left) and sand permeability (right) for the 4th Vedder Sand (Vd4). Red hachured lines denote faults.

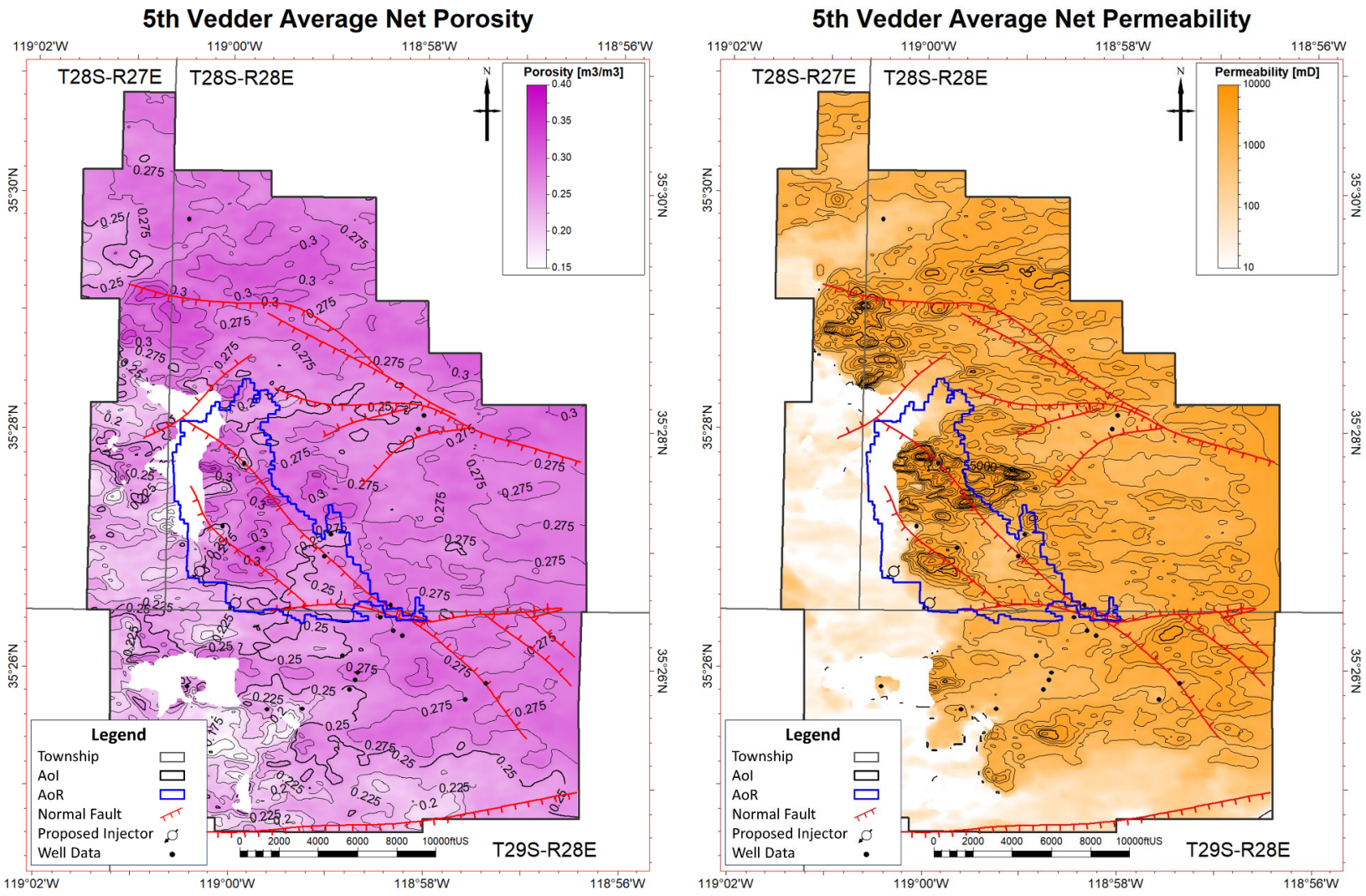

Figure 13. Maps of average sand porosity (left) and sand permeability (right) for the 5th Vedder Sand (Vd5). Red hachured lines denote faults.

Constitutive Relationships and Other Rock Properties

The constitutive relationships modeled are relative permeability with hysteresis, rock compressibility, and CO_2 solubility in reservoir brine.

The relative permeability relationship is shown below in **Figure 14**. This relationship characterizes the multi-phase relative flow between brine and supercritical CO_2 for the Vedder Sands. The curves are developed using a fractional flow analysis (Kamath et. al. 2005) of analog rocks characterized by samples with similar permeability and porosity ranges to the Vedder Sands. A plan for experimentally measuring Vedder core for supercritical CO_2-brine relative permeability is currently underway. For more information on Chevron's future data collection strategy, please refer to the Pre-Operational Logging and Testing Plan. The Freeman-Jewett Silt is prescribed as a no flow boundary, therefore does not follow the relative permeability curve for the Vedder Sand shown in **Figure 14**.

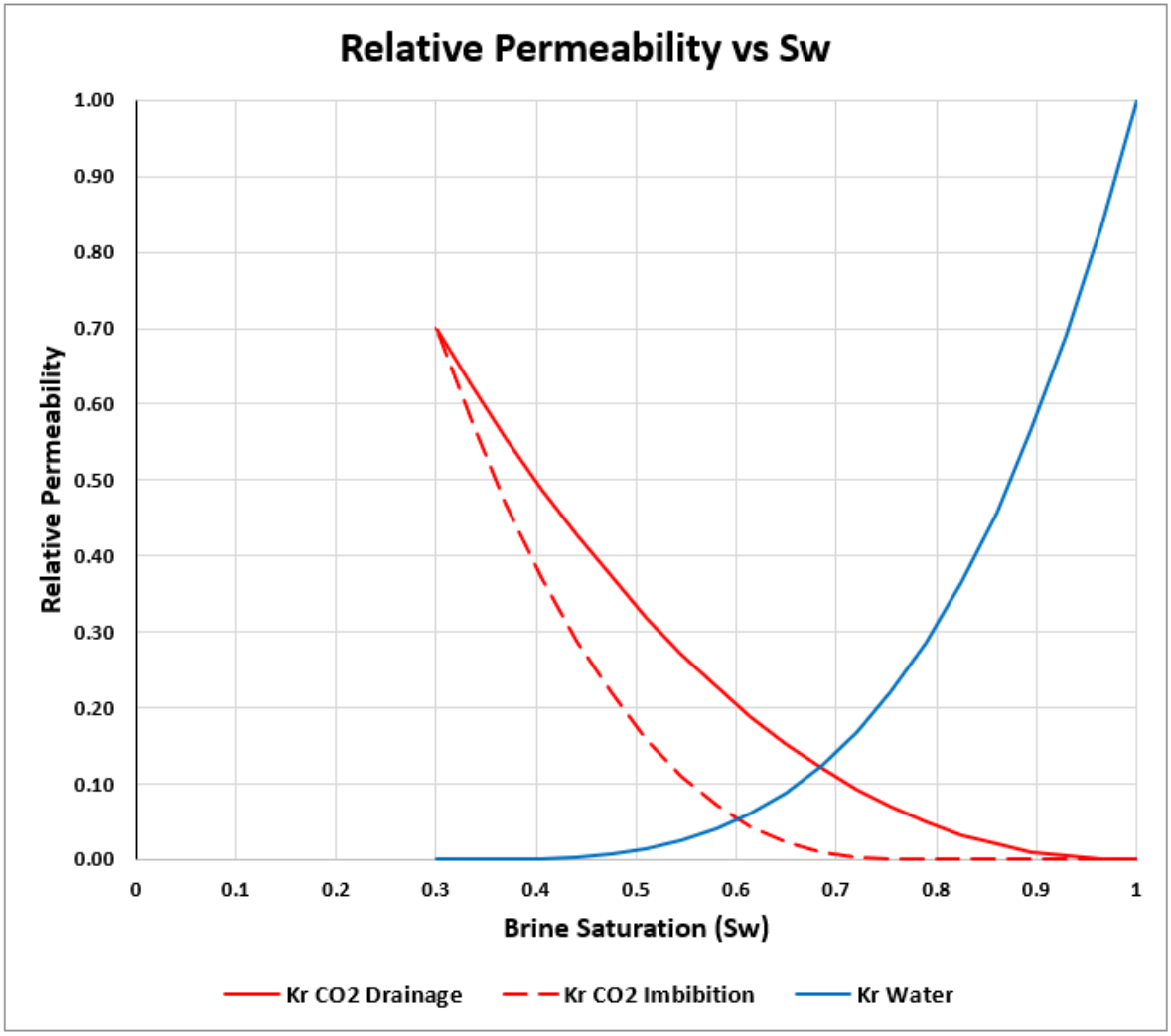

Figure 14. Relative permeability relationship between brine (water) and CO_2

Rock compaction and dilation is implemented within the simulation using **Equation 1**. The compaction/dilation is reversible, and a single value representative of pore volume compressibility/dilation is used.

Equation 1. Compressibility used in the simulation where P represents pressure and ϕ represents porosity.

$$C = \left(\frac{d\varphi}{\mathrm{dP}}\right) \Big/ \varphi$$

To better understand the rock compressibility and geomechanical properties of the Vedder Sands, 3 wells were used (KC20050X_ST1, API# 040304874501; AP_0051X, API# 040296721700; MON0065X, API# 040296758700) (**Figure 15**) to develop a 1-D Mechanical Earth Model (MEM) using the porosity and sonic logs. AP_0051X and MON0065X are within the AoR, while KC20050X is within the AoI, as shown in **Figure 15**. Values of Young's modulus and Poisson's ratio are derived from the three logs. Pore volume compressibility is calculated analytically based on the log derived Young's modulus, Poisson's ratio, and an assumed quartz grain compressibility of 0.181 microsips as shown in **Figure 16** as a continuous curve within the Vedder Sand.

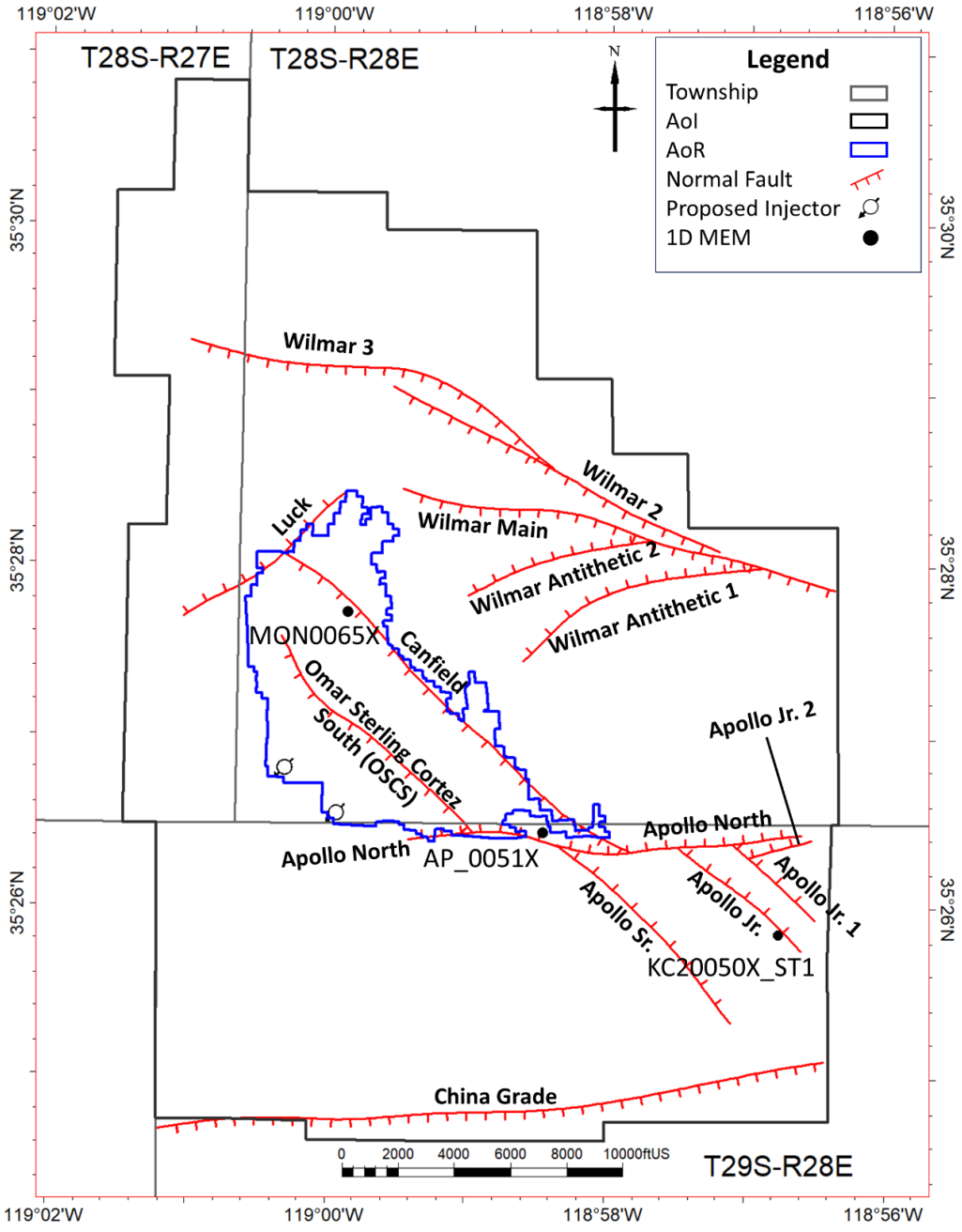

Figure 15. Location of faults intersecting the top of the Vedder Sand and 1D MEMs for wells AP_0051X, MON0065X, and KC20050X_ST1 used for the deterministic fault stability analysis.

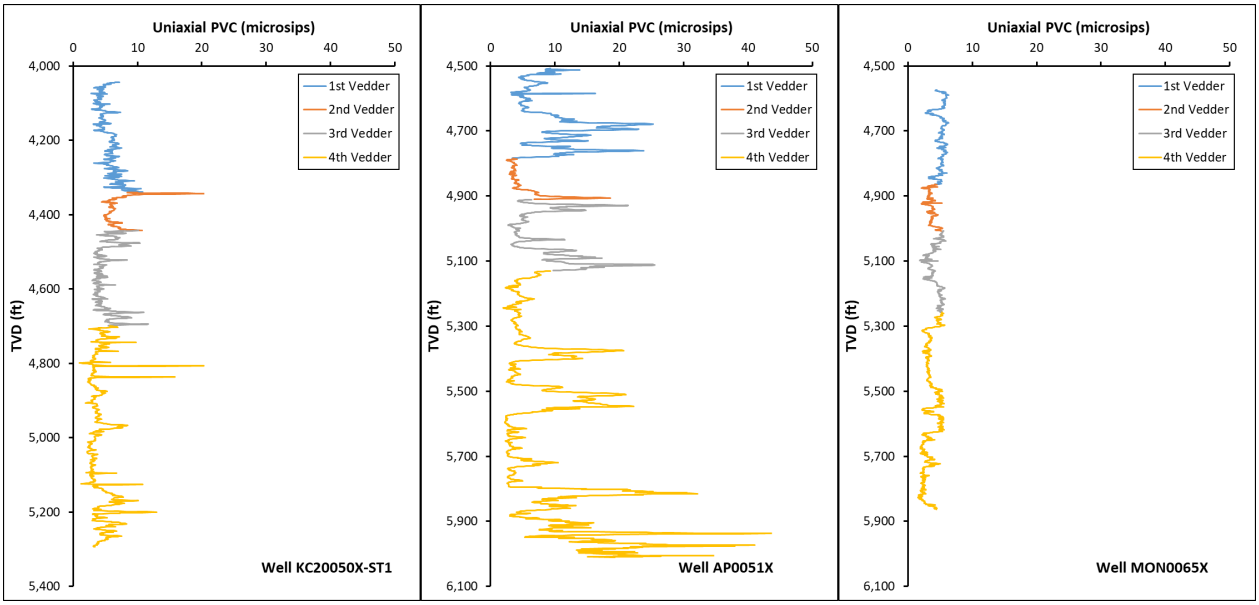

Figure 16. Uniaxial Pore Volume Compressibility vs TVD for wells KC20050X_ST1, AP_0051X, and MON0065X.

Based on this analysis, an approximately average value of 5.0e-6 psi^{-1} (5 microsips) was selected and assigned as formation compressibility for all rock types in the simulation model. Additionally, a plan for experimentally determining rock compressibility for the Vedder Sands is underway. For more information on Chevron's future data collection strategy, please refer to the Pre-Operational Logging and Testing Plan.

The solubility of CO_2 in Vedder brine is described by Ziabakhsh-Ganji & Kooi (2012) as shown below in **Table 5**. This solubility table is used in the simulation model.

Table 5. CO_2 Solubility in brine (Solution GWR) and the impact on formation volume factor of water (Formation Volume Factor)

Pressure (psi)	Solution GWR (MSCF/STB)	Formation Volume Factor (RB/STB)
100	0.011	1.0225
500	0.053	1.0189
1000	0.090	1.0153
1500	0.115	1.0124
2000	0.130	1.0102
2500	0.139	1.0082
3000	0.146	1.0064
3500	0.152	1.0047
4000	0.158	1.0030
5000	0.166	0.9999
6000	0.176	0.9967
7000	0.184	0.9938
8000	0.190	0.9909

Boundary Conditions

The overlying Freeman-Jewett Silt is continuous throughout the model domain with an average thickness of 1140' across the AoI and is proven to have prevented the vertical migration of hydrocarbons within the project area. As such, the Freeman-Jewett Silt has been set as a no flow boundary within the simulation model. Similarly, the lower confining layer, the approximately 50ft shale interval separating the 5th Vedder from the underlying Famoso, is also prescribed as a no flow boundary within the simulation model.

Lawrence Livermore National Laboratory identified the Vedder Sand as a massive, connected saline aquifer that can serve as a key CO_2 sequestration zone in the State of California with 0.9-3.6 billion tons of CO_2 storage capacity (Baker et. al, 2020). Within the AoI, Chevron's historic water disposal in the Vedder Sand and lack of corresponding reservoir pressure increase corroborates Lawrence Livermore National Laboratory's findings. To represent the large, connected pore volume of the Vedder Sand regional aquifer, the model boundaries within the Vedder Sand are open and include pore volume modifiers. The pore volume modifiers are broken into four quadrants (North-West, North-East, South-West, South-East) that contain separate modifier values representing the expected aquifer support in each direction. Aquifer attenuation is accounted for within each quadrant in accordance with the local pore volume modifier. **Figure 17** identifies the separate quadrants, pore volume multiplier cells, and attenuation direction (i versus j), while **Table 6** provides the corresponding pore volume multiplier for each region.

Table 6. Pore volume multipliers applied to simulate each aquifer region.

Aquifer Region (shown on **Figure 17**)	Pore Volume Multiplier
SW i	285
SW j	285
NW i	285
NW j	285
NE i	165
NE j	165
SE i	400
SE j	400

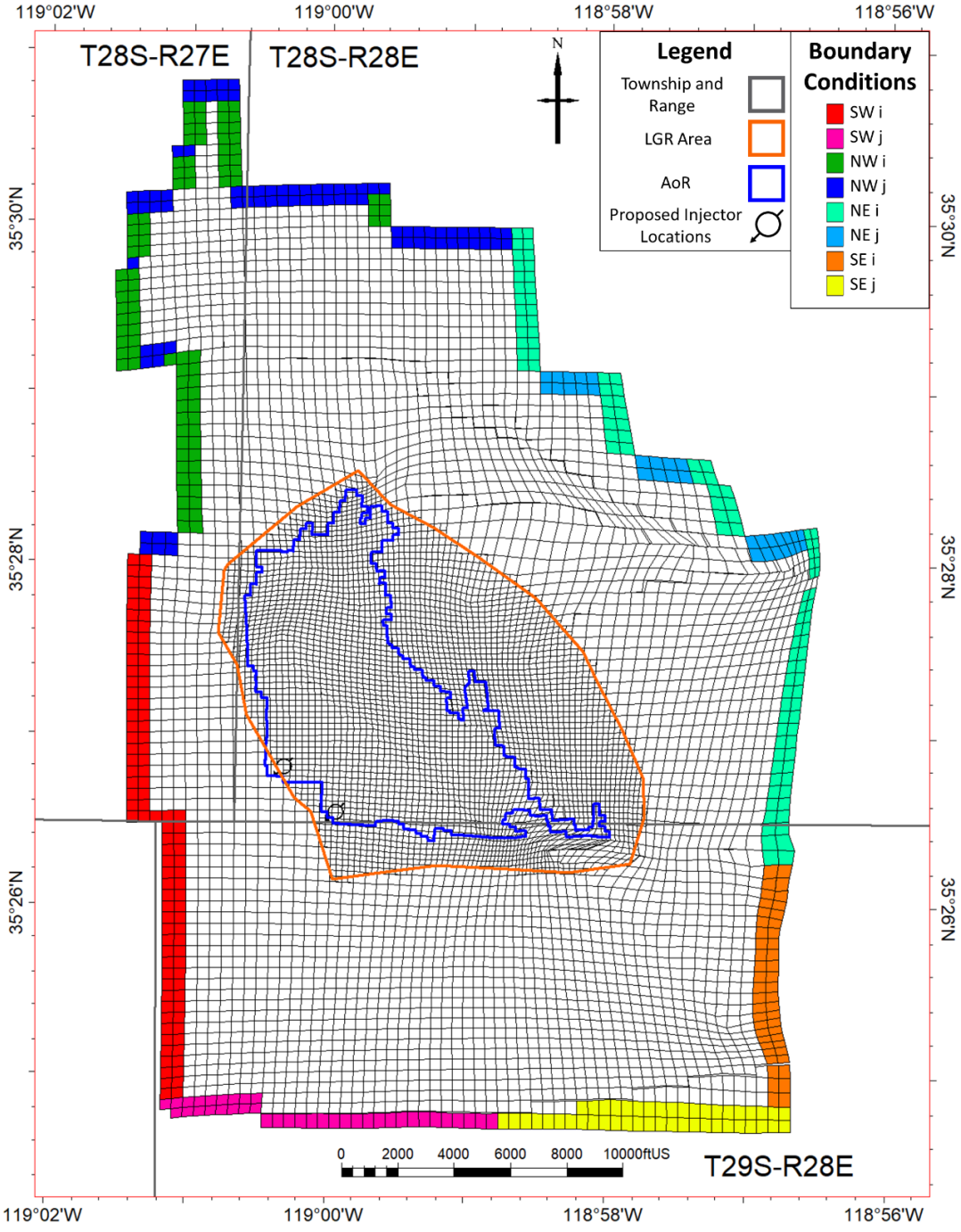

Figure 17. Cells with pore volume multipliers to represent aquifer.

Initial Conditions

Initial conditions for the model are given in **Table 7**. Initially, the model is fully saturated with reservoir brine and is prescribed a hydrostatic pressure gradient which has been calibrated with collected pressure data. No hydrocarbons are included in model initialization.

Table 7. Simulator initial conditions.

Parameter	Value or Range	Units	Corresponding Elevation (ft MSL)*	Data Source
Temperature	160	F	-4293’	Historic well logs within AoR (VES0001WD, API# 040297837500) and AoI (GW_0105, API#: 040290026100; SJ_0002WD, API#: 040296110600)
Formation pressure	1,787	Psi	-3960.5’	Historic well pressure data within AoI (KC20050X, API#: 040304874500) supported by S3_0819X_ST1, API#: 040297371201 and KC20050X_ST1, API#: 040304874501
Fluid density	62.65	lb/ft^3	-4245’	Historic well data within AoI (S3_0719X, API#: 040297135800; S3_0819X, API#: 040297371200)
Salinity (TDS)	10,000	mg/L	-4293’	Historic fluid testing and log data within AoR and AoI
Brine viscosity	0.31	cP	-4245’	Literature correlations based on local salinity
Rock compressibility	$5e^{-6}$	Psi^{-1}	-4245’	Log correlations from within AoR (AP_0051X, API# 040296721700; MON0065X, API# 040296758700) and AoI (KC20050X_ST1, API#: 040304874501)

*In **Table 7**, a negative elevation means below sea level.

Operational Information

Table 8 lists proposed project wells and well types. Details on the injection operation are presented in **Table 9.** Once permitted, Chevron plans to construct MC19001INJ and ANO9004INJ. To ensure disposal deliverability, Chevron plans to retain MC19002INJ and ANO9005INJ as undrilled permitted contingent injectors in the unlikely event that the initially drilled injectors must be abandoned prior to planned injection cessation. Chevron has planned the contingent injectors MC19002INJ and ANO9005INJ to be within 250ft of MC19001INJ and ANO9004INJ, respectively. All simulation modeling in this permit used injectors MC19001INJ and ANO9004INJ, but given the proximity to the contingency injectors, the modeling is also valid for the contingent injectors.

Through the project life, Chevron plans to target individual zones within the Vedder Sand with tubing and packer completions, starting with the deepest target and recompleting into increasingly shallower Vedder Sand intervals through time as necessary based upon monitoring data. With each recompletion, Chevron plans to update operating constraints based upon any wellbore changes (e.g., additional perforations for shallower Vedder Sand targets).

First, Chevron plans to target the 4th Vedder, and after approximately seven years of injection, the injectors will be recompleted into the 3rd Vedder at which point the 4th Vedder will be isolated from injection. After the 3rd Vedder has been targeted for approximately seven years, Chevron plans to recomplete into the 2nd Vedder, at which point the 3rd Vedder will be isolated from injection. Finally, after several years of targeting the 2nd Vedder, the injectors are planned to be recompleted into the 1st Vedder, isolating the 2nd Vedder from injection. Chevron has developed this reconfiguration approach based upon simulation results and plans to use monitoring data during project execution to guide actual recompletion times to optimize pore space. **Figure 18** and **Figure 19** show proposed injection rates and intra-Vedder Sand recompletions through the life of the project.

Using Santa Margarita Sandstone and Vedder Sand pressure data within the AoI, Chevron has made the initial interpretation that the Vedder Sand and the Santa Margarita Sandstone are under hydrostatic conditions. Chevron plans to acquire Santa Margarita Sandstone and Vedder Sand pressure data during well construction, as described in detail in the Pre-Operational Logging and Testing Plan.

Chevron plans to drill and operate water producers in the Vedder Sand through injection life to slightly decrease the reservoir pressure to the point that the AoR is purely a function of CO_2. The simulated pressure response at the monitoring wells highlights the effectiveness of this strategy, shown in **Figure 28, Figure 29, Figure 30 and Figure 31**. The planned producer locations are shown in **Figure 22**. Chevron plans to leverage existing surface facilities to handle Vedder Sand produced water.

As previously mentioned, this Project plans to source the CO_2 from a variety of sources (e.g., direct air capture) Chevron expects capturable volumes to increase through the life of the Project, as reflected in the rate schedules shown in **Figure 18** and **Figure 19**. All CO_2 streams will be analyzed and shared with the Environmental Protection Agency (EPA) prior to any inclusion in the injection stream.

Table 8. Project Well Names and Well Types.

Well Name	Well Type
MC19001INJ	CO_2 Injector
ANO9004INJ	CO_2 Injector
MC19002INJ	Contingent CO_2 Injector
ANO9005INJ	Contingent CO_2 Injector
DDA9001OB	Deep Monitoring Well
COR9001OB	Deep Monitoring Well
RCA9001OB	Deep Monitoring Well
HK_9001OB	Deep Monitoring Well
KER9001OB	Shallow Monitoring Well
IR_9001OB	Shallow Monitoring Well
ANO9003OB	Shallow Monitoring Well
ANO9001OB	Shallow Monitoring Well
GW_9001OB	Shallow Monitoring Well
GW_9002OB	Shallow Monitoring Well
FEA9001P	Pressure Management Producer
FEA9002P	Pressure Management Producer

Table 9. Operating details.

Operating Information	**Injection Well 1 MC19001INJ**	**Injection Well 2 ANO9004INJ**	**Contingent Injection Well 2 ANO9005INJ**	**Contingent Injection Well 1 MC19002INJ**
Location (surface hole) X Y	 1702883.99 707652.89	 1702047.20 709910.70	 1702099.43 709783.20	 1702940.99 707531.07
Location (bottomhole) X Y	 1702415.6 708383.07	 1700588 709996.78	 1700731.93 709857.64	 1702276.04 708526.23
No. of perforated intervals	4	4	4	4
Perforated interval (ft. MD) 1st Vedder Top Perforation- Bottom Perforation 2nd Vedder Top Perforation- Bottom Perforation 3rd Vedder Top Perforation- Bottom Perforation 4th Vedder Top Perforation- Bottom Perforation	 5036'-5096' 5300'-5360' 5574'-5634' 5843'-5903	 5357'-5417' 5609'-5669' 5864'-5924' 6168'-6228'	 5311'-5371' 5564'-5624' 5819'-5879' 6121'-6181'	 5161'-5221' 5427'-5487' 5690'-5750' 5970'-6030'
Wellbore diameter (Inches)	7"	7"	7"	7"
Planned injection period Start End	 2030 2050	 2030 2050	 2030 2050	 2030 2050
Injection duration (years)	20	20	20	20
Injection rate (MSCF/day & tonne/annum)	Provided in **Figure 18**.	Provided in **Figure 19**.	Provided in **Figure 19**.	Provided in **Figure 18**.

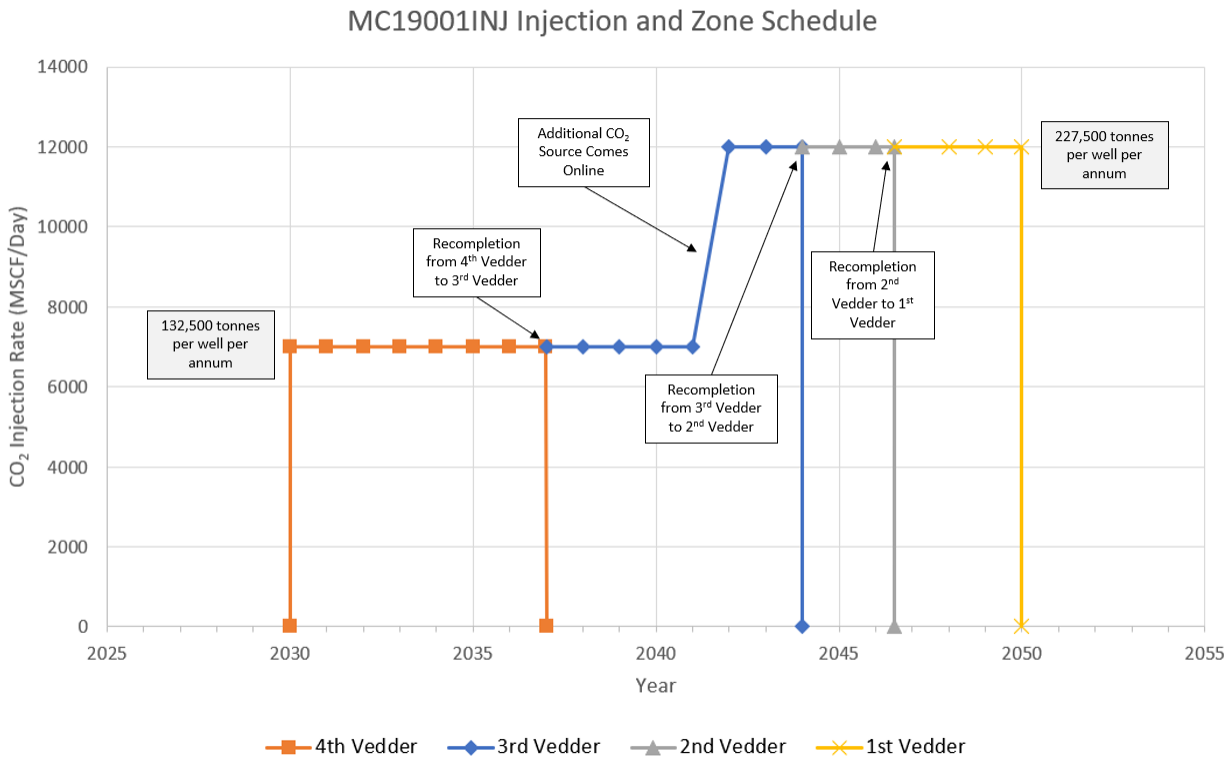

Figure 18. Injection and zonal recompletion schedule for injector MC19001INJ. If it is ever needed to be drilled, contingent injector MC19002INJ follows the same zonal recompletion and injection schedule where MC19001INJ left off.

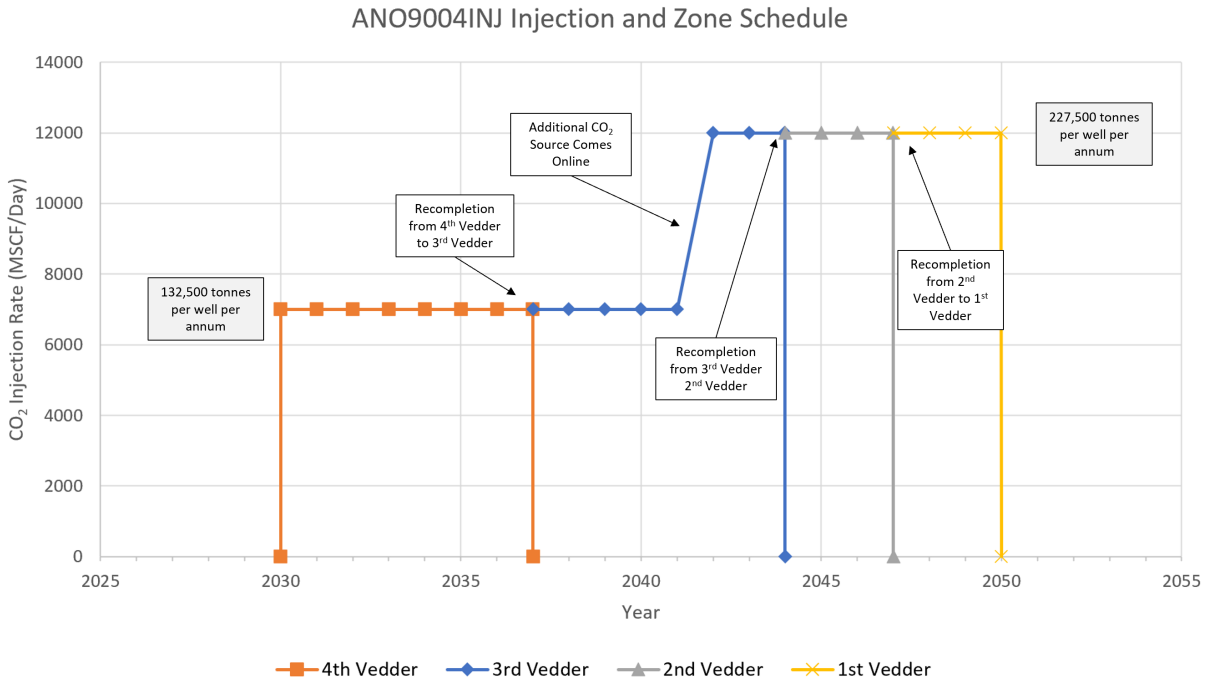

Figure 19. Injection and zonal recompletion schedule for injector ANO9004INJ. If it is ever needed to be drilled, contingent injector ANO9005INJ follows this same zonal recompletion and injection schedule where ANO9004INJ left off.

Fracture Pressure and Fracture Gradient

Determination of the fracture gradient is detailed in the Geomechanical and Petrophysical Information section of the Project Narrative. In 2022, Chevron executed a step rate test within the target Vedder Sand within the AoI using well KCL20050X (API #040304874500). The test was conducted with 10' of perforations, 4654'- 4664' MD. The observed Fracture Propagation Pressure from this test was found to be 2,871.6 psi as shown in **Figure 20**. This equates to a fracture gradient of 0.642psi/ft. Chevron plans to operate proposed injectors with automated, fail-safe control systems to ensure bottomhole injection pressures never reach more than 90% of the observed Vedder Sand fracture pressure. Resultant maximum injection pressures for the proposed injectors are listed in **Table 10** The results from this 2022 step rate test are consistent with nearby publicly available observed fracture gradients within the Vedder Sand. Examples include a 0.682 psi/ft gradient observed in Young Fee WD4 (API# 040305916200) in 2016 in Kern Front Oil field, which directly neighbors the AoI to the west (California Resources Corporation, 2019). Based on the evidence presented here, there is sufficient data to characterize fracture pressure gradient of the Vedder Sand within the Project AoI. Unless required by the UIC Region 9 Director, Chevron does not plan to conduct additional Vedder Sand fracture testing in future construction phases of the Project.

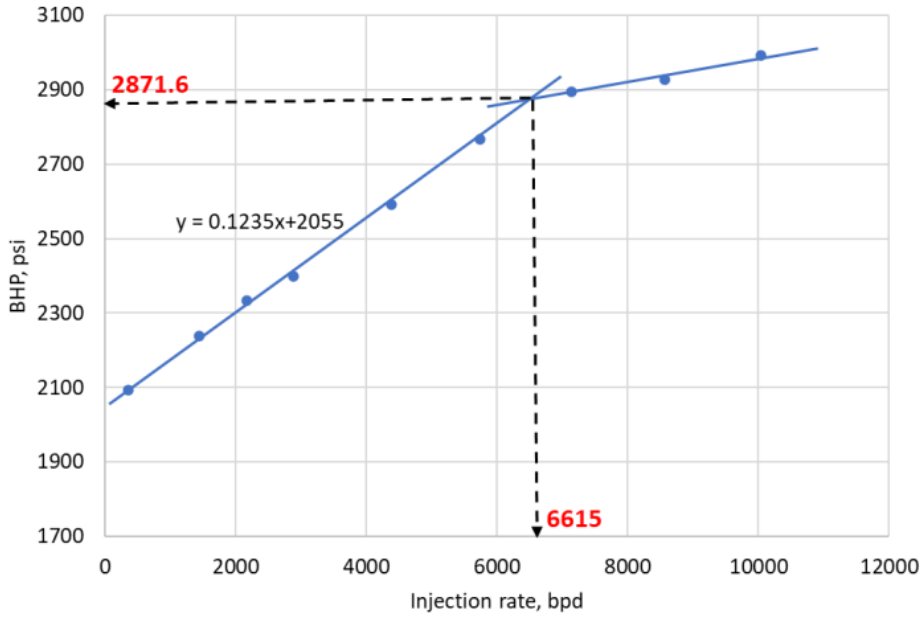

Figure 20. Results from 2022 Step Rate Test within the Vedder Sand, obtaining a Fracture Propagation Pressure of 2,871.6 psi, equivalent to 0.642 psi/ft.

As mentioned in the Operational Information section of this document, Chevron plans to start with the deepest injection target, the 4th Vedder, and recomplete vertically through the life of the project as dictated by the monitoring plan. During injection, each target zone is planned to be isolated from all other wellbore perforations with packers. The completion zones will change through time, and each recompletion will result in a newly calculated fracture gradient based upon only the perforations that are open to flow (reflected in **Table 10**).

Table 10. Injection pressure details.

Injection Pressure Details	**Injection Well MC19001INJ**	**Injection Well ANO9004INJ**	**Contingent Injection Well ANO9005INJ**	**Contingent Injection Well MC19002INJ**
Fracture gradient (psi/ft)	0.642	0.642	0.642	0.642
Maximum injection bottomhole pressure for each isolated zone (90% of fracture pressure, psi)				
Perforation 1st Vedder	2829	2891	2892	2826
Perforation 2nd Vedder	2982	3037	3038	2979
Perforation 3rd Vedder	3140	3184	3185	3131
Perforation 4th Vedder	3295	3360	3360	3293
Elevation corresponding to maximum injection pressure (ft TVD)				
Perforation 1st Vedder	4896’	5004’	5005’	4891’
Perforation 2nd Vedder	5160’	5256’	5258’	5157’
Perforation 3rd Vedder	5434’	5510’	5513’	5419’
Perforation 4th Vedder	5703’	5814’	5815’	5700’
Elevation at the top of the perforated interval (ft TVD)				
Perforation 1st Vedder	4896’	5004’	5005’	4891’
Perforation 2nd Vedder	5160’	5256’	5258’	5157’
Perforation 3rd Vedder	5434’	5510’	5513’	5419’
Perforation 4th Vedder	5703’	5814’	5815’	5700’
Maximum expected injection pressure at the top of the perforated interval based on computational simulation (psi)				
Perforation 1st Vedder	1940	1940	N/A	N/A
Perforation 2nd Vedder	2045	2045	N/A	N/A
Perforation 3rd Vedder	2160	2160	N/A	N/A
Perforation 4th Vedder	2290	2290	N/A	N/A

Computational Modeling Results

Predictions of System Behavior

Chevron plans to perforate the bottom section of each Vedder Sand and target each sand body individually, starting with the deepest target, the 4th Vedder, and recompleting vertically to the 3rd, 2nd, and finally 1st Vedder through time as dictated by monitoring data.

When the CO_2 is injected, a fraction of the stream will dissolve into the reservoir brine while the remaining buoyant supercritical CO_2 begins to migrate vertically within the target interval until it reaches a baffle or confining shale layer, and up-dip to the northeast until it reaches the Omar-Sterling-Cortez-South fault. Over time, CO_2 builds up against this baffling fault, and can eventually migrate through the fault when enough of a CO_2 column has developed, overcoming the required capillary entry pressure, and pushing through the reduced permeability of the fault deformation zone. The CO_2 that breaks through or travels around the Omar-Sterling-Cortez-South fault to the northwest next encounters the Canfield fault, where the CO_2 again begins to build a column against the fault until capillary forces are overcome, and CO_2 can migrate through the fault deformation zone. This same general migration path is followed independently in each sand once that sand is targeted for CO_2 injection. This described behavior through time is highlighted in **Figure 23 and Figure 24.**

Chevron recognizes that the faults have an impact on the CO_2 migration path and plume shape, therefore Chevron has exerted significant effort to characterize and model the faults within the AoR as well as throughout the entire administrative field boundary. The data sources, analytical methodologies, and how the data has been incorporated into the simulation model are described in detail within the Model Calibration and Validation section of this document. Chevron has incorporated the characterization of these faults into the design of the monitoring well network as described in the Testing and Monitoring Plan, which is designed to observe CO_2 plume migration for a range of fault seal scenarios and will serve as a guide for simulation validation and target recompletion times (planned recompletion times highlighted in (**Figure 18** and **Figure 19**).

Chevron plans to acquire additional Santa Margarita pressure data during well construction, as described in detail in the Pre-Operational Logging and Testing Plan. Based on historical Santa Margarita and recent Vedder Sand pressure data within the AoI, Chevron has made the initial interpretation that the Vedder Sand and the Santa Margarita are in hydrostatic conditions.

Given this assumption, Chevron plans to include water producers targeting the Vedder Sand through the injection life to slightly decrease the reservoir pressure to the point that no section of the reservoir rises above the critical pressure, resulting in an AoR which is purely a function of the CO_2 plume. The simulated pressure response at the monitoring wells highlights the effectiveness of this strategy, as shown in **Figure 28, Figure 29, Figure 30,** and **Figure 31**. Chevron plans to drill new water producers FEA9001P and FEA9002P and operate the wells with electric submersible pumps. The planned locations for these two (2) wells are shown in **Figure 22**. During the life of injection, Chevron plans to produce formation water from the Vedder Sand to slightly decrease reservoir pressure. **Figure 21** shows the schedule of produced fluids used in simulation. The producers are planned to follow a vertical recompletion strategy similar to the injectors, so that the producers target individual zones to effectively dewater and depressurize zones being targeted with CO_2 at that time. The increase in production rate correlates to the increase in injection rate.

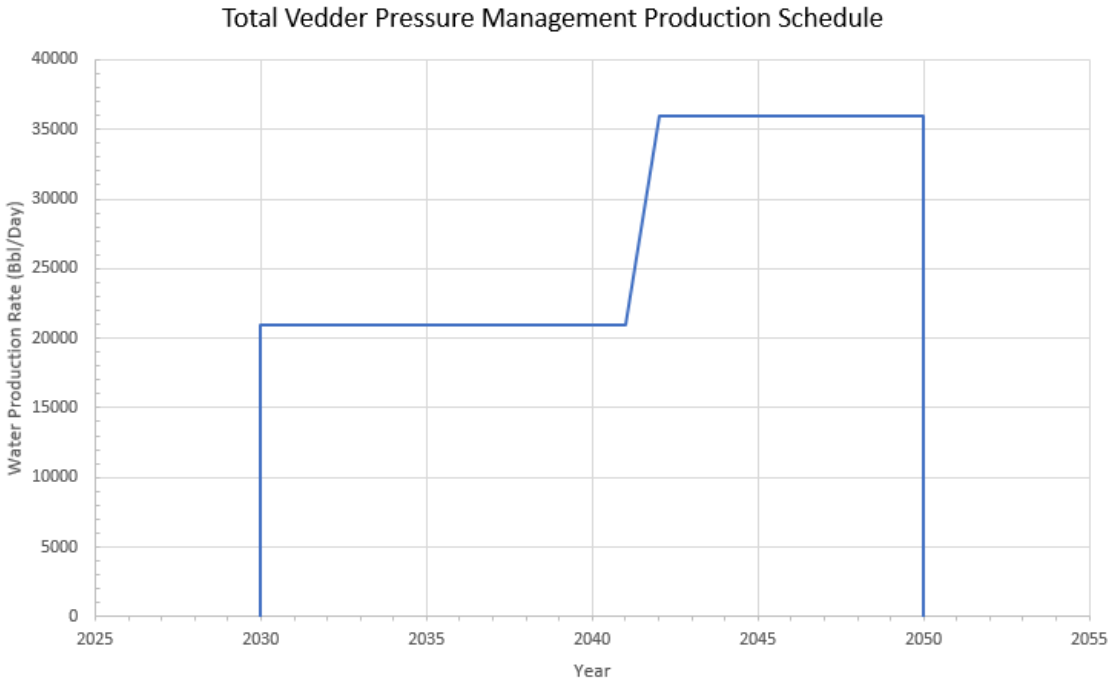

Figure 21. Schedule of pressure management produced fluids used in all simulation cases presented in this report. The increase in production rate is to keep up with the increase in injection rate, as shown in **Figure 18** and **Figure 19**.

As part of ongoing hydrocarbon production and operation in the shallower Kern River Series, Chevron has existing surface facilities for the treatment and disposition of produced water. Chevron plans to use these facilities to handle produced water from the Vedder Sand.

Figure 22 shows the AoR as well as the monitoring wells and their detection boundaries. **Figure 23** and **Figure 24** display the migration of CO_2 at various time steps throughout the project life. The boundaries of the simulated CO_2 plume have been defined with a minimum saturation cutoff of 5% based on detectable limits of monitoring equipment. Additional details and cross sections of pressure changes through the life of the project are provided in the AoR Delineation section of this document.

As shown in **Figure 23** and **Figure 24**, the CO_2 extent approaches stability after 20 years of injection. Over the next 40-60 years of post-injection monitoring, there is a small amount of additional growth as CO_2 continues to migrate up-dip and builds a column against the Canfield fault, a small portion of which eventually overcomes the capillary forces and reduced permeability of the fault zone.

Figure 25 and **Figure 26** display the evolution of the pressure front through the life of the Project. Several of the images appear blank, meaning that due to pressure management, there are no regions of the model at that time with a pressure change greater than the critical pressure.

Throughout the life of the injection, the free phase CO_2 is anticipated to remain supercritical. **Figure 27** presents the forecast mass quantities of CO_2 by phase and trapping mechanism over the Project life.

During project execution, Chevron plans to compare computational pressure changes and CO_2 forecasts with observed monitoring data to identify any discrepancies and, if necessary, update computational model parameters (within reason) to better match observed data. Please refer to the AoR Reevaluation Cycle section of this document for further details on this topic.

Chevron has disposed of over 50,000,000 barrels of water across the Vedder Sand within the AoI over the past 40 years with no observed seismic response or pressure build up. The AoRs of the Vedder Sand water disposal and proposed CO_2 injection do not overlap with one another.

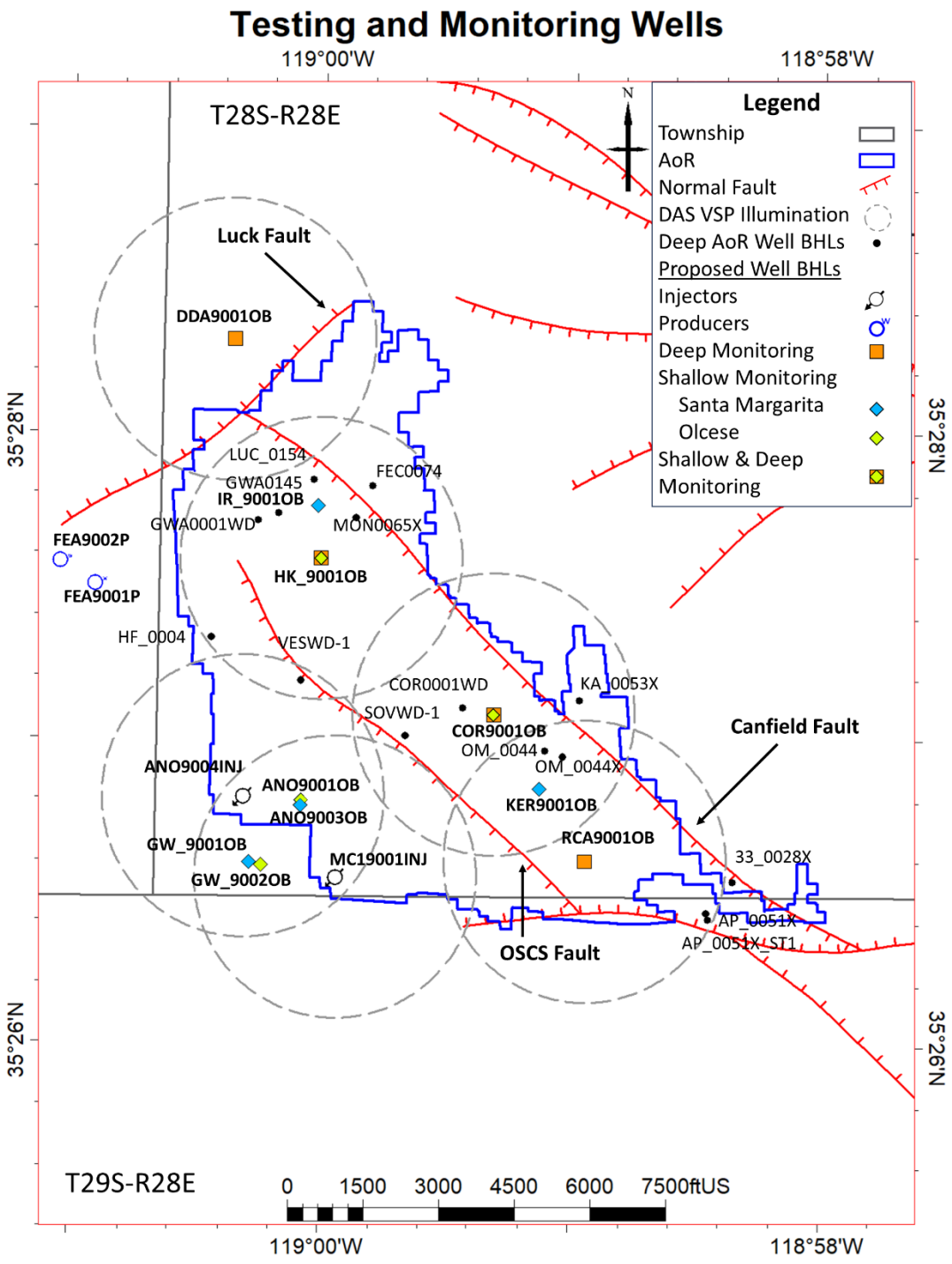

Figure 22. AoR (blue) shown with injectors (black open circles with arrows) MC19001INJ and ANO9004INJ, deep monitoring wells (orange squares) DDA9001OB, HK_9001OB, COR9001OB, RCA9001OB with their expected supercritical CO_2 detection boundaries (dashed radii around monitoring wells), shallow water observation wells (blue and yellow diamonds) GW_9001OB, GW_9002OB, ANO9001OB, and ANO9003OB and pressure management producers FEA9001P and FEA9002P.

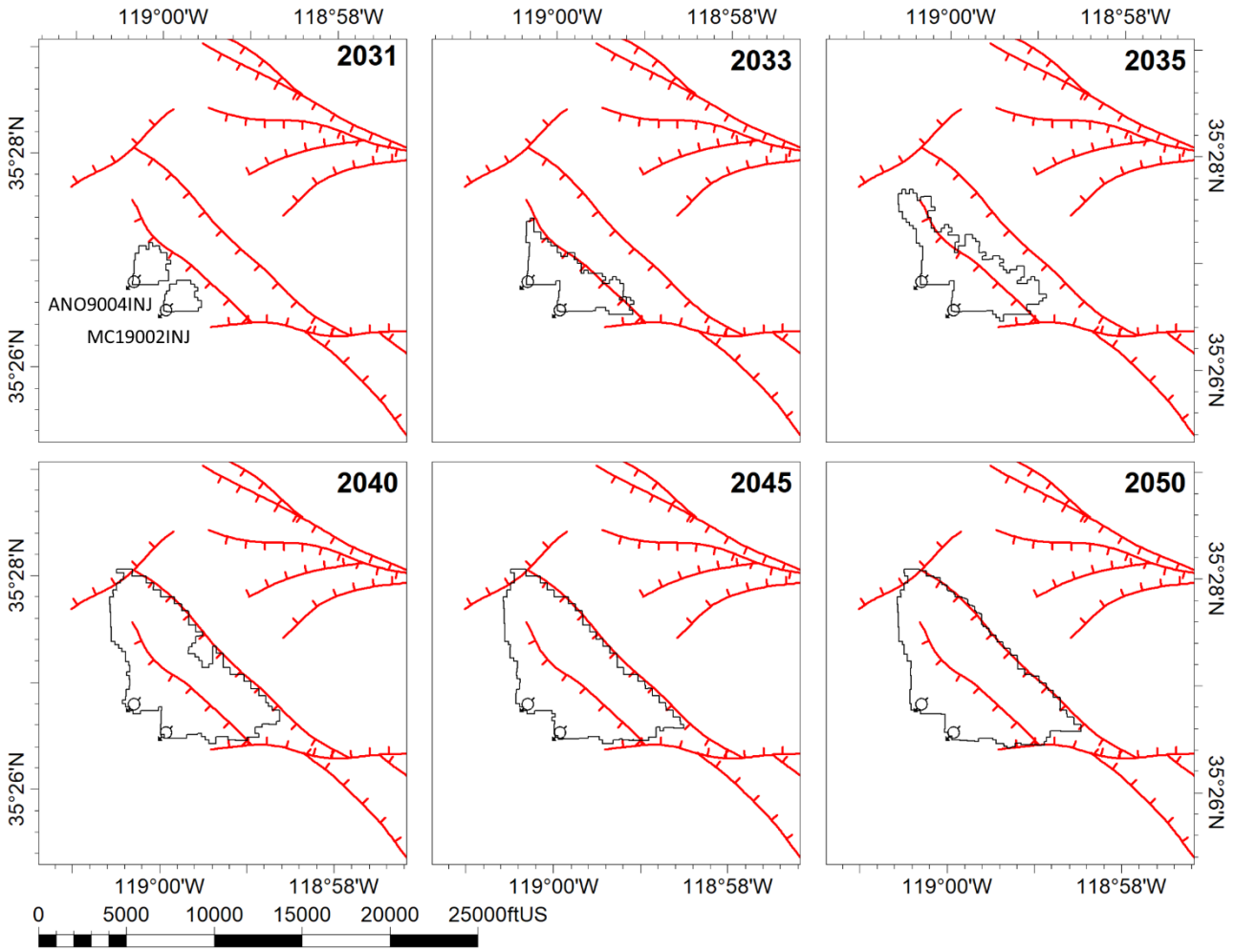

Figure 23. AoR evolution over the 20-year injection, beginning in 2030. Image is taken at the beginning of the year shown in the top right corner of each pane. Well locations are bottomhole locations.

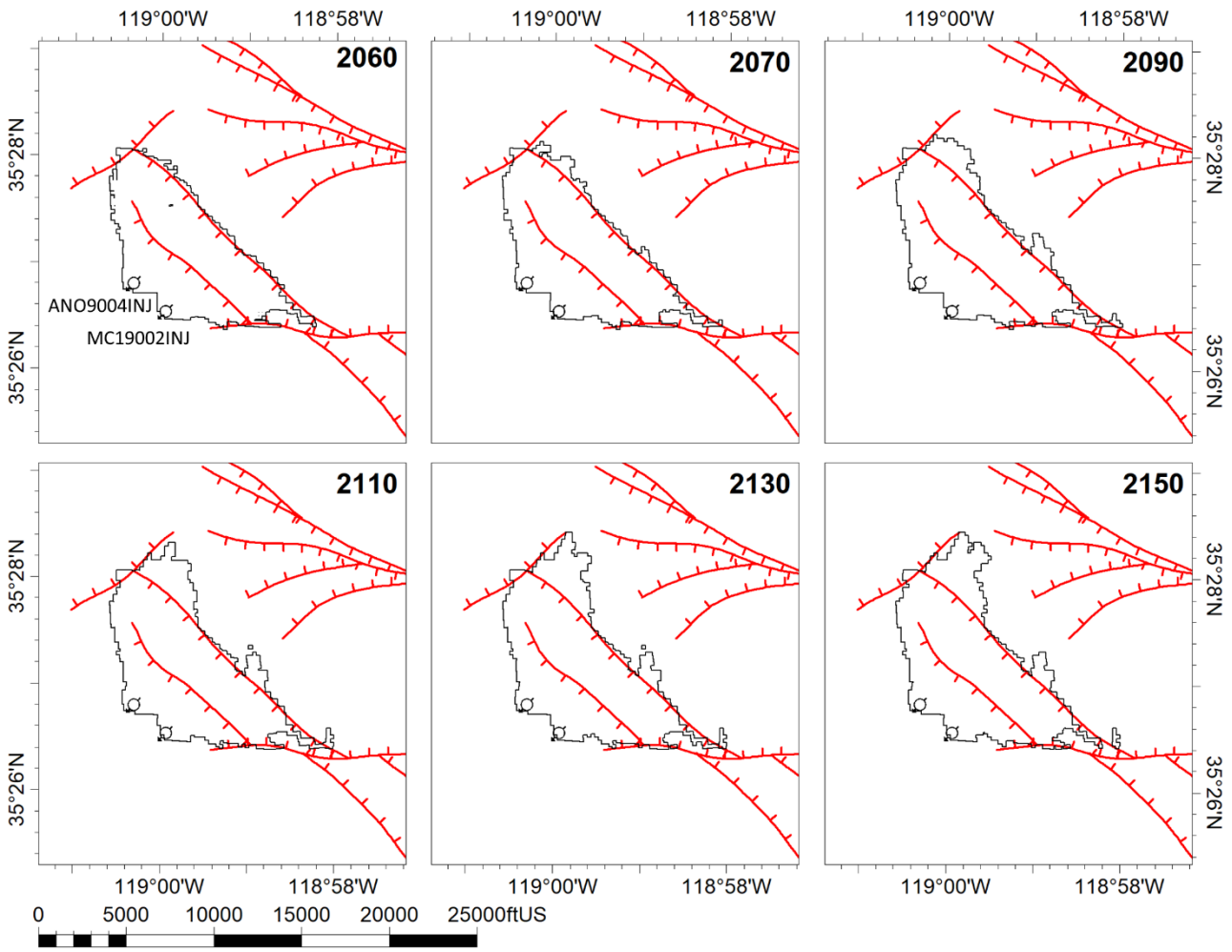

Figure 24. AoR evolution after cessation of injection at the beginning of 2050. Image is taken at the beginning of the year shown in the top right corner of each pane. Well locations are bottomhole locations.

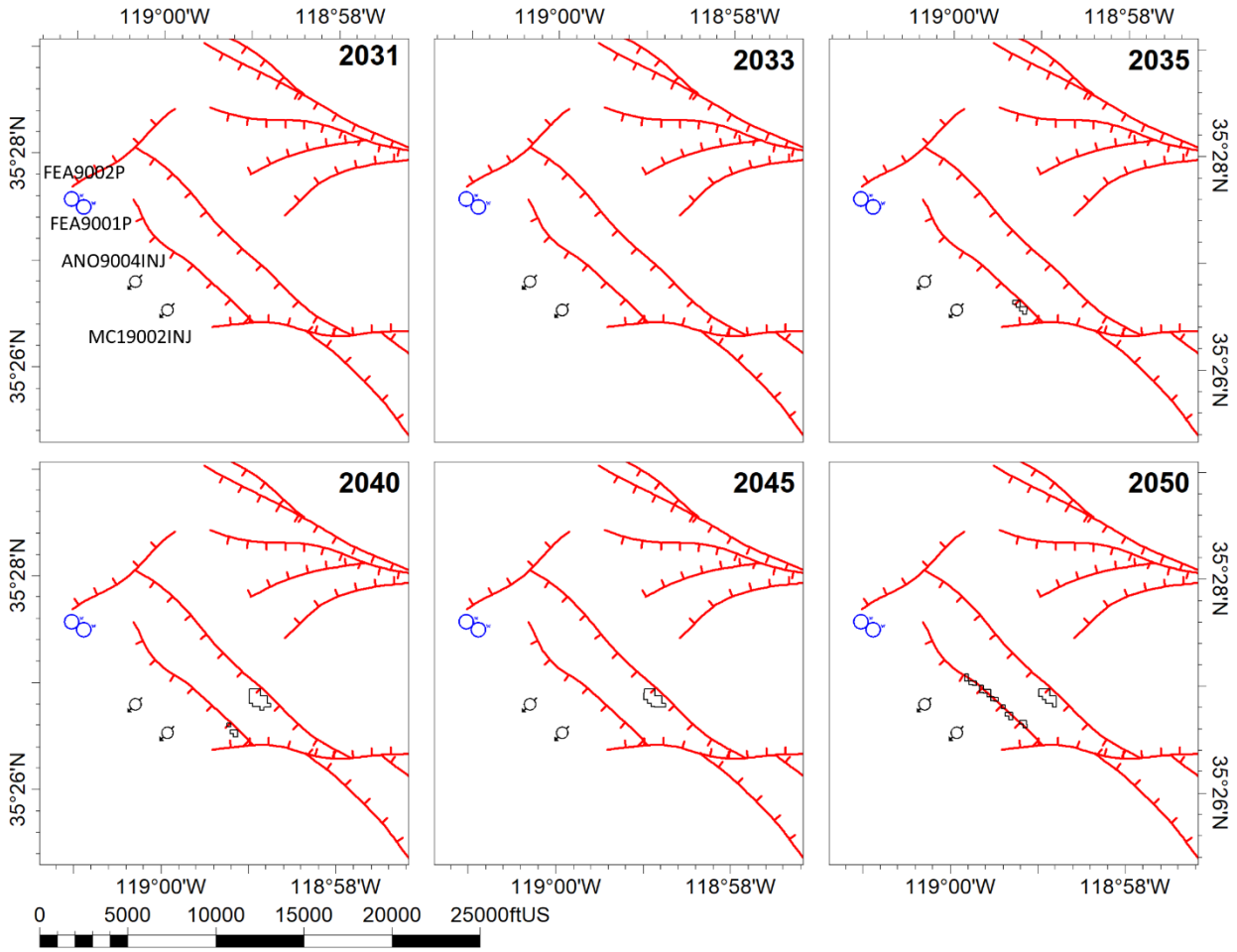

Figure 25. Critical pressure evolution over the 20-year injection, beginning in 2030. Image is taken at the beginning of the year shown in the top right corner of each pane. Well locations are bottomhole locations. Black wells as injectors, blue wells are pressure management producers. Many of the time slices appear blank, meaning there are no regions of the model with an elevated pressure greater than 3.6 psi.

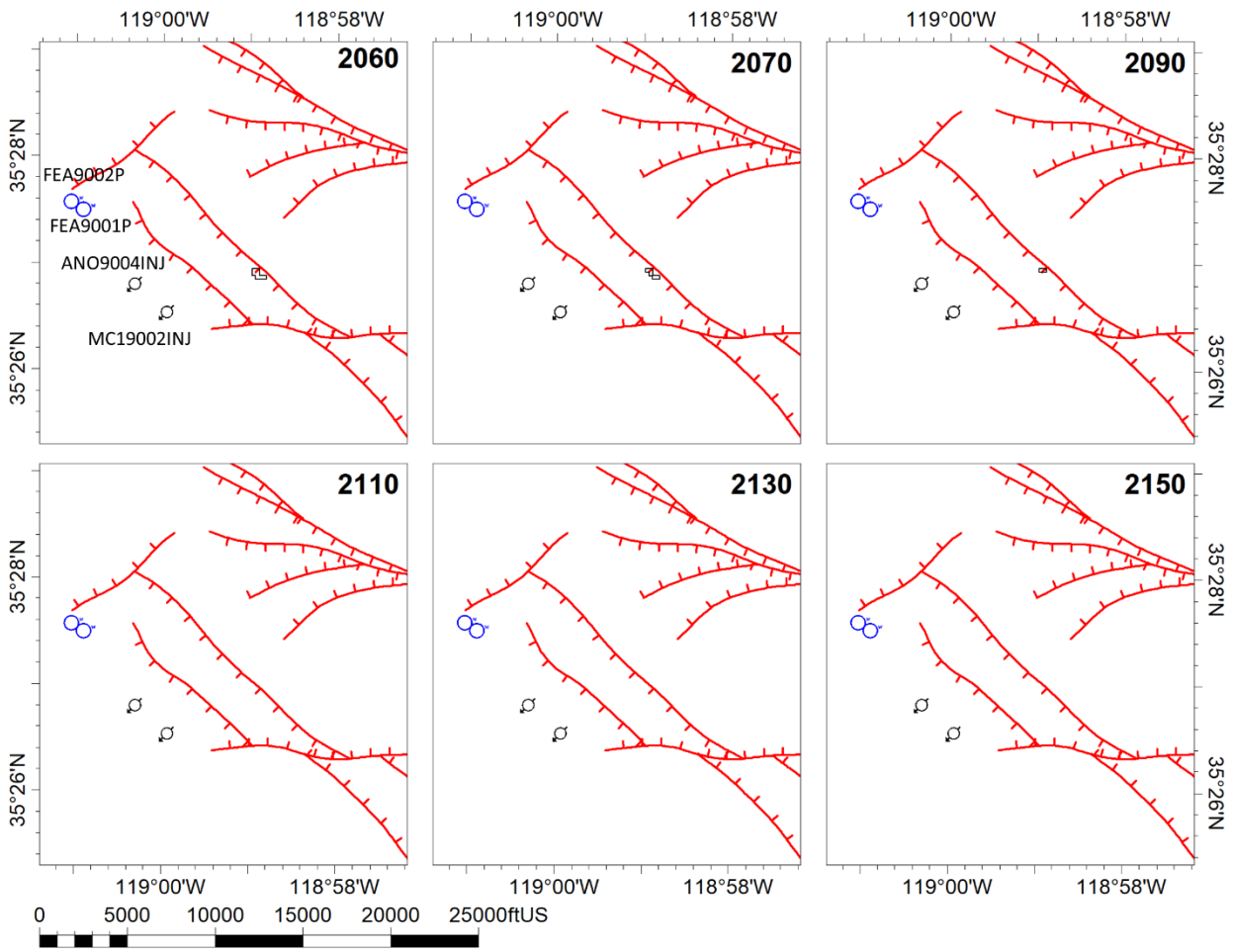

Figure 26. Critical pressure evolution after cessation of injection at the beginning of 2050. Image is taken at the beginning of the year shown in the top right corner of each pane. Well locations are bottomhole locations. Many of the time slices appear blank, meaning there are no regions of the model with an elevated pressure greater than 3.6 psi.

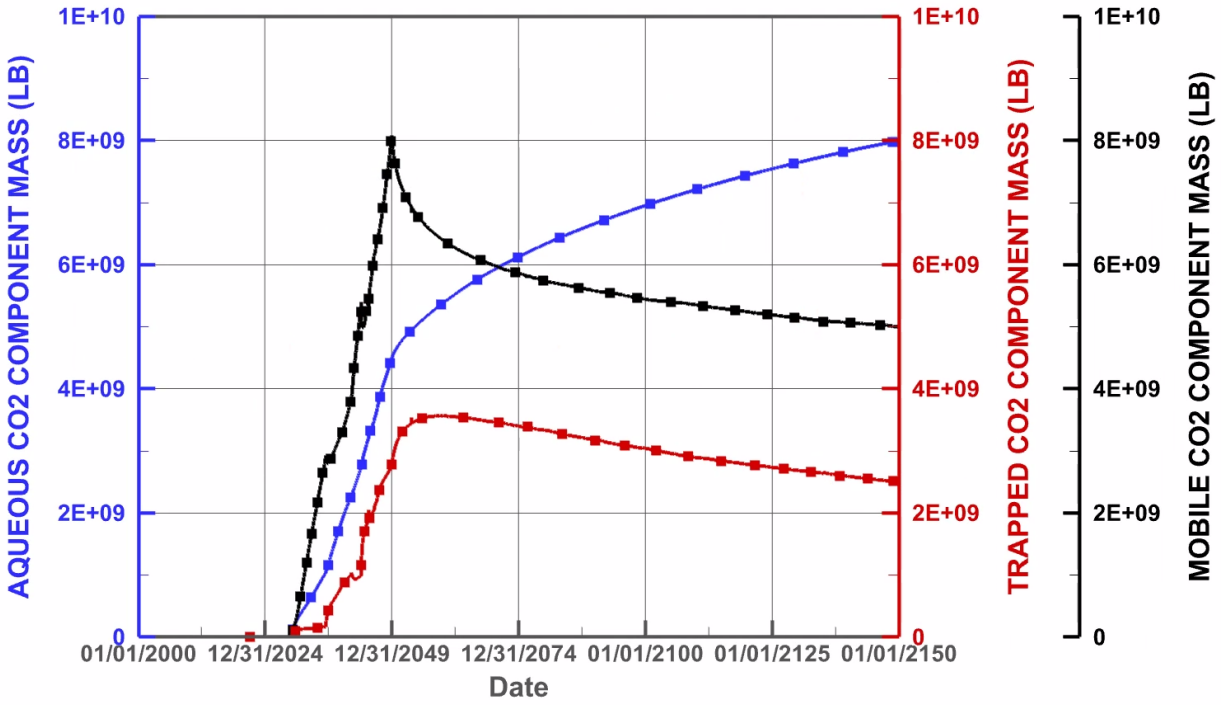

Figure 27. Mass quantities of CO_2 by phase and trapping mechanism over full Project life.

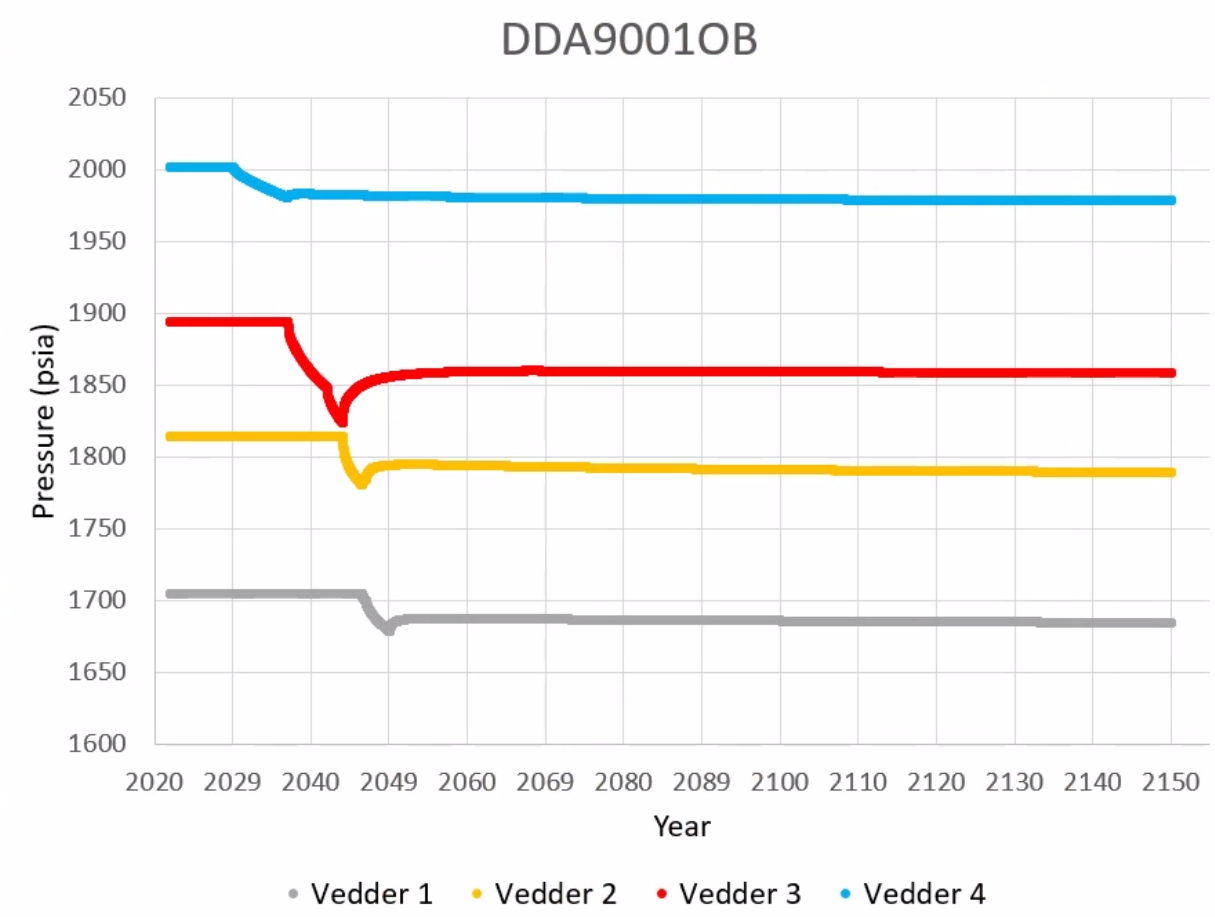

Figure 28. Pressure response by sand at monitoring well DDA9001OB through the life of the Project. Each sand is targeted individually for production as it is simultaneously individually targeted for CO_2 injection.

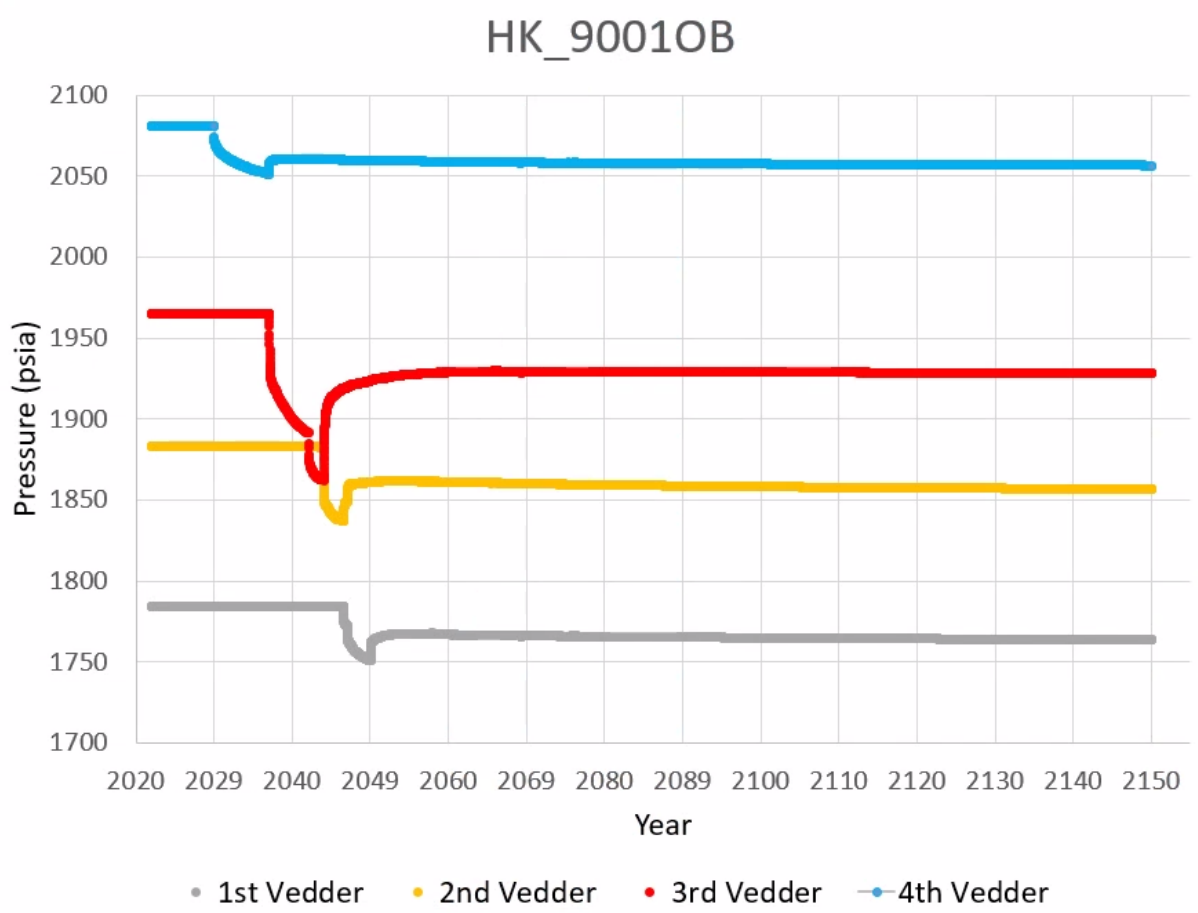

Figure 29. Pressure response by sand at monitoring well HK_9001OB through the life of the Project. Each sand is targeted individually for production as it is simultaneously individually targeted for CO_2 injection.

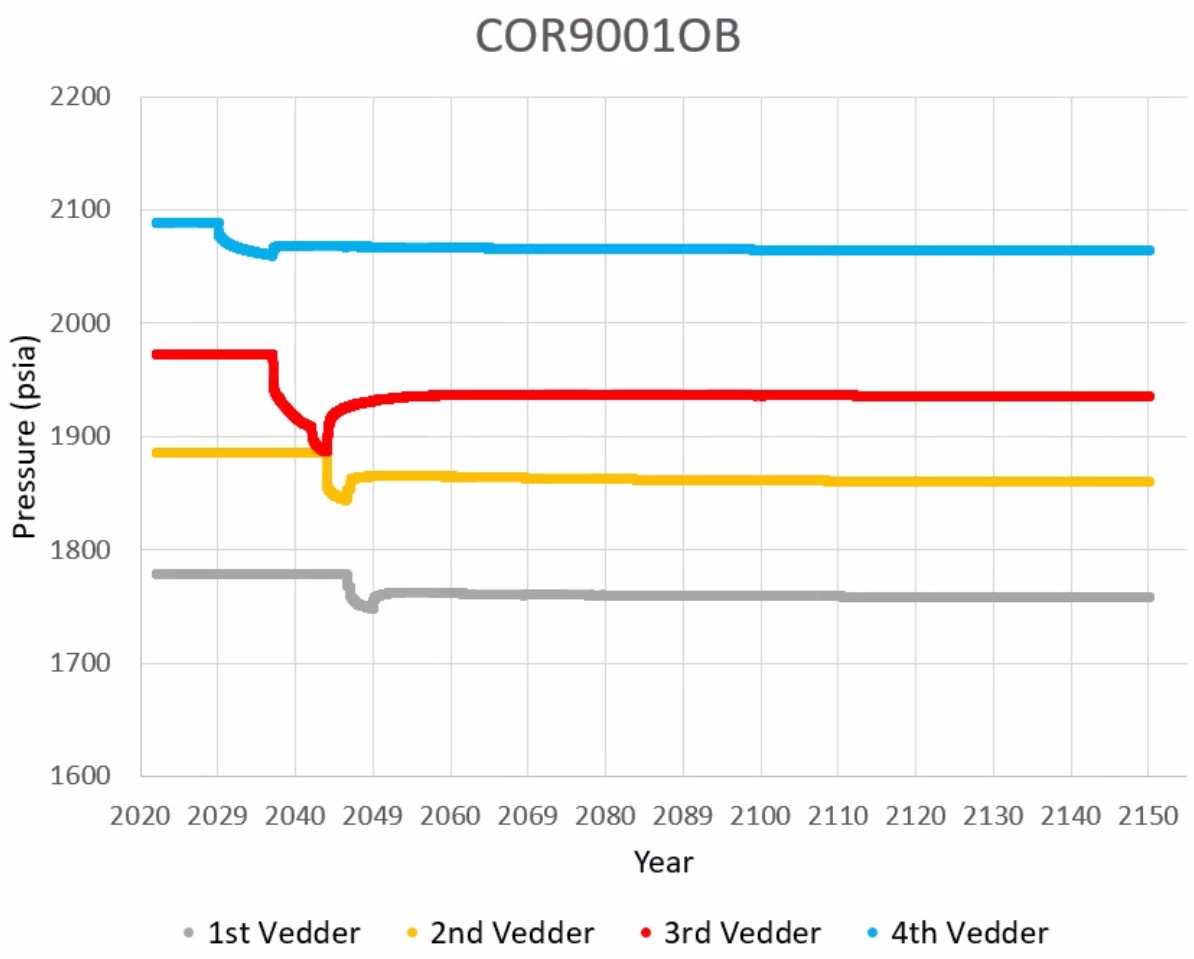

Figure 30. Pressure response by sand at monitoring well COR9001OB through the life of the Project. Each sand is targeted individually for production as it is simultaneously individually targeted for CO_2 injection.

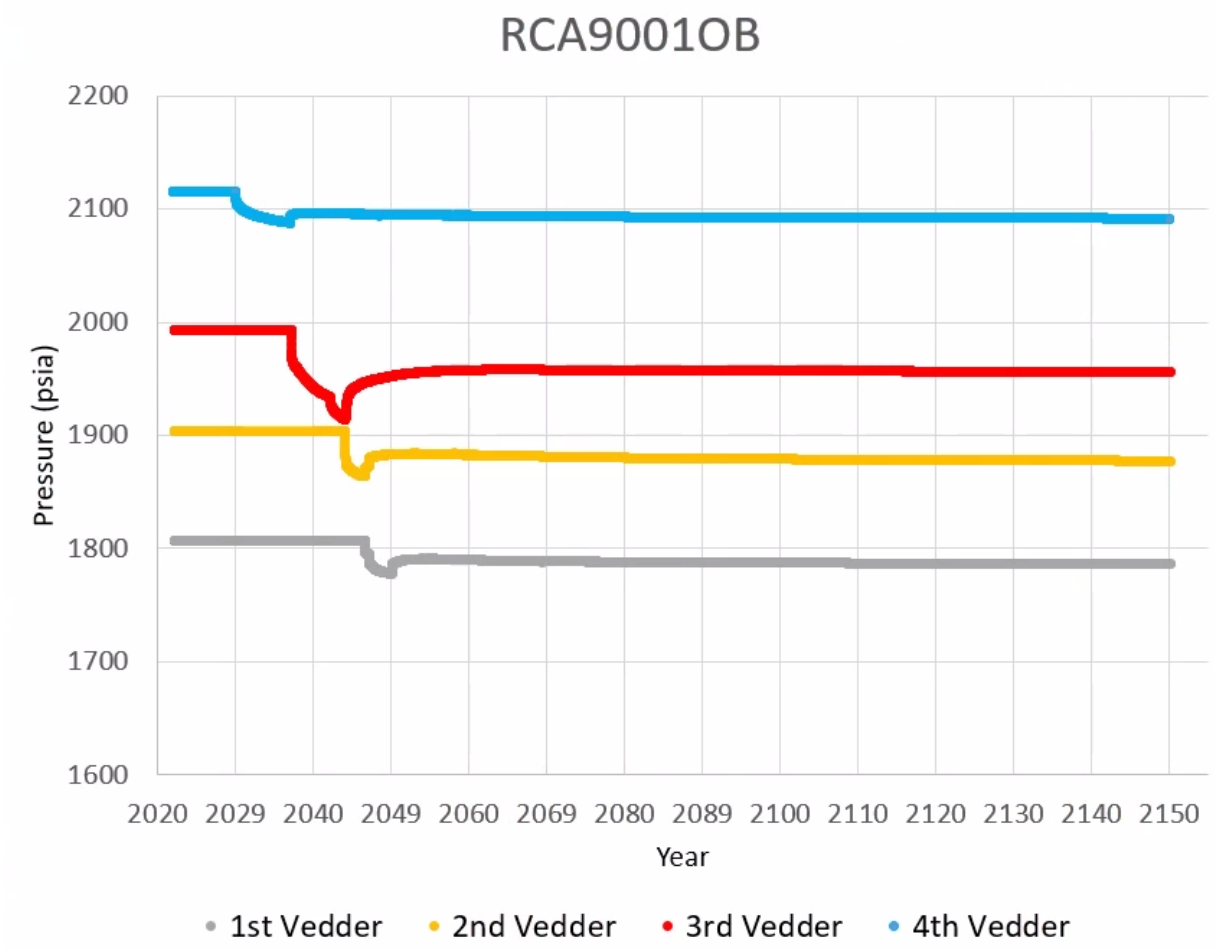

Figure 31. Pressure response by sand at monitoring well RCA9001OB through the life of the Project. Each sand is targeted individually for production as it is simultaneously individually targeted for CO_2 injection.

Model Calibration and Validation – Data Sources

The model is calibrated with a variety of data types from within the AoI ranging from recent direct measurements in the Vedder Sand to historical log measurements and fluid samples in the Vedder Sand.

Pressure Transient Well Test Results

Well KC20050X (API#: 0403048745, **Figure 1**) was used to perform a fall-off test and a step-rate test on the 3rd Vedder. The 3rd Vedder at this location is 195 ft thick and was testing through a 10 ft perforation interval.

The first injection period (injection period #1) lasted for 110 hours (4.6 days) at a target injection rate of 1440 barrels of fresh water per day (BPD). Following the injection period, the well was shut-in to enable real-time monitoring of the fall-off test for 110 hours. After the fall-off, a step rate test was performed. **Figure 32** shows the rate schedule and resultant pressure response during the flow testing. All pressures from this analysis were collected using a downhole pressure gauge placed at the center of the 10 ft perforation interval.

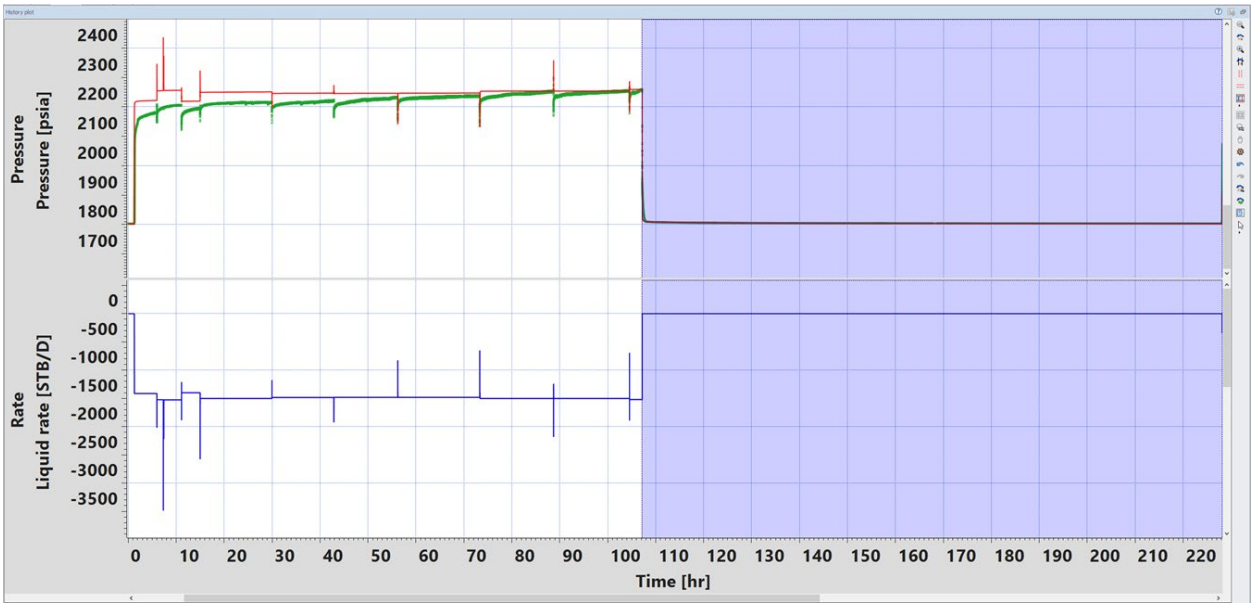

Figure 32. Rate and pressure schedule during the injection period #1 and the fall-off period #1. The green pressure curve is the observed pressure with corresponding injection (blue), while the red is the modeled pressure response. A negative liquid rate represents injection into the well.

The initial injection period followed by the fall-off test #1 was analyzed using Kappa Engineering's Saphir® pressure transient analysis software. Kappa Engineering's Saphir® software module is a tool used to analyze pressure transient fall-off and build-up data from well tests. More can be read about Saphir on the following website (https://www.kappaeng.com/software/saphir/overview).

In transient well test analysis, the pressure derivative is normally used to define the flow regimes such as wellbore storage, radial flow, and pseudo-steady state. The difference in pressure from the shut-in time is calculated and plotted on a log-log plot of pressure difference versus time along with the derivative of pressure difference. Each flow regime exhibits different characteristics in the log-log plot. For example, the radial flow is characterized by a zero slope for the pressure derivative. From the radial flow regime, the formation permeability can be calculated. Late time phenomena are also used to characterize the state of the boundary conditions in the system.

Figure 33 shows the raw data and the simulated analytical match. Interpretation of this analysis is summarized in **Table 11.**

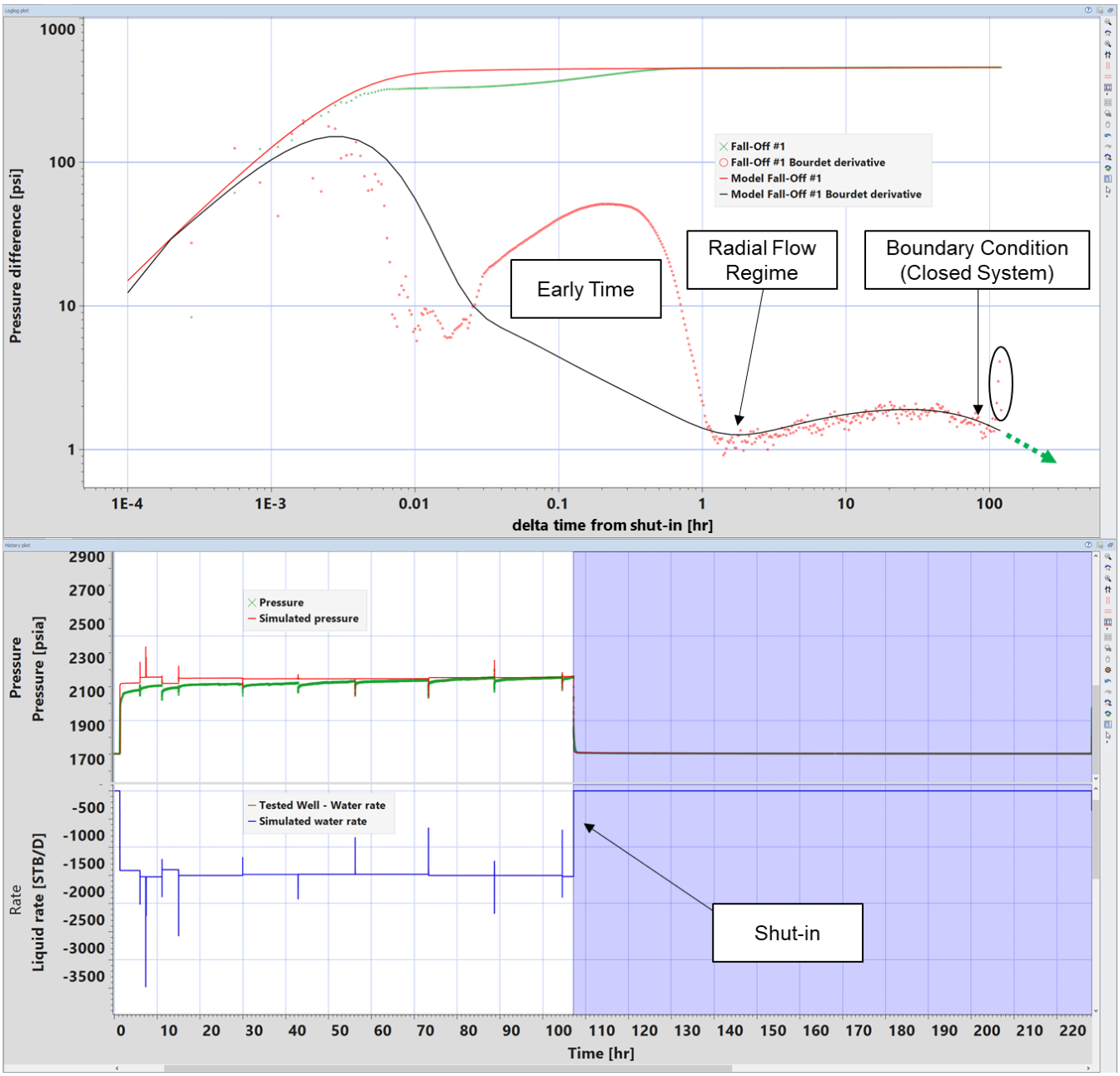

Figure 33. Liquid rate and pressure response of the injection well test (lower image) and the pressure transient analysis (top image). The top image is history match of well test pressure response (solid black line) and data (red dots). Mismatch of early time data does not affect the detection of the radial flow regime and the boundary conditions observed (closed outer boundary, as indicated by the trend at the end with a similar slope to the dashed green arrow). The data in black circle is an artifact of the numerical derivative and is ignored.

Table 11. Interpretation of the analytical model for Fall-Off #1.

Parameter	Value	Boundary	Estimated Distance
Permeability * Thickness	49,335 mD*ft	North (no flow)	7,000 ft
Thickness	195 ft	East (no flow)	700 ft
Average Permeability	253 mD	South (no flow)	4,000 ft
		West (no flow)	5,000 ft

The pressure derivative (**Figure 33**, red circles labelled "Fall-Off #1 Bourdet derivative") of the field data plateaus ~2 hours after shut-in during Fall-Off #1, indicating radial flow, which enables an estimate of permeability-thickness. Afterwards, the pressure derivative increases and plateaus again at ~20 hours. The pressure derivative value at the second plateau is approximately twice that of the first plateau, indicating the presence of a linear no-flow boundary. Towards the end of the 120-hour falloff test, the pressure derivative decreases (the last few points of the pressure derivative, circled in **Figure 33**, on the log-log plot are artificial effects and can be ignored). The derivate drop shows pressure is stabilizing to a constant value, indicating a closed system around the well. The early time deviation of the model and the data (0.03 to 1 hour) is a near wellbore effect that will not principally change the flow regime where radial flow occurs (at 2 hours) or the boundary conditions indicated by the dropping derivative.

The analysis of this Fall-Off test shows two important features. The first is that the Vedder Sand at this depth has a bulk average permeability of 253 mD (approximately 1.5 times lower than estimated in the permeability characterization). The second is that the well is surrounded by 4 sealing faults at distances aligned with the seismically imaged faults near the KC20050X well.

The step rate test established that the Vedder Sand at 4650 ft (through just 10 ft of perforated interval) can inject water up to 10,000 BPD and has a parting pressure of 2872 psi. The change in the slope of the step-rate test at 6615 barrels of water per day indicates the parting pressure of the formation. From the step-rate test analysis, the injectivity of water is calculated from the slope of the line from 0 to 6615 bpd as 8.1 bbl/d/psi. **Figure 20** shows the data for the step-rate test.

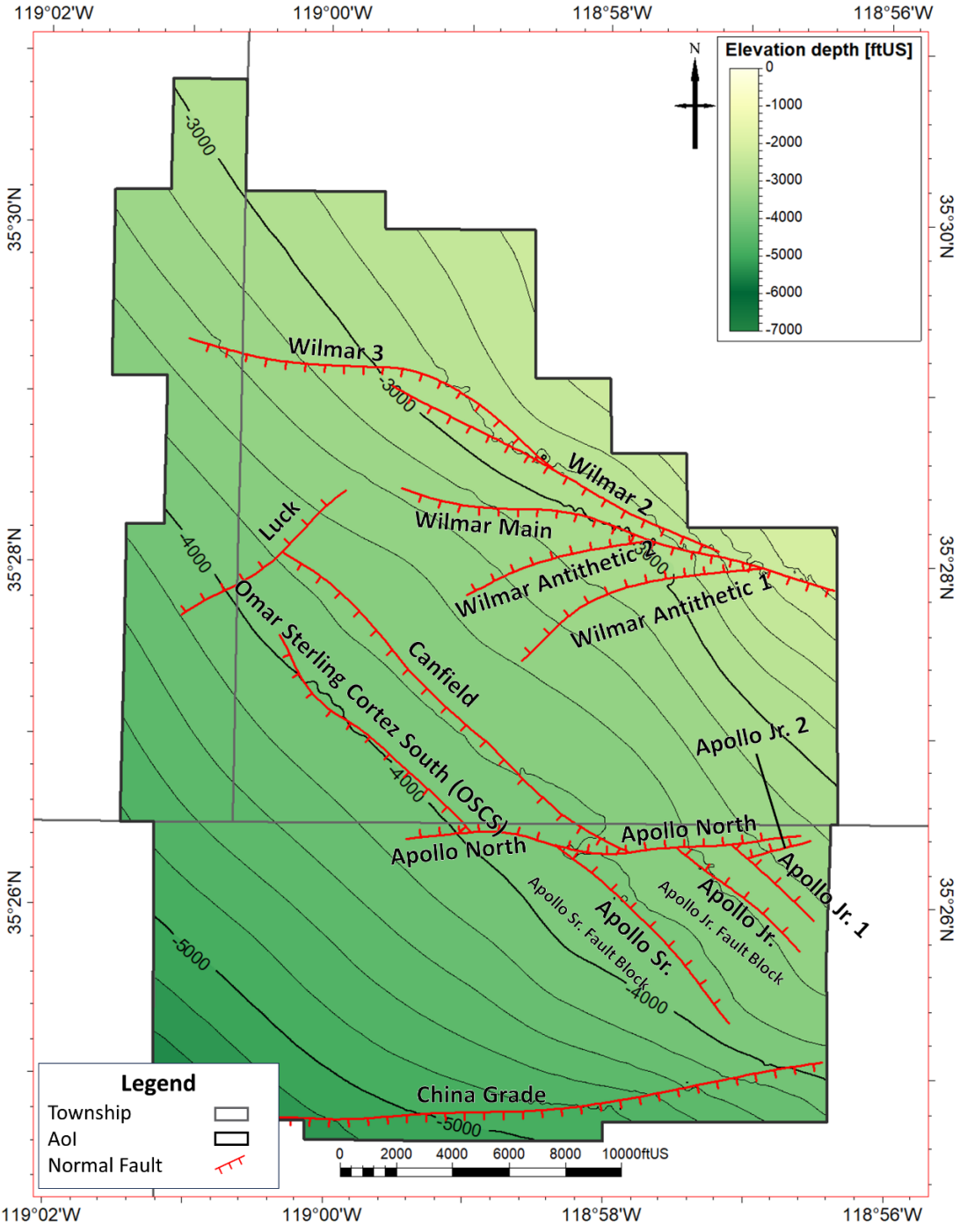

Figure 34. Fault framework with labeled faults and key fault blocks. Structure contours and fault intersections are shown at the top of the 1st Vedder.

Interpretation of the Pressure transient analysis (PTA) shows sealing faults in the Vedder Sand with fault throws as low as 29 ft. (**Table 12** shows the Apollo Jr fault with a mean displacement of 29 ft).

Log Measurements and Fluid Samples

Over the course of the Kern River Oil field development, wells occasionally targeted the Vedder Sand. Oil accumulations were discovered against the Apollo Sr and Apollo Jr faults as shown in **Figure 35** below. These accumulations further demonstrate the sealing potential of faults in the Vedder Sand.

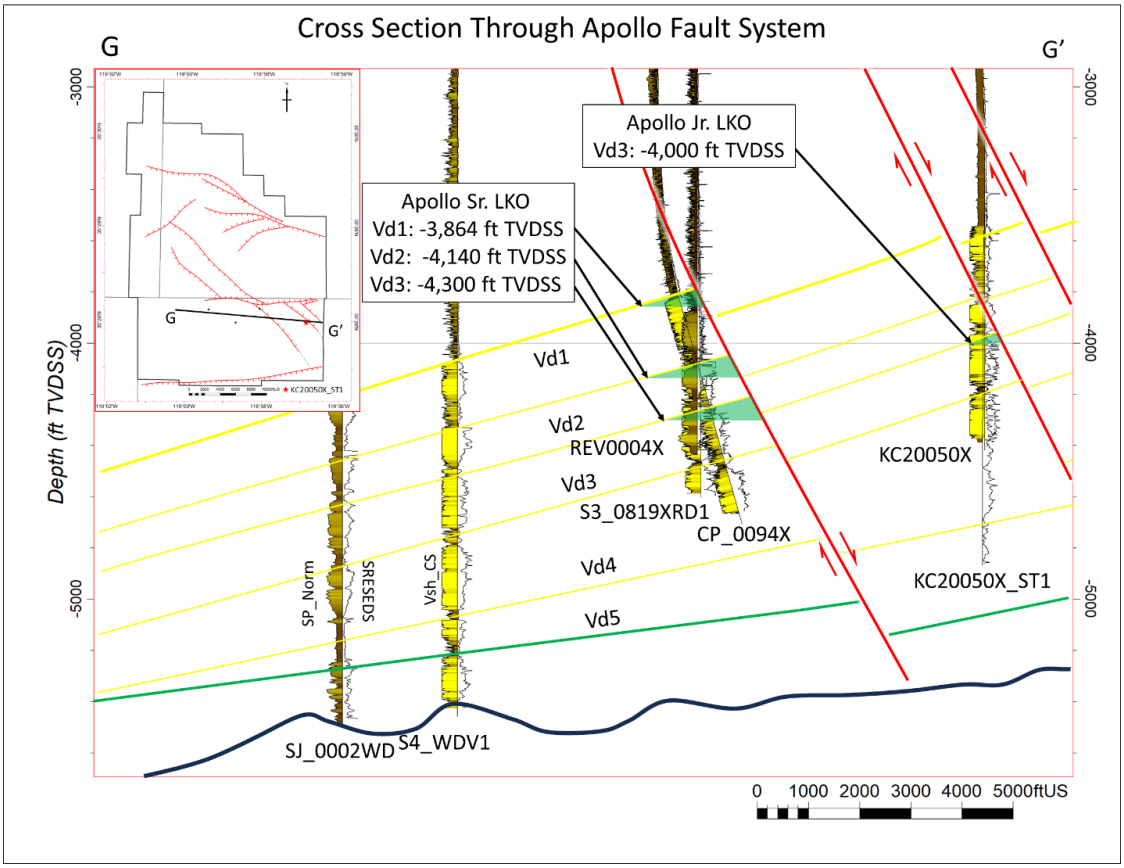

Figure 35. Cross section G-G' showing the hydrocarbon accumulations against the Apollo Sr and Apollo Jr faults. Revenue 4X (REV0004X), Section 3 819X (S3_0819X), & Kern Lease 2 50X (KC20050X) wells labelled.

Geochemical gas chromatographic (GC) analysis of oils from the 2nd and 3rd Vedder Sands shows a lack of lateral fluid communication through the faults in the 3rd Vedder Sand and a lack of vertical fluid communication through the faults or intraformational shales between the 2nd and the 3rd Vedder Sand. **Figure 36** is 4 GC samples where the two top samples are from the 3rd Vedder for the Section 3 819X (S3_0819X) and Revenue 4X (REV0004X) wells (from left to right, respectively) and the two bottom samples are from the 2nd Vedder for the same two (2) wells. These two (2) wells are in the same accumulation of oil, as shown in **Figure 35**. The

difference between the GC signatures between the 2nd and 3rd Vedder Sand are distinct. In the 2nd Vedder samples, a larger relative presence of the NC19 through NC30 components is clearly visible when compared to the 3rd Vedder samples.

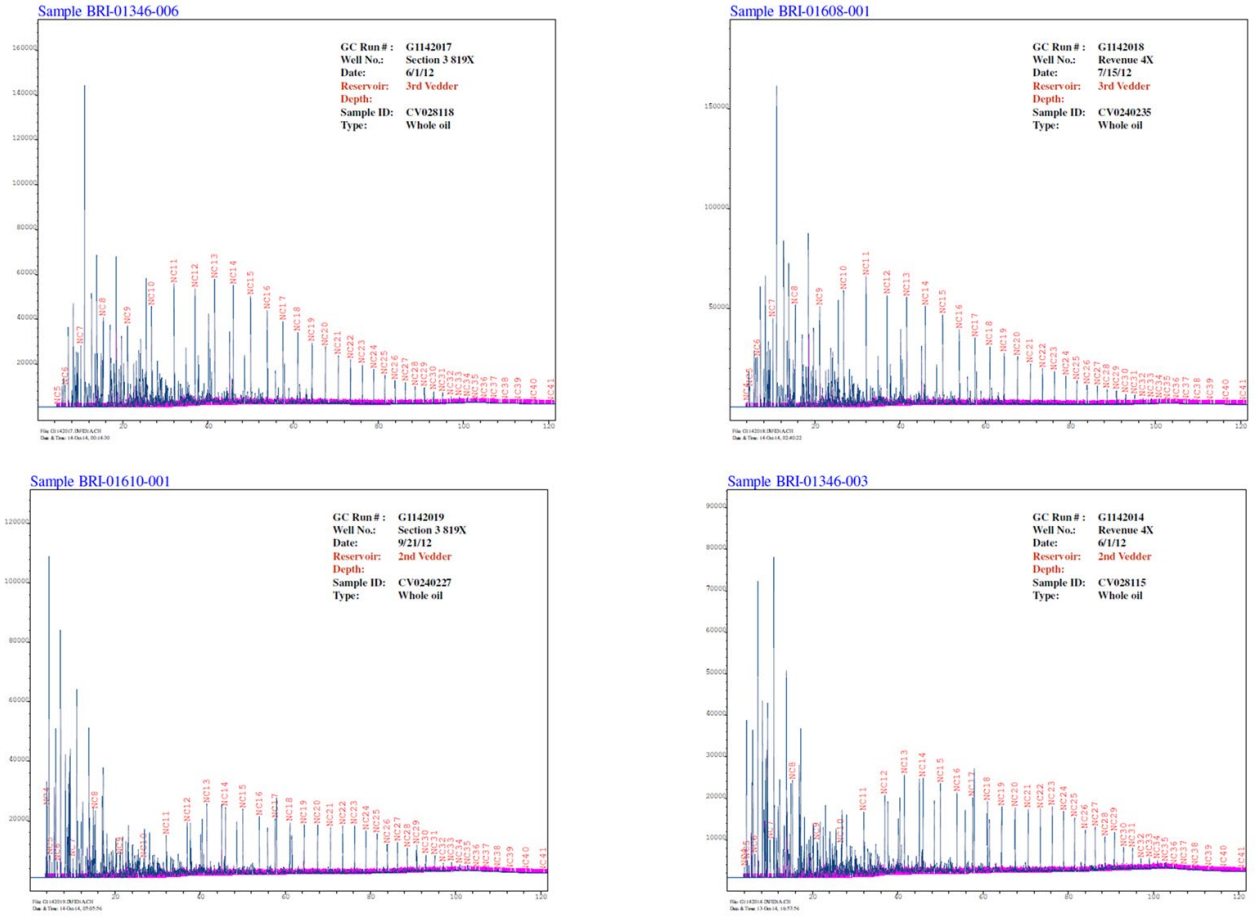

Figure 36. Gas chromatograph (GC) samples from the 3rd Vedder oil samples (top) and 2nd Vedder oil samples (bottom) for wells Section 3 819X (S3_0819X) and Revenue 4X (REV0004X) (left to right, respectively). 2nd Vedder oil samples show more presence of the heavier end components (NC19 to NC30) than the 3rd Vedder samples. This demonstrates a lack of vertical communication between the 2nd and 3rd Vedder Sand.

Below in **Figure 37** are three (3) GC samples from the 3rd Vedder for the Section 3 819X (S3_0819X, top), Revenue 4X (REV0004X, middle), and Kern Co. Lease 2 50X (KC20050X, bottom) wells. Revenue 4X and Section 3 819X are in the same fault block, whereas KC20050X is in a separate fault block, as shown in **Figure 35**. The difference between the GC signatures of the top two (S3_0819X & REV0004X) and the bottom well (KC20050X) is visible in the relative presence of the NC7 through NC11 components when compared to the other components.

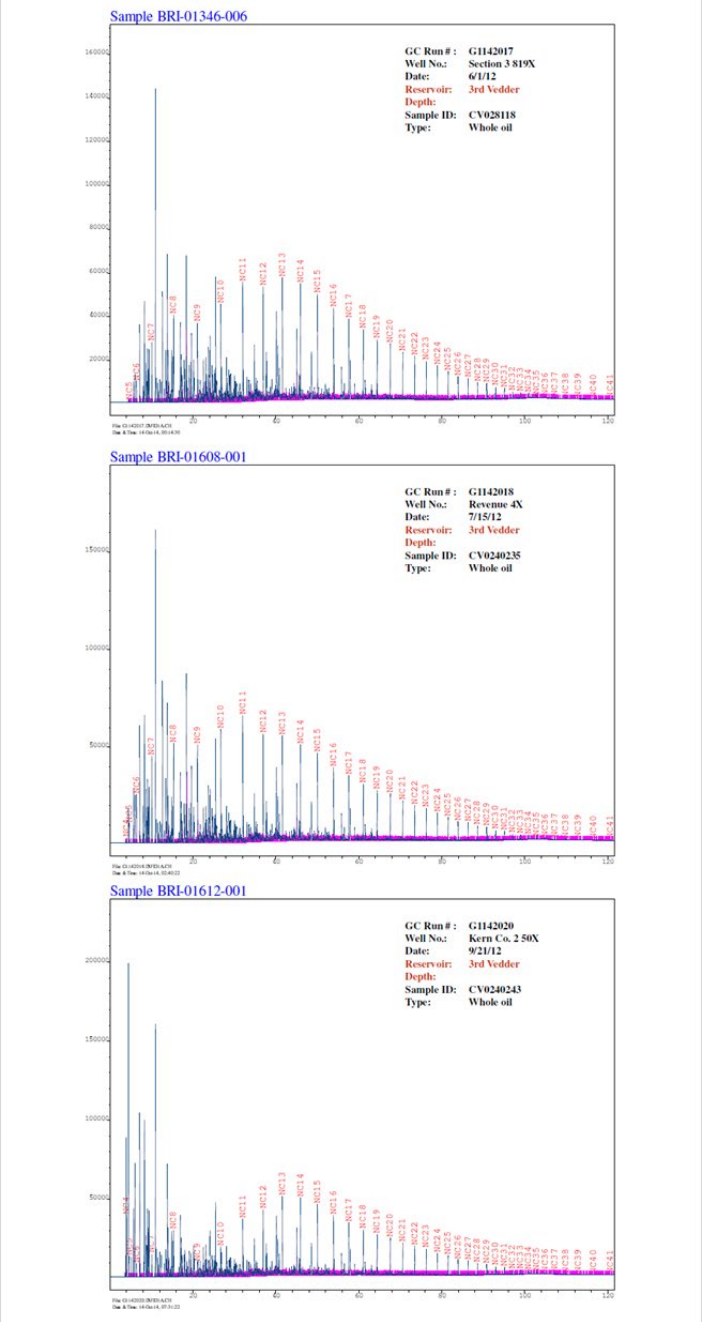

Figure 37. GC oil samples from the 3rd Vedder for the Section 3 819X (S3_0819X), Revenue 4X (REV0004X), and Kern Co. Lease 2 50X (KC20050X) wells. 3rd Vedder oil sample from the Kern Co. Lease 2 50X (KC20050X) well (on the footwall of the Apollo Jr. fault) shows less relative presence of the lighter components (NC7 through NC11) when compared to the other two (2) wells on the footwall of the Apollo Sr fault.

This data demonstrates that the subunits of the Vedder Sand do not communicate vertically or laterally through the faults or vertically through intraformational shale layers.

Summary of Data Sources

In summary, several sources of data are used to form our assessment of the faults within the Vedder Sand. Direct flow measurements from pressure transient analysis show sealing faults in the Vedder Sand. Historical well logs, proven trapped hydrocarbon volumes, and gas chromatic analysis of those hydrocarbons demonstrate faults acting as seals both vertically and horizontally.

Model Calibration and Validation – Analysis

Evidence shows faults seal and prevent the migration of hydrocarbons in the Vedder Sand. However, the nature of subsurface characterization lends itself to uncertain outcomes. For this reason, a fault seal analysis study was performed to quantify the sealing nature of the faults within the Vedder Sand and validate those results with direct measurements recently taken.

Fault Seal Analysis

Fault seal analysis (FSA) is used to quantify the flow characteristics of faults with sand-on-sand juxtaposition. Approaches focusing on characterizing the thickness and the permeability of the fault zone are used to inform the impact on fluid flow (Manzocchi et. al., 1999) through modifications to the permeability changes in fault zones. These approaches can be implemented easily in flow simulations by calculating the impact of the fault thickness and permeability on the transmissibility of gridblocks where the fault intersects the grid. Additionally, the clay content of the strata and the impact of smearing and cataclasis within the fault zone can impact the capillary properties of a fault zone modifying the threshold entry pressure as a function of the shale gouge ratio or SGR (Bretan et. al. 2003). Both approaches are used to model the transmissibility multipliers and the average threshold entry pressure of the faults within the Vedder Sand.

Fault seal analysis (FSA) is done on the seismically identifiable faults within the Vedder Sand in the AoI. The inputs and outputs are shown in **Table 12.**

Table 12 Fault name, mean displacement, mean shale-gouge-ratio, mean thickness, mean permeability, and mean threshold pressure.

Fault Name	Fault Displacement Mean (ft)	Shale-Gouge-Ratio (SGR) Mean	Fault Thickness Mean (ft)	Fault Perm Mean (mD)	Threshold Press Mean (psi)
Omar Sterling Cortez South	30	0.250	0.300	0.260	8.4
Canfield	38	0.280	0.380	0.160	15.7
Ap North	66	0.260	0.660	0.200	11.7
Luck	68	0.310	0.680	0.130	23.8
Ap Sr	91	0.340	0.910	0.140	20.8
Wilmar 2	256	0.370	2.560	0.050	51.4
Wilmar Main	212	0.390	2.120	0.070	27.4
Wilmar 3	167	0.320	1.670	0.070	31.3
Wilmar_Antithetic_2	100	0.270	1.000	0.230	11.6
Wilmar_Antithetic_1	41	0.220	0.410	0.310	8.4
Apollo Jr & Jr 1	29	0.210	0.290	0.300	7.7

The FSA outputs are fault thickness and fault permeability which are used in combination with the geocellular model to calculate the fault transmissibility multipliers along each fault surface. The algorithm used is consistent with Manzocchi et al. 1999 and is shown in **Figure 38**.

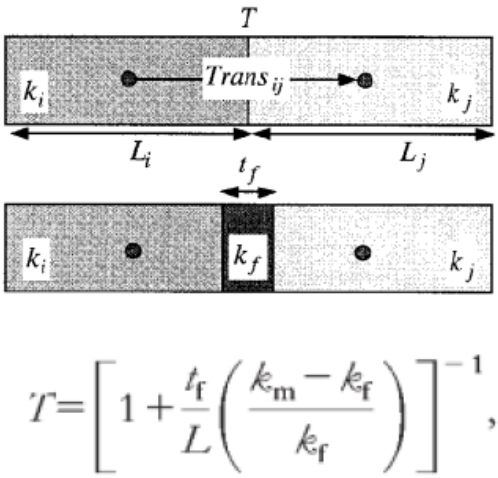

Figure 38. From Manzocchi et al. 1999. Picture and formula of how a fault transmissibility multiplier, T, is calculated by using the fault thickness (t_f) and fault permeability (k_f) assuming that permeability and length of the cells on either side of the fault are approximately equivalent. The finite fault grid block is not included in the reservoir simulation model, but it's impact to flow is accounted for in the multiplier, T.

Threshold pressures are used directly in the reservoir simulation model and are assigned independently to each of the faults as a single value. Computational simulator INTERSECT uses the assigned threshold pressures as a switch for each gridblock connection across the fault. When a differential pressure for two gridblocks across the fault exceeds the threshold pressure, that gridblock pair begins to flow. Once the criteria are satisfied, the connection remains flowing.

Model Calibration and Validation – Synthesis

Multiple data types validate faults within the Vedder Sand and shallower sands seal. The data indicative of 4 sealing faults around well KC20050X (API#: 0403048745, **Figure 1**) is an important piece of information that we consider further in the synthesis.

Pressure transient analysis (PTA) is a dynamic test used to assess formation permeability-thickness (through identification of the radial flow regime) and patterns in the late time transient pressure derivative that indicate boundary conditions. The interpretation of the injection well test performed at KC20050X indicates a closed system bounded by sealing faults. Resolving this information with the fault seal analysis is an important step towards validating the nature of the faults within the Vedder Sand.

The simulation model is used to validate the PTA. Starting with the system containing no fault seal analysis (100% open), the same rate schedule used in the injection well test is implemented inside of the simulator along with the shut-in time. Pressures throughout the injection and shut-in time are output from the simulator and analyzed to test the response pattern in the transient pressure derivative (**Figure 39 (a)**). The same analysis is done and compared to the un-validated or raw fault seal analysis (**Figure 39 (b)**). The comparison between these two shows that the un-validated FSA (**Figure 39 (b)**) looks like the case where faults are 100% open (**Figure 39 (a)**). A scalar multiplier on the faults in the simulation model is used to progressively test less transmissibility across the faults. Multiplying the raw fault seal analysis transmissibility multiplier by 0.025 provided the best match to the raw data shown in **Figure 33** while still allowing the faults to leak. The comparison of these three scenarios with the raw data is shown in **Figure 39**.

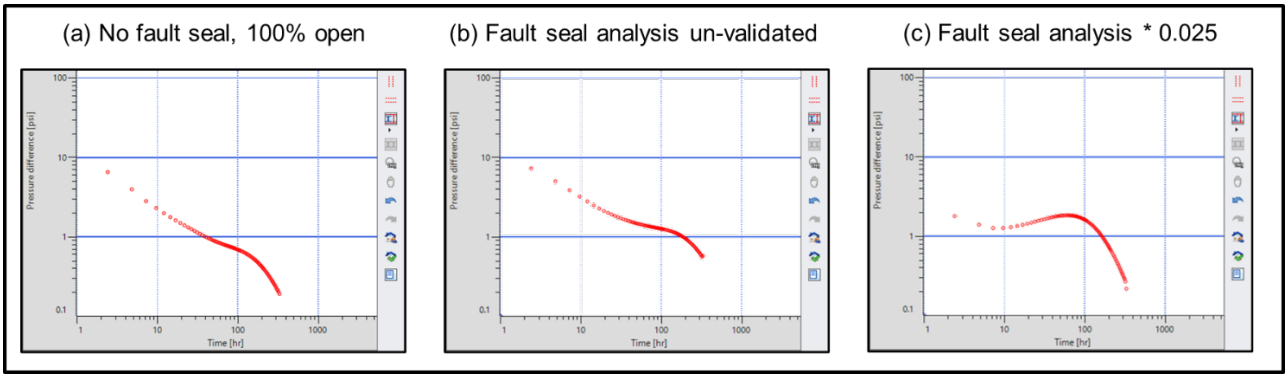

Figure 39. Computationally simulated transient pressure derivative of scenarios starting from left to right **(a)** Faults are open and have no sealing capacity **(b)** Faults seal analysis is raw and un-validated by PTA and **(c)** Fault seal analysis validated with pressure transient analysis using an additional transmissibility multiplier of 0.025.

In all cases, the model permeability was multiplied by a factor of 0.66 to match the observed permeability calculated using the radial flow regime identified in the PTA. Transformed well logs from the 3rd Vedder of well KC20050X show the highest average permeability among all wells used in site characterization, and the well log permeability is well represented in the static earth model. Based on the findings from this dynamic testing, Chevron globally reduces the dynamic model permeability by a multiplication factor of 0.66.

Additionally, using the analytical pressure transient analysis, a sensitivity was performed to understand how much a fault system could leak and still provide the pressure transient derivative in **Figure 33**. Using progressively smaller transmissibility multipliers we find the largest multiplier that allows a match of the data reasonably well is 0.01. When larger multipliers are used in the model, they do not match the data for late time. **Figure 40** is a zoomed in view of the PTA during the late time regime and shows the result of the sensitivity and the mismatch of larger multiplier values of 0.1 an 0.05.

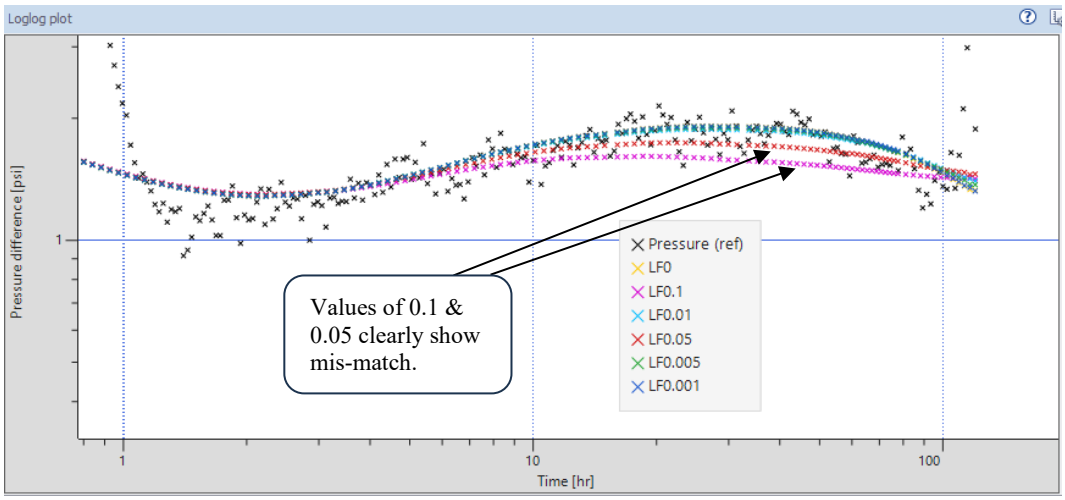

Figure 40. Sensitivity study of the analytical pressure transient analysis for well KC20050X. Convergence of totally sealing (LF0) and progressively less sealing cases using a transmissibility multiplier of 0.001, 0.005, 0.01 (LF0.001, LF0.005, LF0.01, respectively). Departure from observed data occurs with transmissibility multipliers of 0.05 and 0.1 (LF0.05 and LF0.1, respectively).

In summary, evidence suggests faults within the Vedder Sand seal. Direct measurements by pressure transient analysis corroborate the sealing nature. The faults are analyzed using fault seal analysis (Manzocchi et. al 1999), output as fault transmissibility multipliers, and tested in the simulator. An additional scalar multiplier is used to condition the model to field data, which results in the most transmissible (leakiest) fault that satisfies a good match to the transient analysis data, a direct measurement on the faults in the Vedder Sand.

Fault seal analysis provides a consistent transmissibility modification relative from one fault to another based upon each fault's characteristics (e.g. throw, SGR, etc). PTA validates the faults surrounding well KC20050X where the flow test was performed. That validation adds only the minimum seal required to corroborate the PTA data and is applied across all faults to maintain a consistent fault-to-fault transmissibility character.

Chevron has designed the Testing and Monitoring Plan to collect the necessary data to verify injected CO_2 migrates as expected through the life of the project and if needed, modify computational models and the AoR.

AoR Delineation

Critical Pressure Calculations

The AoR was delineated based upon the methods of Nicot et al. (2008) mentioned in the EPA Class VI Well Area of Review Evaluation and Corrective Action Guidance Document and shown below in **Equation 2**. Based on Santa Margarita Sandstone and Vedder Sand pressure data from within the AoI Chevron assumes the Vedder Sand and the Santa Margarita Sandstone to be under hydrostatic conditions. Chevron plans to acquire additional Santa Margarita Sandstone and Vedder Sand pressure data during well construction to verify this assumption, as described in detail in the Pre-Operational Logging and Testing Plan.

Equation 2. Equation used to calculate critical pressure.

$$\Delta P = g\,(z_v - z_I)\left(\frac{\lambda-\xi}{2}\,(z_v - z_I) + \rho_{I,\lambda} - \rho_I\right)$$

Where,

g	acceleration due to gravity
z_v	depth, base of USDW
z_I	depth, top of injection zone
λ	density gradient at constant salinity
ζ	initial density gradient in borehole
$\rho_{I,\lambda}$	fluid density at the base of USDW after flow
ρ_I	fluid density at base of USDW, initial conditions

The Vedder Sand is an exempt aquifer within the AoI. Salinity data from fluid samples and log resistivity curves from within the AoR and AoI shows the Vedder Sand total dissolved solids (TDS) increasing with dip to the southwest corner of the AoI. Within the up-dip portion of the AoR, fluid sample TDS data from the Vedder Sand shows roughly 5,000-7,000 mg/L. Due to the increase in salinity with dip, the TDS at the injector locations is expected to be 10,000 mg/L.

The Santa Margarita is the lowermost USDW throughout the administrative field boundary, though the exact salinity in the Santa Margarita is uncertain. For critical pressure calculations, the Santa Margarita is assumed to have a TDS of 1,000 mg/L. Historical records show Santa Margarita salinity ranging between 490- 1,584 mg/L TDS within the AoI. Chevron plans to collect Santa Margarita salinity information during the Pre-Operational Phase, which is described in detail in the Pre-Operational Testing and Logging Plan.

Top of CO_2 injection zone and base of USDW depths are based on well correlations within the AoI. Fluid density and fluid density gradients are calculated as a function of temperature and salinity using the correlations provided by McCutcheon et al. (1993). Using **Equation 2**, the critical pressures are calculated as shown below in **Table 13** and **Table 14** at the injectors and compared against simulated pressure changes (relative to initial pressure) throughout the entire grid at timesteps through the life of injection and post-injection monitoring listed in **Table 15**. AoR maps are generated for each of the listed timesteps throughout the life of the project based on the elevated pressures above the critical pressure and supercritical CO_2 saturation above a minimum cutoff of 5% based on detection limits of monitoring equipment. The AoR maps for each timestep are compiled into a single figure to generate the comprehensive project AoR, as shown in **Figure 22.**

Table 13. Calculated Critical Pressures for injectors ANO9004INJ and MC19001INJ. All calculations are carried out using the top of the 1st Vedder as the top of the injection zone.

ANO9004INJ	
Base of USDW	
Depth (ft TVD)	2354
Temperature (F)	113
TDS (ppm)	1000
Top of 1st Vedder	
Depth (ft TVD)	4947
Temperature (F)	160
TDS (ppm)	10000
Base of USDW	
Initial Density @ USDW (lb/ft3)	61.86
Top of 1st Vedder	
TDS (ppm)	10000
Initial Density @ Top of Vedder (lbm/ft3)	61.46
Final Density @ Top of USDW (lbm/ft3)	62.28
Gravitational Constant (ft/s2)	32.174
Density Gradient Initial, ξ (lbm/ft3/ft)	-0.00015
Density Gradient Final, λ (lbm/ft3/ft)	-0.00031
Final Density Differential @ USDW (lbm/ft3)	0.41138
Depth Differential (ft)	2593
Critical Pressure (Psi)	**3.70**

MC19001INJ	
Base of USDW	
Depth (ft TVD)	2274
Temperature (F)	113
TDS (ppm)	1000
Top of 1st Vedder	
Depth (ft TVD)	4838
Temperature (F)	160
TDS (ppm)	10000
Base of USDW	
Initial Density @ USDW (lb/ft3)	61.86
Top of 1st Vedder	
TDS (ppm)	10000
Initial Density @ Top of Vedder (lbm/ft3)	61.46
Final Density @ Top of USDW (lbm/ft3)	62.28
Gravitational Constant (ft/s2)	32.174
Density Gradient Initial, ξ (lbm/ft3/ft)	-0.00016
Density Gradient Final, λ (lbm/ft3/ft)	-0.00032
Final Density Differential @ USDW (lbm/ft3)	0.41138
Depth Differential (ft)	2564
Critical Pressure (Psi) calculated	**3.66**

Table 14. Calculated Critical Pressures for contingent injectors ANO9005INJ and MC19002INJ. All calculations are carried out using the top of the 1st Vedder as the top of the injection zone.

Backup Injector ANO9005INJ	
Base of USDW	
Depth (ft TVD)	2355
Temperature (F)	113
TDS (ppm)	1000
Top of 1st Vedder	
Depth (ft TVD)	4947
Temperature (F)	160
TDS (ppm)	10000
Base of USDW	
Initial Density @ USDW (lb/ft3)	61.86
Top of 1st Vedder	
TDS (ppm)	10000
Initial Density @ Top of Vedder (lbm/ft3)	61.46
Final Density @ Top of USDW (lbm/ft3)	62.28
Gravitational Constant (ft/s2)	32.174
Density Gradient Initial, ξ (lbm/ft3/ft)	-0.00015
Density Gradient Final, λ (lbm/ft3/ft)	-0.00031
Final Density Differential @ USDW (lbm/ft3)	0.41138
Depth Differential (ft)	2592
Critical Pressure (Psi) calculated	**3.70**

Backup Injector MC19002INJ	
Base of USDW	
Depth (ft TVD)	2274
Temperature (F)	113
TDS (ppm)	1000
Top of 1st Vedder	
Depth (ft TVD)	4836
Temperature (F)	160
TDS (ppm)	10000
Base of USDW	
Initial Density @ USDW (lb/ft3)	61.86
Top of 1st Vedder	
TDS (ppm)	10000
Initial Density @ Top of Vedder (lbm/ft3)	61.46
Final Density @ Top of USDW (lbm/ft3)	62.28
Gravitational Constant (ft/s2)	32.174
Density Gradient Initial, ξ (lbm/ft3/ft)	-0.00016
Density Gradient Final, λ (lbm/ft3/ft)	-0.00032
Final Density Differential @ USDW (lbm/ft3)	0.41138
Depth Differential (ft)	2562
Critical Pressure (Psi) calculated	**3.66**

Table 15. Model timesteps analyzed to generate computational AoR

Timestep Date	Project Status at Corresponding Timestep
2029 January 1	Initial conditions, no injection
2030 January 1	First injection into Vedder 4 with both MC19001INJ and ANO9004INJ; begin Vedder 4 pressure management
2031 January 1	Injection into Vedder 4; active Vedder 4 pressure management
2032 January 1	
2033 January 1	
2034 January 1	
2035 January 1	
2036 January 1	
2037 January 1	Recomplete both MC19001INJ and ANO9004INJ to inject into Vedder 3; cease Vedder 4 pressure management and begin Vedder 3 pressure management
2038 January 1	Injection into Vedder 3; active Vedder 3 pressure management
2039 January 1	
2040 January 1	
2041 January 1	
2042 January 1	
2043 January 1	
2044 January 1	Recomplete both MC19001INJ and ANO9004INJ to inject into Vedder 2; cease Vedder 3 pressure management and begin Vedder 2 pressure management
2045 January 1	Injection into Vedder 2; active Vedder 2 pressure management
2046 January 1	
2046 July 7	Recomplete MC19001INJ to inject into Vedder 1; active pressure management in both Vedder 2 and Vedder 1
2047 January 1	Recomplete ANO9004INJ to inject into Vedder 1; cease Vedder 2 pressure management; active Vedder 1 pressure management
2048 January 1	Injection into Vedder 1; active Vedder 1 pressure management
2049 January 1	
2050 January 1	End of Injection and pressure management
2051 January 1	Post Injection Monitoring
2055 January 1	

2060 January 1	
2065 January 1	
2070 January 1	
2075 January 1	
2080 January 1	
2085 January 1	
2090 January 1	
2095 January 1	
2100 January 1	
2105 January 1	
2110 January 1	
2115 January 1	
2120 January 1	
2125 January 1	
2130 January 1	
2135 January 1	
2140 January 1	
2145 January 1	
2150 January 1	

AoR Delineation

The AoR is delineated as the union of the regions with elevated pressures above the critical pressure and regions with supercritical CO_2 saturations above a minimum cutoff of 5% based on detection limits of monitoring equipment.

As previously mentioned, Chevron plans to drill two water producers targeting the Vedder Sand through the injection life to slightly decrease the reservoir pressure of each targeted Vedder Sand to the point that no region of the reservoir experiences elevated pressure above the critical pressure, resulting in an AoR which is purely a function of the CO_2 saturation map. Chevron plans to operate these producing wells, FEA9001P and FEA9002P, with electric submersible pumps. The planned locations for these two wells are shown in **Figure 22**. **Figure 21** shows the schedule of produced fluids used in simulation. The producers are planned to follow a vertical recompletion strategy similar to the injectors, so that the producers target individual zones to effectively dewater and depressurize zones being targeted with CO_2 at that time. The increase in production rate is to keep up with the increase in injection rate.

Though Chevron accounts for both the pressure and saturation components in delineation of the AoR, the pressure management system effectively decreases the pressure in each Vedder Sand to the point that the AoR is dictated completely by the saturation component.

Figure 22 highlights the AoR relative to injector and producer locations, identified faults, and monitoring wells with their radii of detection.
Figure 41 is a snapshot of the Vedder Sand in the year 2150 showing the extent of the plume migration 120 years after first injection. This image forms the basis of the AoR delineation as the composite union of the critical pressure front and CO_2 plume for each of the sands using a critical pressure of 3.6 psi and CO_2 saturation equal to or greater than 5% as the criteria (based on monitoring well detection limits). **Figure 42** is a snapshot of the gas saturation extent in each individual Vedder Sand in the year 2150 alongside the AoR. **Figure 43** provides a snapshot in time for each of the Vedder Sand injection targets at the end of injection for each target zone.

Figure 44 illustrates the locations for **Figure 45** and **Figure 46,** cross sections K-K’ and L-L’ respectively. These cross sections through the model show CO_2 saturation at various time steps through the life of the Project.

Figure 47 shows dip cross section K-K’ through ANO0004INJ illustrating pressure changes across the Vedder Sand at various times through the life of injection. **Figure 48** shows dip cross section L-L’ through MC19001INJ with pressure changes across the Vedder Sand at various times through the life of injection. **Figure 49** shows a strike cross section M-M’ through the project injectors and producers demonstrating pressure changes across the Vedder Sand at various times through the life of injection. Locations for the cross sections in **Figure 47**, **Figure 48**, and **Figure 49** are shown on **Figure 44.**

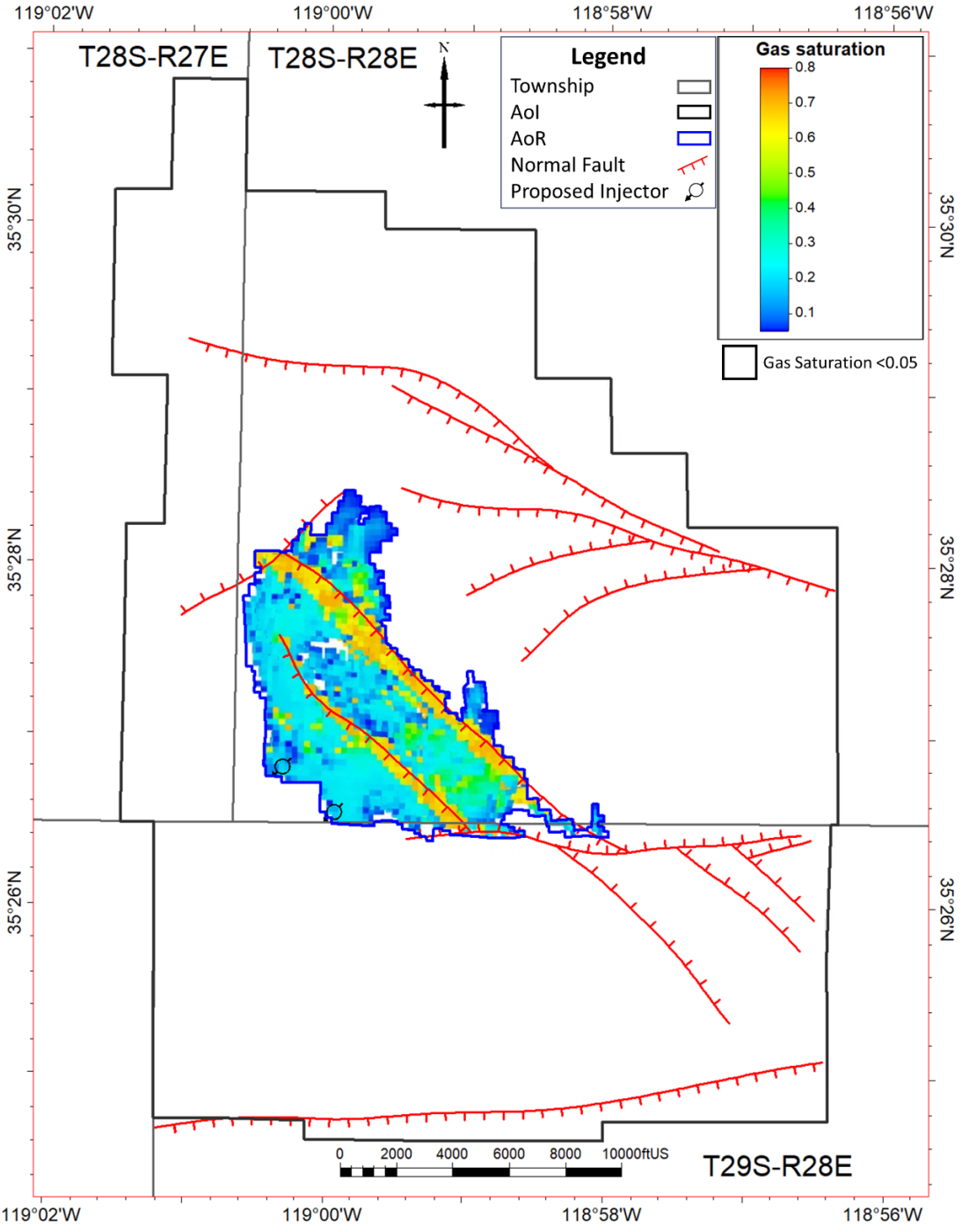

Figure 41. CO_2 saturation for all Vedder Sand target zones in the year 2150, 100 years after the 20-year injection period. Colored cells show the shallowest cell that has a CO_2 saturation greater than 5% (based on monitoring detection limits).

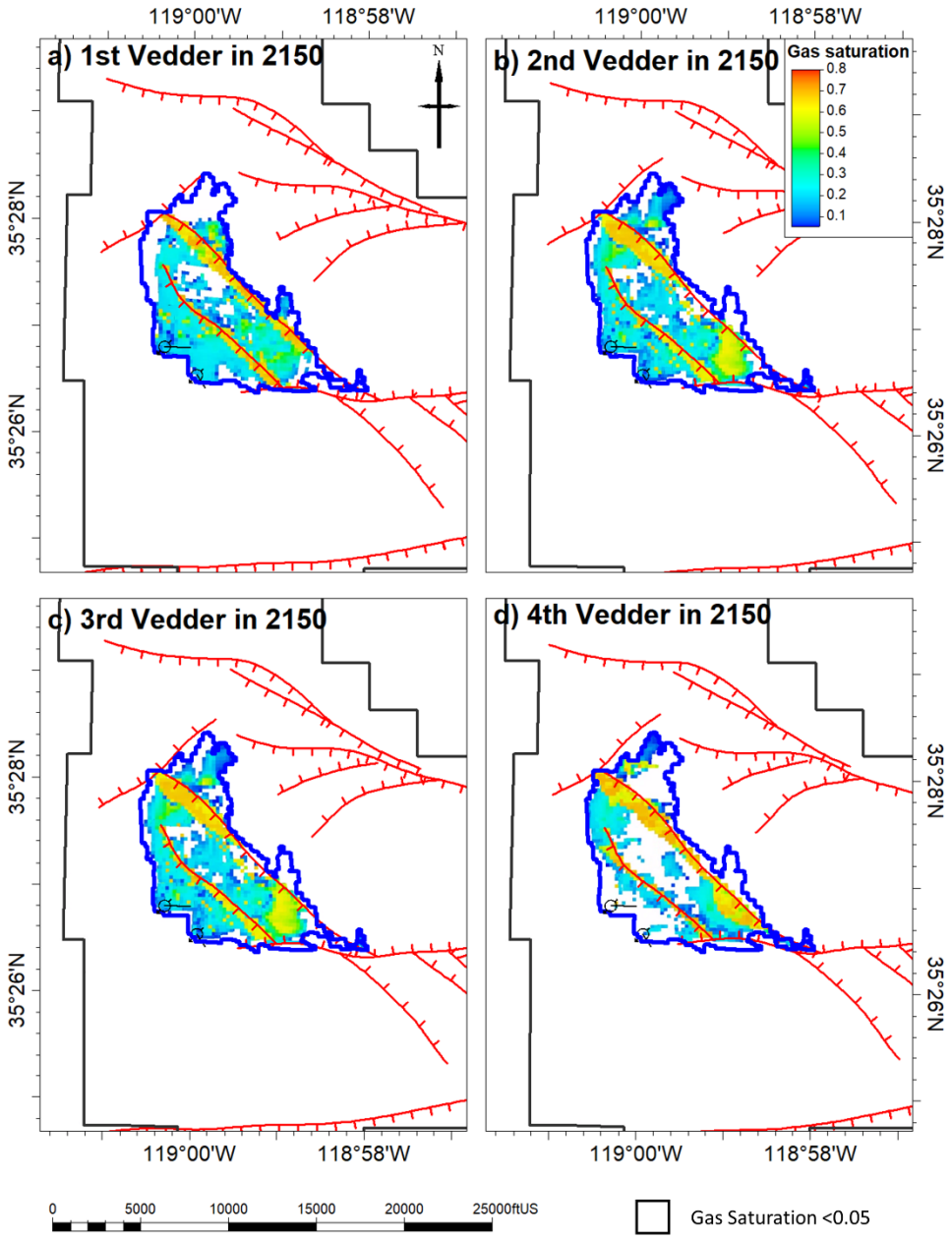

Figure 42. Map view the Vedder Sand injection zones on January 1, 2150, along with the AoR outline in blue. The map illustrates the gas saturation in the topmost saturated cell of each zone, as noted in the top left corner of each pane. The minimum gas saturation displayed is 5% based on detection limits of monitoring technology. 1st Vedder is the shallowest and the 4th Vedder is the deepest.

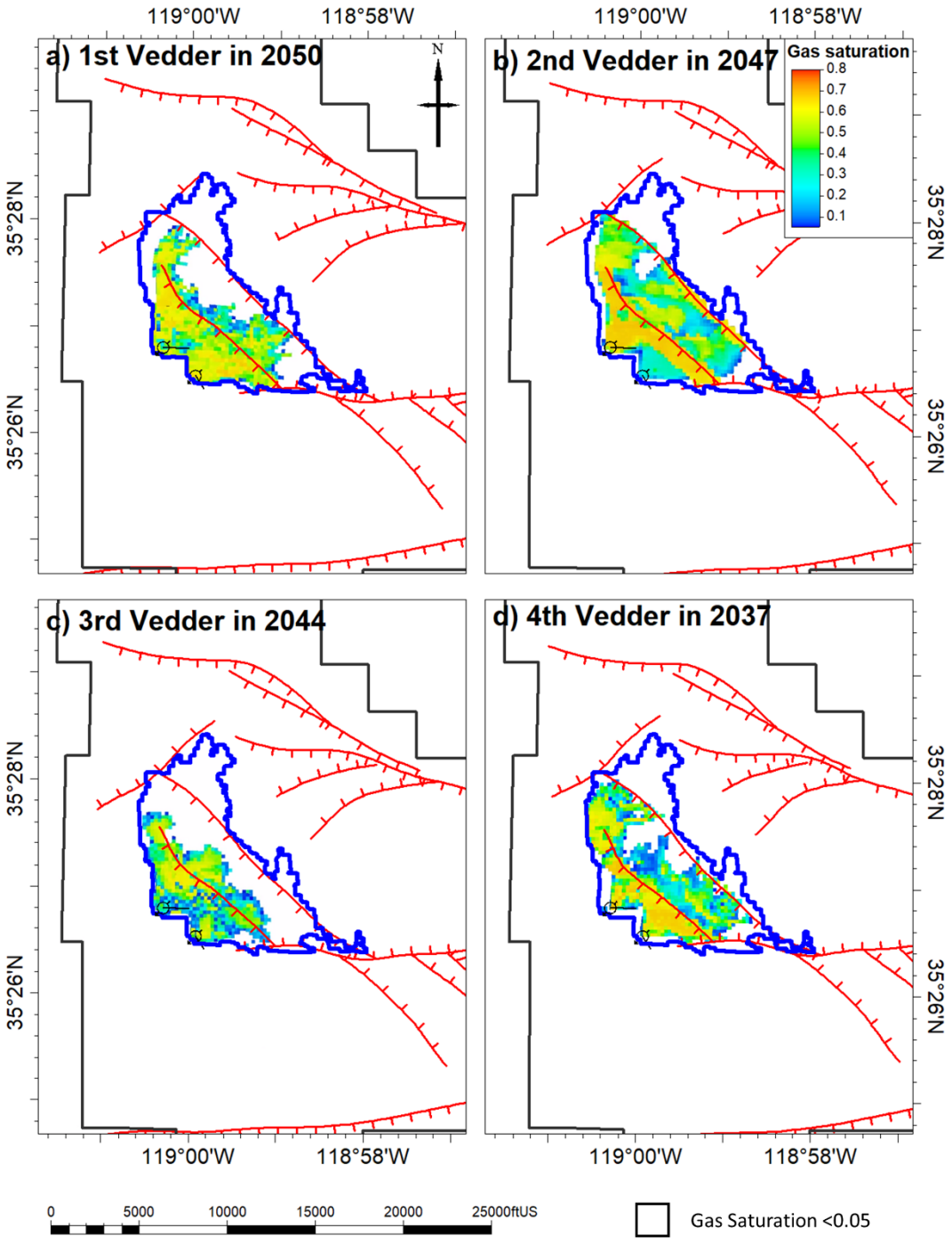

Figure 43. Map view of the Vedder Sand injection zones at the last point in time when active injection is occurring in each zone (labeled in top left corner of each pane). The figure shows the saturation value in the topmost saturated cell in each zone. The minimum gas saturation displayed is 5% based on detection limits of monitoring equipment. The AoR outline is shown in all images in blue. The 1st Vedder is the shallowest and the 4th Vedder is the deepest.

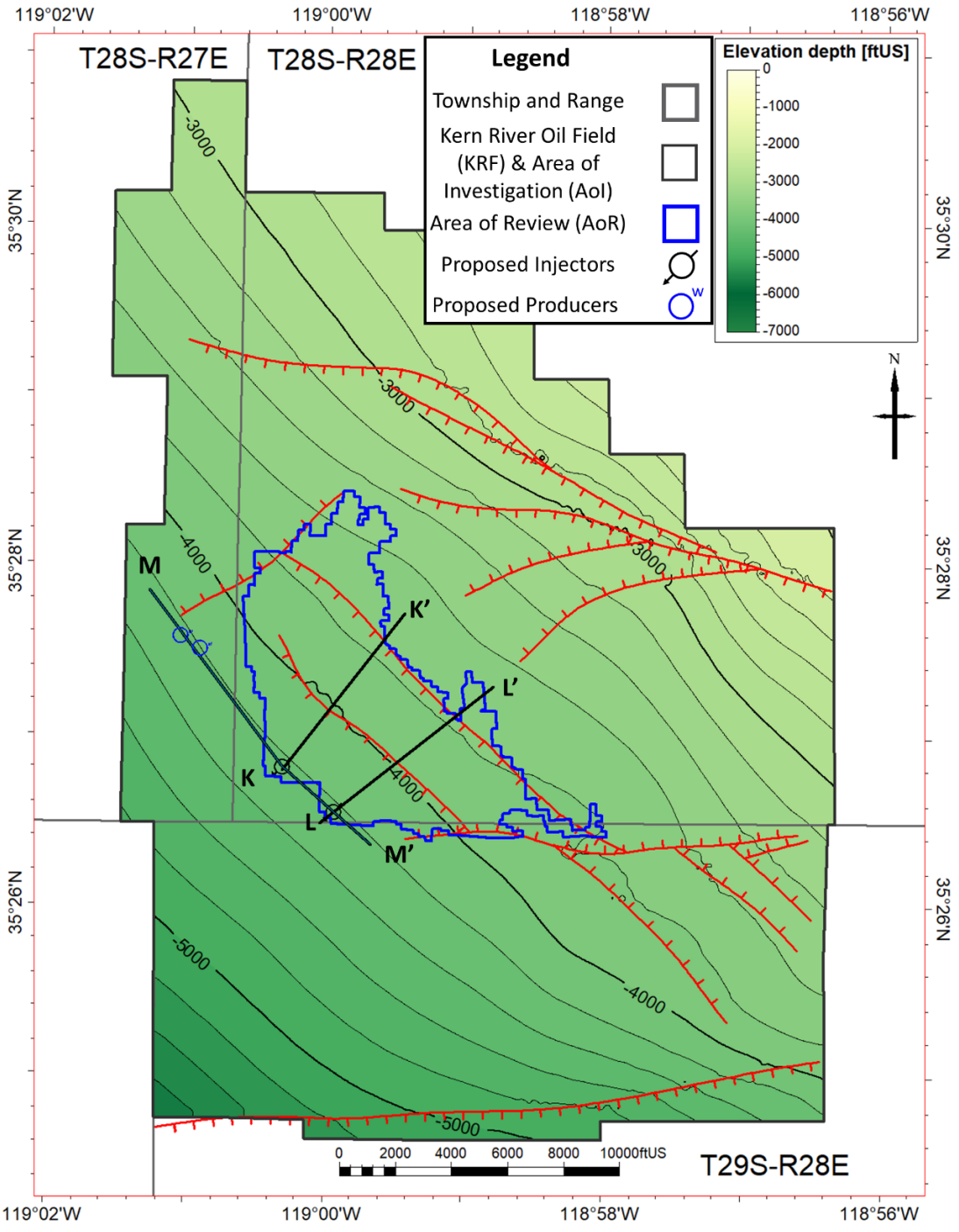

Figure 44. Location map for **Figure 45, Figure 46, Figure 47, Figure 48, and Figure 49.** AoR for Eastridge is shown in blue area compared to the AoI shown in dark black.

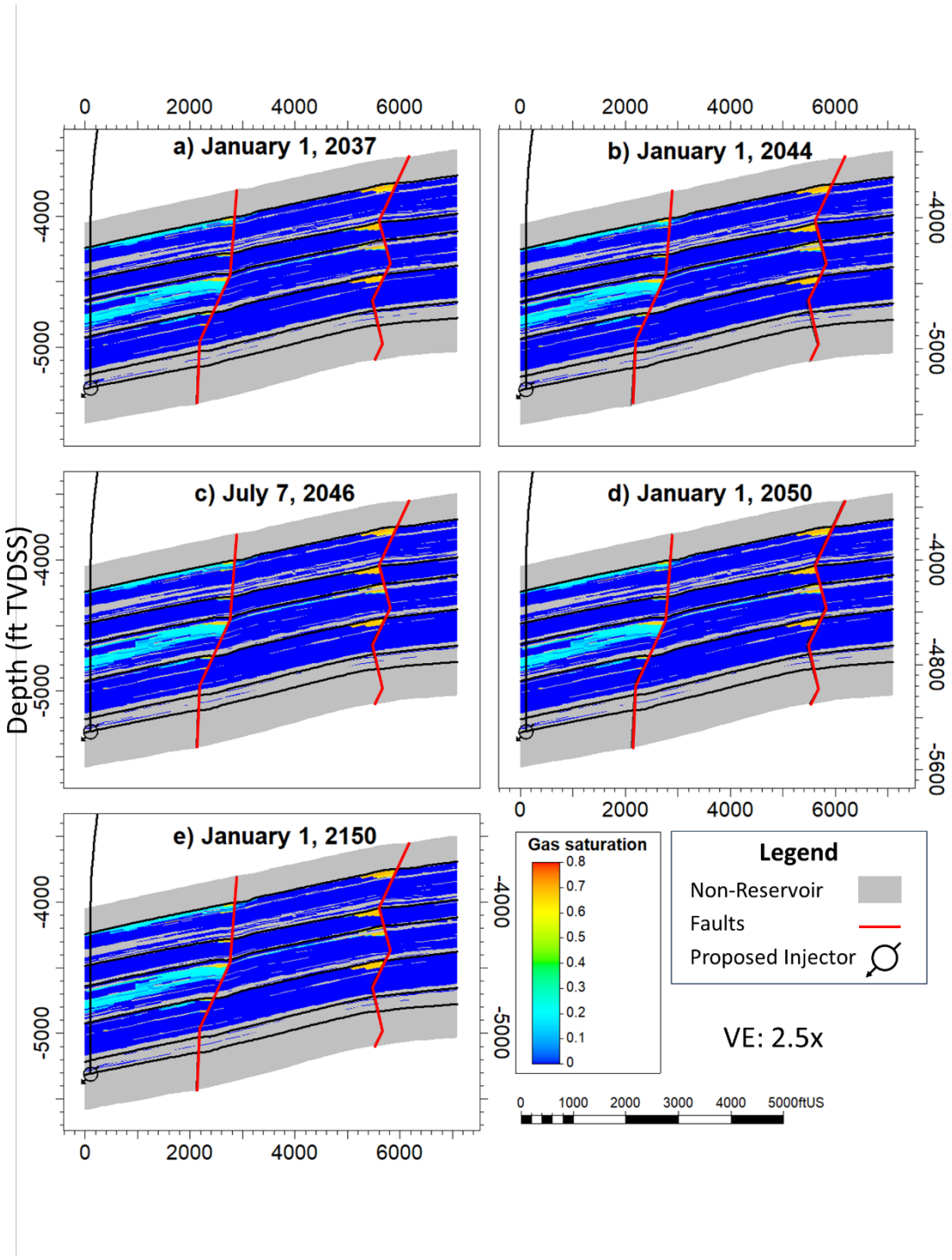

Figure 45. Cross section K-K' showing CO_2 saturation at different times a) January 1, 2037, last CO_2 injection in Vedder 4 b) January 1, 2044 last CO_2 injection in Vedder 3 c) July 7, 2046 last CO_2 injection in Vedder 2 d) January 1, 2050 last CO_2 injection in Vedder 1 e) January 1, 2150, 100 years after the 20-year injection life.

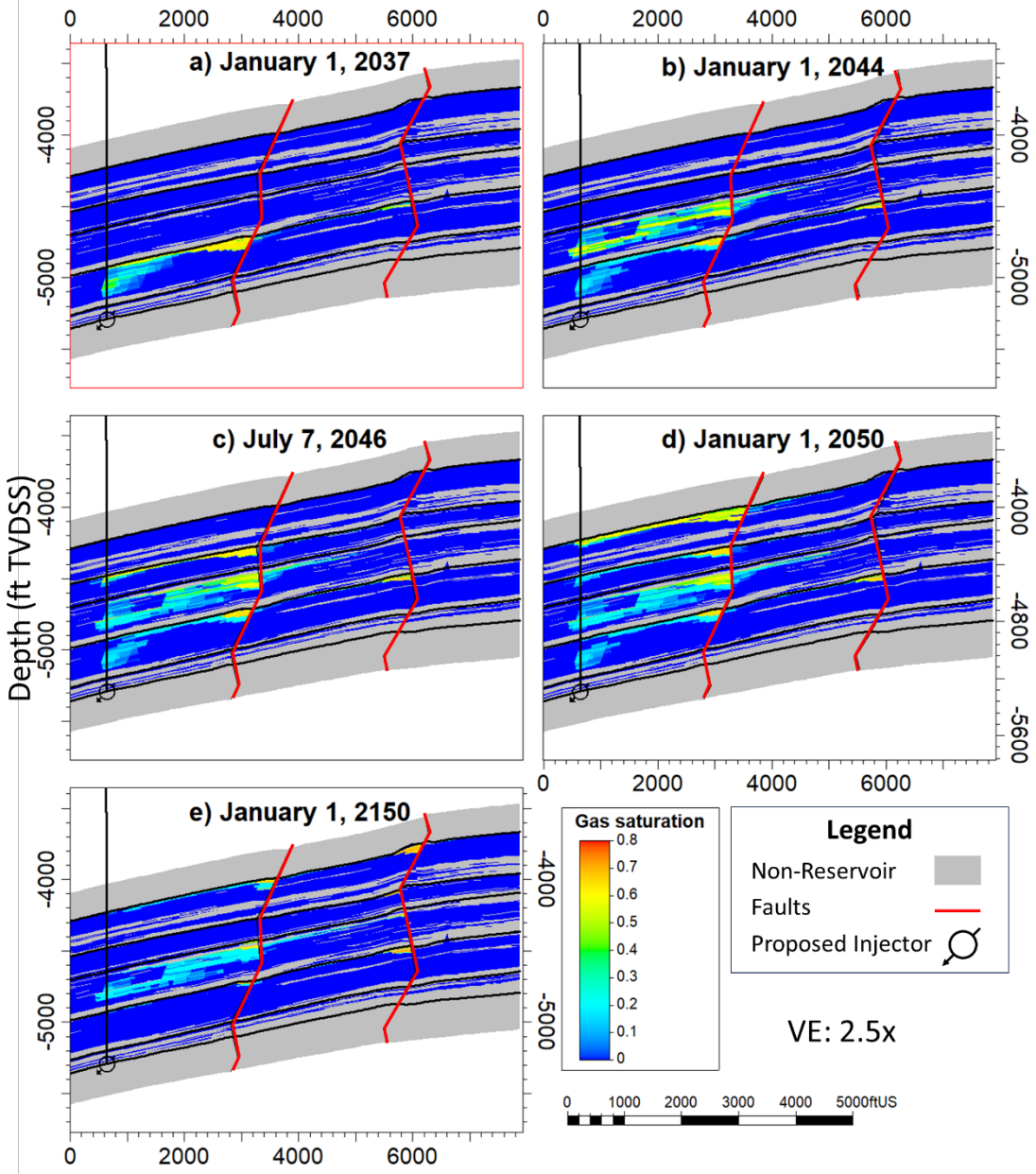

Figure 46. Cross section L-L' showing CO_2 saturation at different times a) January 1, 2037, last CO_2 injection in Vedder 4 b) January 1, 2044 last CO_2 injection in Vedder 3 c) July 7, 2046 last CO_2 injection in Vedder 2 d) January 1, 2050 last CO_2 injection in Vedder 1 e) January 1, 2150, 100 years after the 20-year injection life.

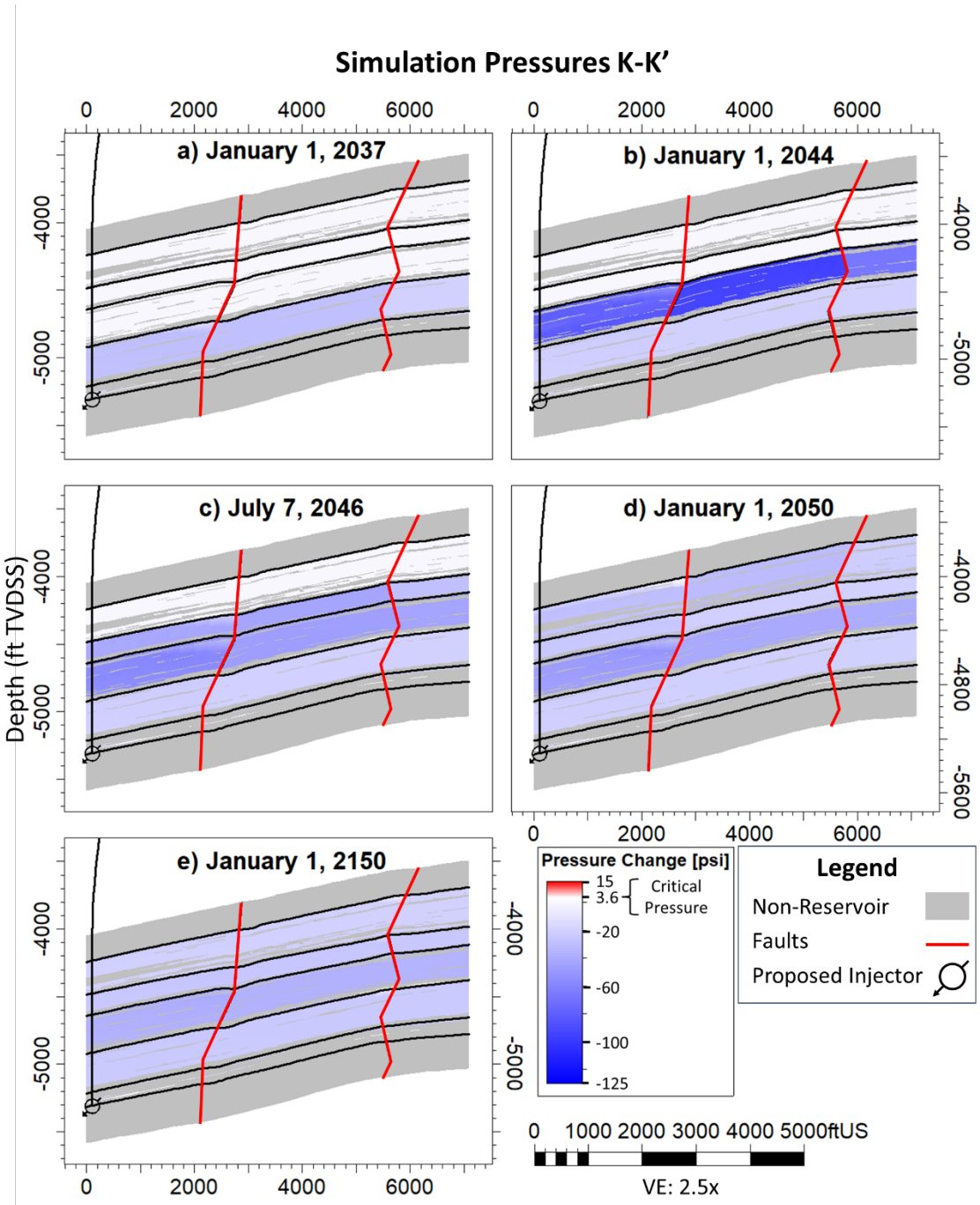

Figure 47. Cross section K-K' illustrating pressures across the Vedder Sand along a dip section up dip of proposed injector ANO9004INJ through time. a) January 1, 2037, last CO_2 injection in Vedder 4 b) January 1, 2044 last CO_2 injection in Vedder 3 c) January 1, 2047 last CO_2 injection in Vedder 2 d) January 1, 2050 last CO_2 injection in Vedder 1 e) January 1, 2150, 100 years after the 20-year injection life.

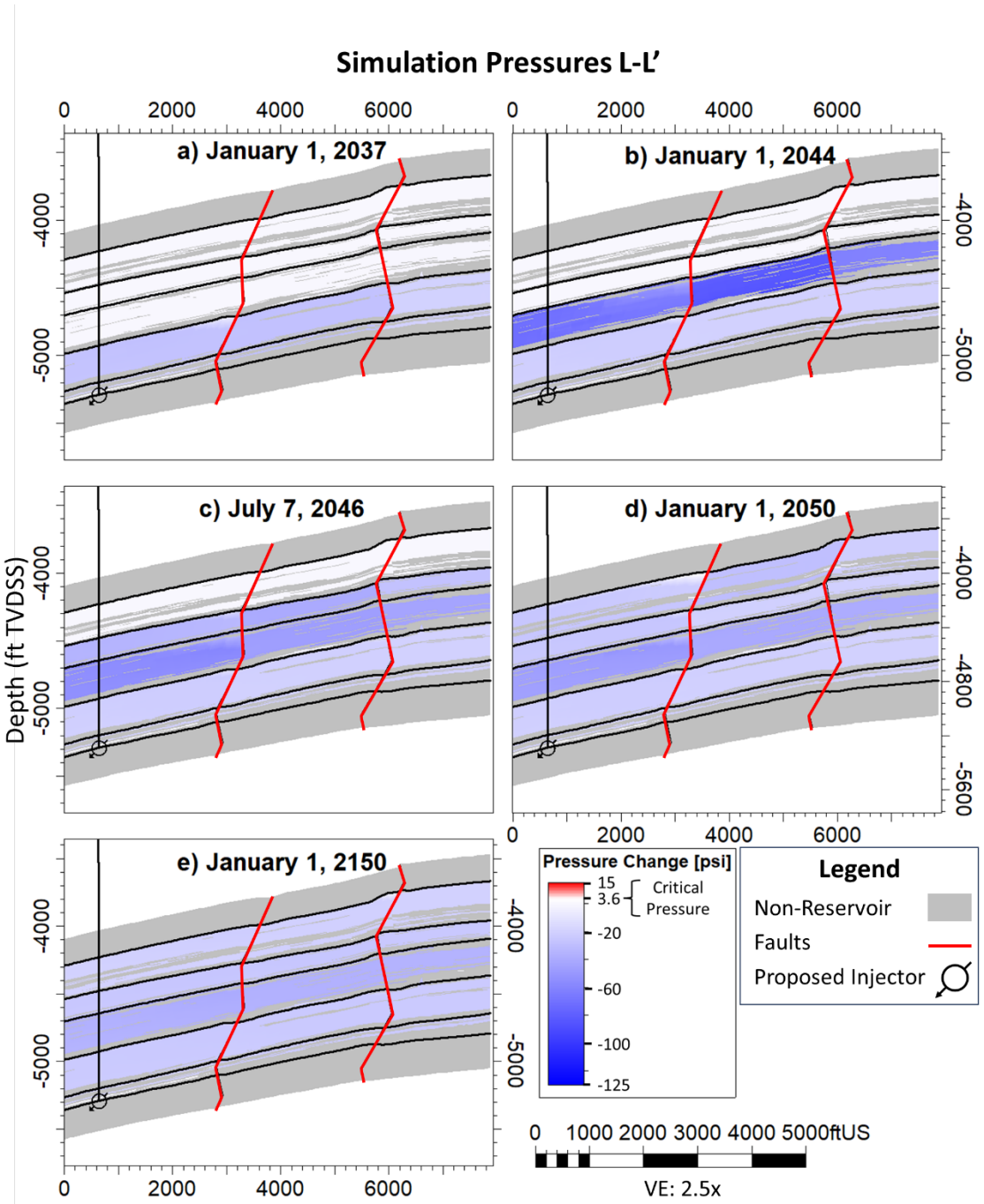

Figure 48. Cross section L-L' illustrating pressures across the Vedder along a dip section up dip of proposed injector MC19001INJ through time. a) January 1, 2037, last CO_2 injection in Vedder 4 b) January 1, 2044 last CO_2 injection in Vedder 3 c) July 7, 2046 last CO_2 injection in Vedder 2 d) January 1, 2050 last CO_2 injection in Vedder 1 e) January 1, 2150, 100 years after the 20-year injection life.

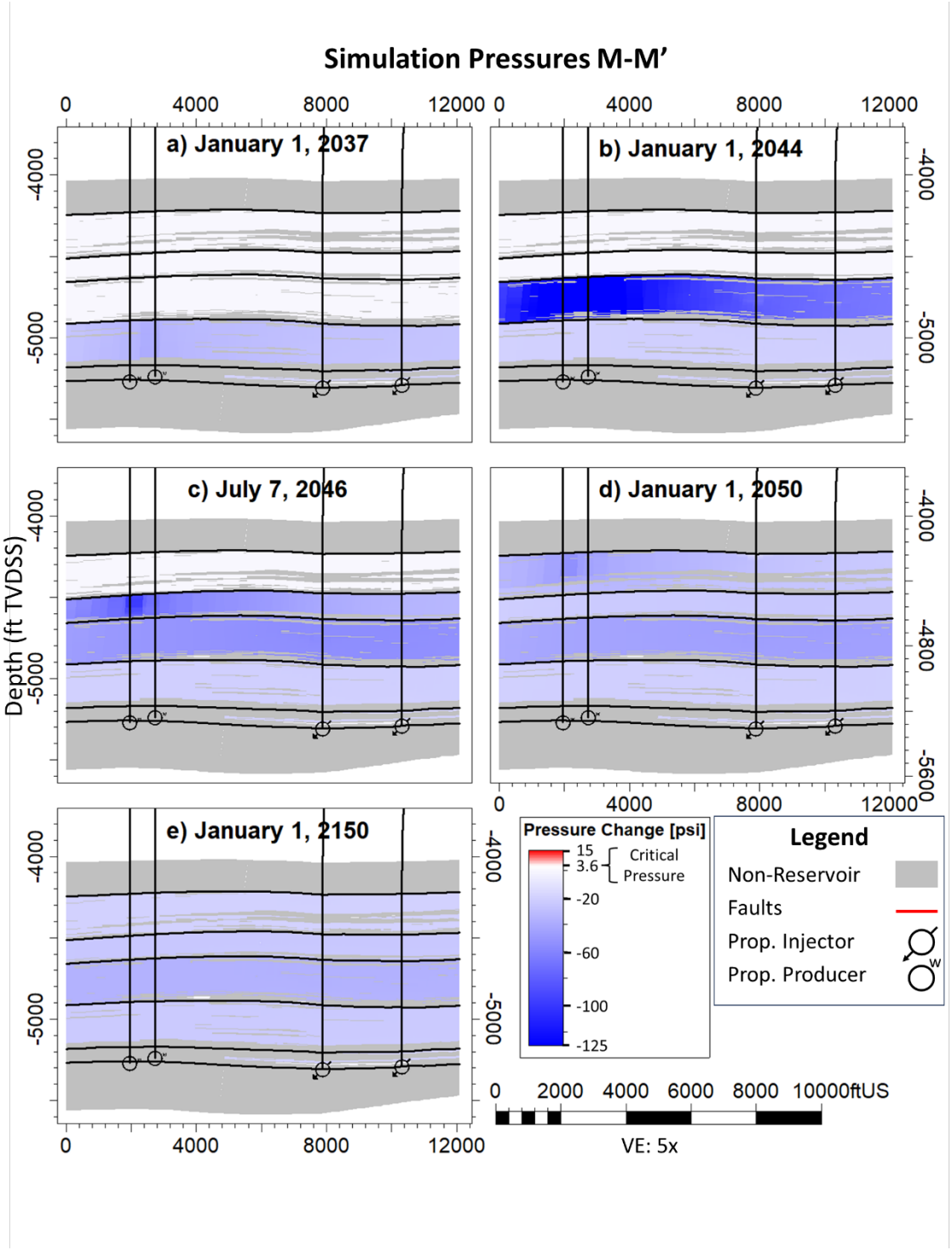

Figure 49. Cross section M-M' illustrating pressures across the Vedder Sands along strike between the proposed producers and the proposed injectors through time. a) January 1, 2037, last CO_2 injection in Vedder 4 b) January 1, 2044 last CO_2 injection in Vedder 3 c) July 7, 2046 last CO_2 injection in Vedder 2 d) January 1, 2050 last CO_2 injection in Vedder 1 e) January 1, 2150, 100 years after the 20-year injection life.

AoR Sensitivity Analysis

The data from wells within the AoR and AoI combine with the seismic survey across the project area to provide reasonable certainty on the geologic structure and general geologic environment of the Vedder Sand and overlying Freeman-Jewett Silt within the AoR. However, Chevron recognizes that localized variations in reservoir properties could still exist, and with this in mind, has generated and analyzed a range of sensitivities.

Table 16. Sensitivity analysis of each variable compared to the base case.

Run	Description	Base	Sensitivity
Run_1_01	Relative Permeability - smaller amount of trapped CO2 due to hysteresis and higher CO_2 mobility (kr) for all saturations.	Sg-trapped - 0.23, Ng - 2.2, Nw - 3.5	Sg-trapped - 0.17, Ng - 1.8, Nw - 3
Run_1_02	Permeability modifier low	Model Permeability As-Is adjusted based upon PTA	Permeability * 0.5
Run_1_03	Porosity modifier	Model Porosity As-Is	Porosity - 2pu (Porosity * 0.93)
Run_1_04	Investigating sensitivity to different injection schemes where the sands are perforated in the lower portion of the zone or completed from top to bottom.	All sands completed in the lowest part of the sand	All sands completed in the entire sand
Run_1_05	Fault threshold pressure sensitivity to investigate assumptions used in IFT*CosTheta	Cos Theta = 40	Cos Theta = 50 (multiply threshold pressure by 0.84)
Run_1_06	Fault transmissibility sensitivity to test the leaky or sealing nature of our faults	Calculated transmissbility multipliers adjusted for the PTA with a scalar of **0.025**	scalar adjustment of **0.005** (more sealing)
Run_1_07	Relative Permeability - larger amount of trapped CO2 due to hysterisis and lower CO_2 mobility (kr) for all saturations.	Sg-trapped - 0.23, Ng - 2.2, Nw - 3.5	Sg-trapped - 0.30, Ng - 2.2, Nw - 4
Run_1_08	Permeability modifier high	Model Permeability As-Is adjusted for PTA	Permeability * 2.0
Run_1_09	Porosity modifier	Model Porosity As-Is	Porosity + 2pu (Porosity * 1.07)
Run_1_10	**Best Technical Case (Base Case)**	none	none
Run_1_11	Fault threshold pressure sensitivity to investigate assumptions used in IFT*CosTheta	Cos Theta = 40	Cos Theta = 30 (multiply threshold pressure by 1.13)
Run_1_12	Fault transmissibility sensitivity to test the leaky or sealing nature of our faults	Calculated transmissibility multipliers adjusted for the PTA with a scalar of **0.025**	scalar adjustment of **0.05** (less sealing)

Table 16 shows the sensitivities run to test the impact of variability in key properties on the AoR. In each run, the base case and sensitivity modification are described. Each sensitivity modification is done as an uncertainty both above and below the base case assumption to test for the variance. The one exception is the injection scheme where only two cases are tested, the base case assumption and an alternative.

The outcome of the sensitivity analysis is summarized towards the end of this section with two separate summary maps of the base case AoR with sensitivities that result in an expanded AoR and the base case AoR with sensitivities that result in a shrunken AoR.

Sensitivity – Relative Permeability

The base case uses a set of relative permeability curves with a Corey exponent of 2.2 and 3.5 for the CO_2 and brine phase, respectively, and a hysteresis trapped CO_2 saturation of 0.23. Run_1_01 tests a case where there is less trapped CO_2, and the relative permeability of CO_2 is higher than the base case. More CO_2 is available to move with a higher mobility resulting in the CO_2 moving further up-dip. Run_1_07 tests the case where more CO_2 is trapped via hysteresis and the relative permeability is lower than the base case. Less CO_2 is available to move (due to trapping) and with a lower mobility resulting in less CO_2 migration up-dip. **Figure 50** illustrates the sensitivity of the AoR to the relative permeability variable tested in the two runs.

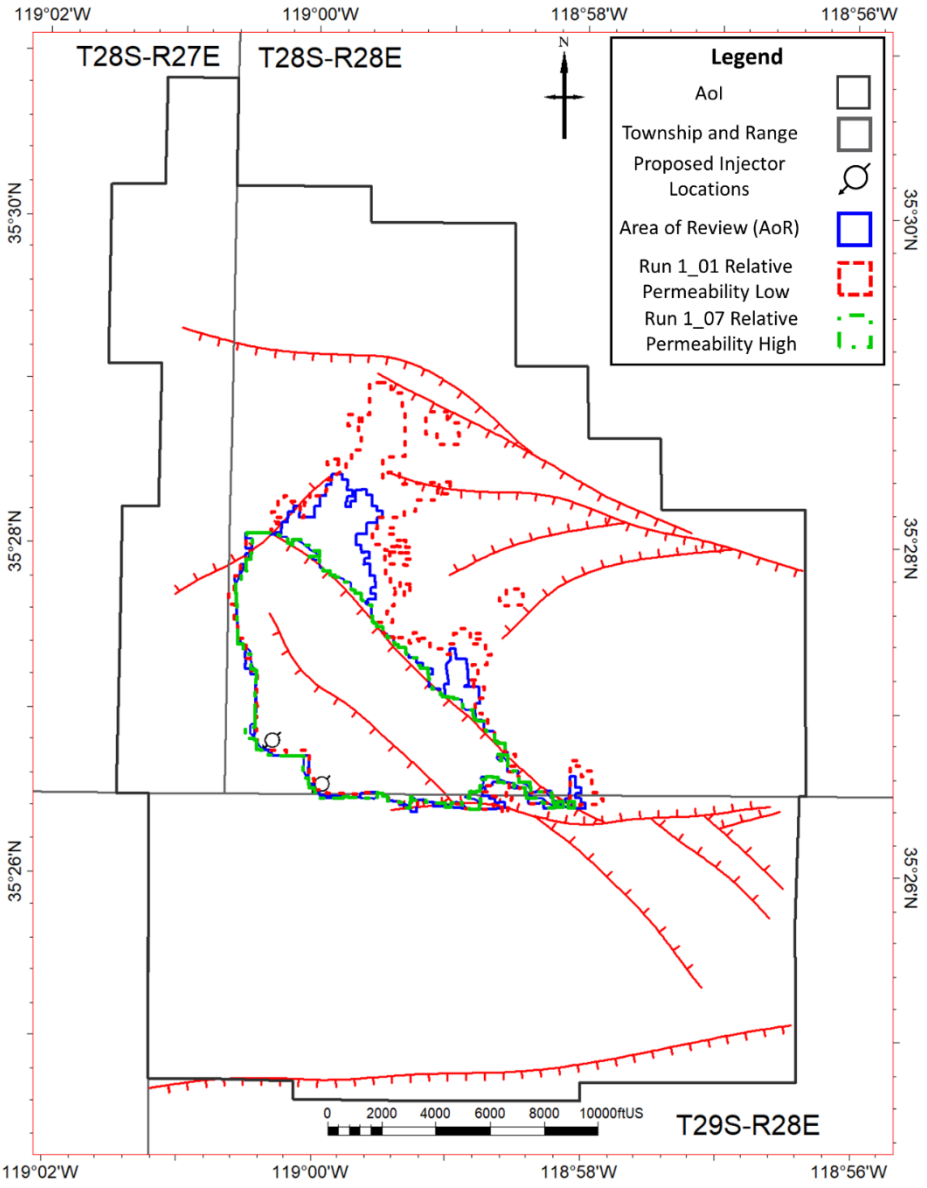

Figure 50. Deviation from the base case as a function of relative permeability. Run_1_01 has less CO_2 trapped via hysteresis and a higher mobility overall, allowing it to move up-dip further than the base case AoR. Run_1_07 has more trapped CO_2 and lower overall mobility, preventing the CO_2 from migrated further up-dip.

Sensitivity – Permeability

The base case model permeability field was tested for a high and low outcome by multiplying all permeability values by 2.0 and 0.5, respectively. Permeability was transformed from a log-normal distribution to a normal distribution by taking the logarithm. The variance of this normal distribution was used to calculate a range of one half a standard deviation from low to high which results in the multipliers of 2.0 and 0.5. The higher permeability sensitivity allows the CO_2 to move more rapidly through the system and the lower permeability multiplier inhibits the CO_2 from moving rapidly through the system. **Figure 51** illustrates the AoR for the low and high permeability cases.

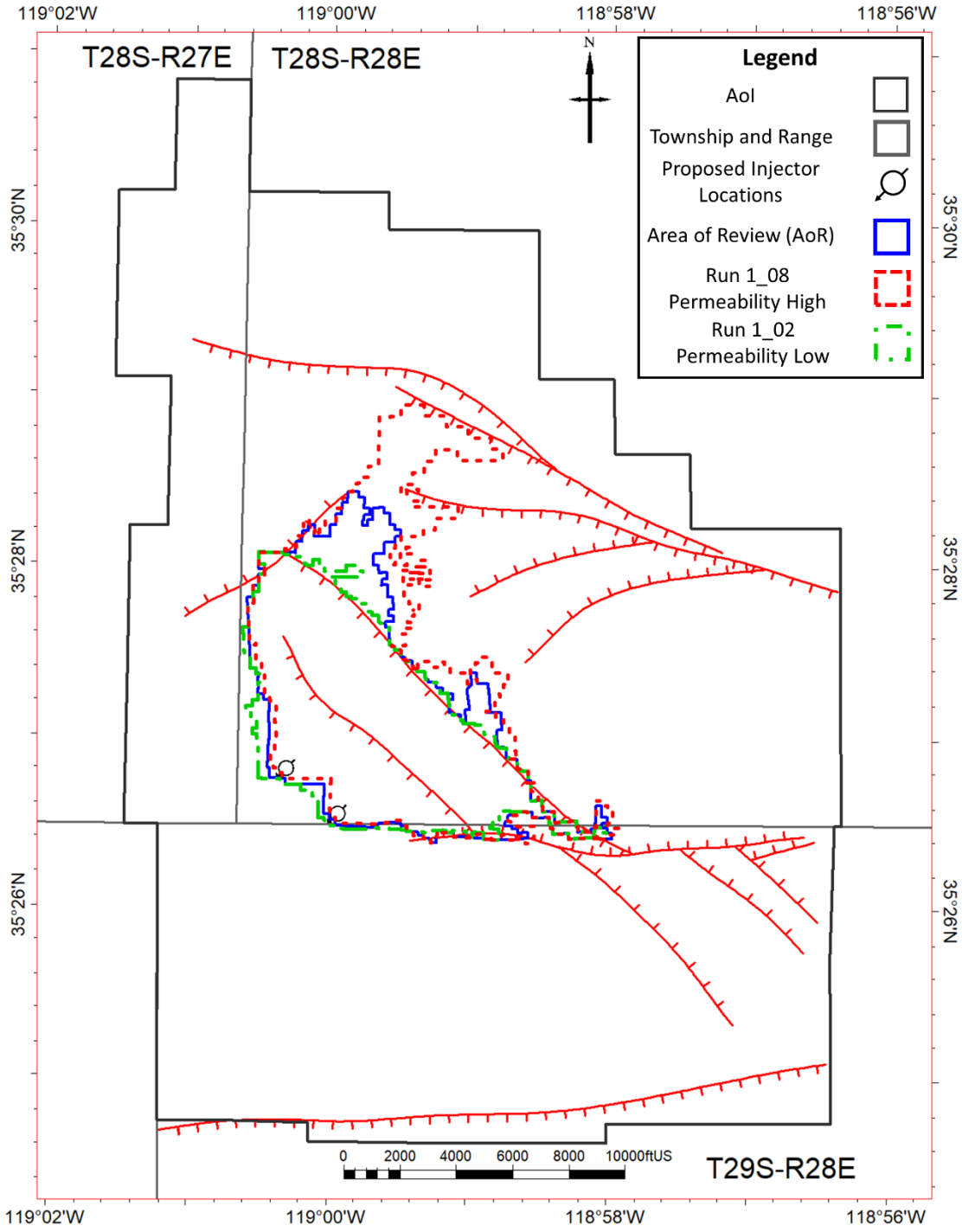

Figure 51. AoR Sensitivity to permeability. Run_1_08 shows the AoR when permeability is multiplied by 2.0 and Run_1_02 when permeability is multiplied by 0.5.

Sensitivity – Porosity

The base case porosity shows a mean pay porosity of 29%. The distribution from the model defines a standard deviation of 4 porosity units. Porosity is varied by 2 porosity units (percent) for the sensitivity analysis. This results in a mean porosity of 27% and 31% in the low and high cases, respectively. **Figure 52** illustrates the impact on the AoR. The results are reasonable and easily explained by the overall greater availability of pore space.

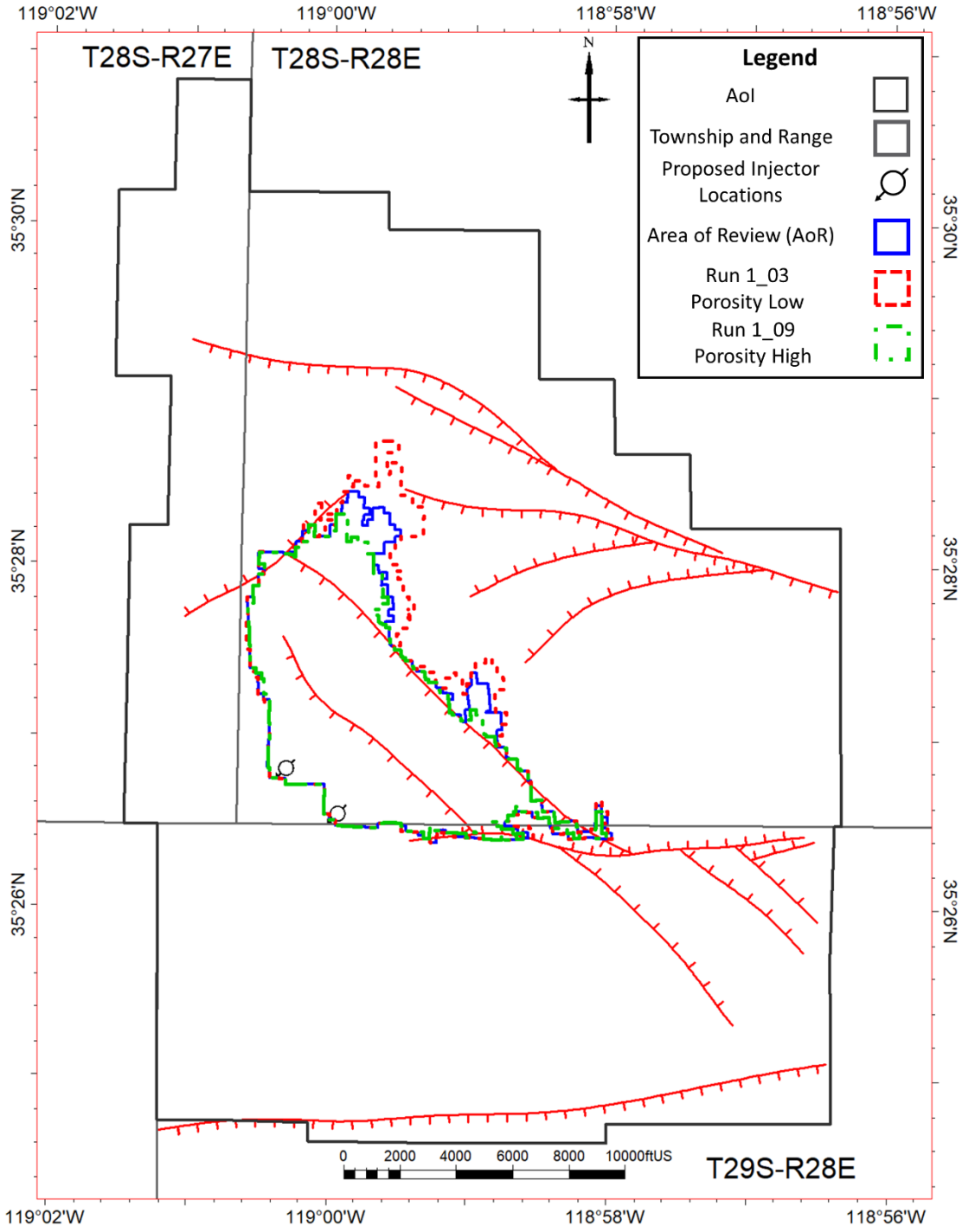

Figure 52. AoR Sensitivity to porosity field. Run_1_09 shows the AoR when porosity is multiplied by 1.07 (+2 pu) and Run_1_02 when all porosity is multiplied by 0.93 (-2 pu).

Sensitivity – Injection Scheme

Testing the sensitivity of the AoR to how each of the sands is completed is referred to as Injection Scheme. The base case uses a completion in the deepest section of the sands. The sensitivity tests the AoR when the entire sand is completed**. Figure 53** illustrates how the AoR is impacted. Injecting only in the deepest section of each sand allow for the CO_2 to sweep additional area as buoyancy forces drive the CO_2 toward the top of the zone. Conversely, if the top of the zone is targeted, CO_2 enters the reservoir near the top of the zone and sweeps less area, resulting in less total trapping prior to the CO_2 reaching the fault. With more CO_2 accumulating at the fault, more CO_2 can migrate through the fault, explaining why the entire sand results in a larger AoR.

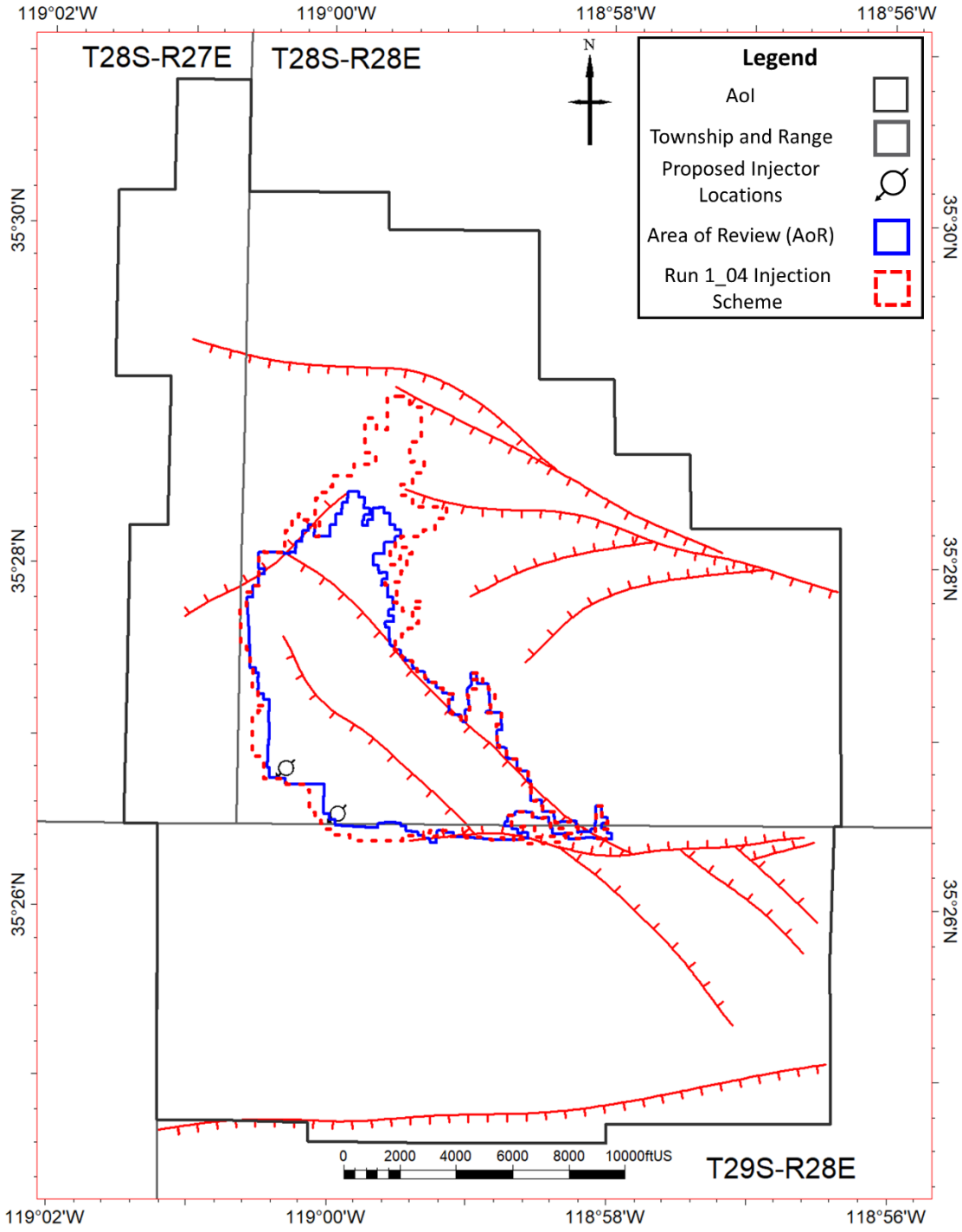

Figure 53. AoR as a function of injection scheme. In the base case AoR, the wells are completed in the deepest section of the sand. In Run_1_04, the wells are completed throughout the entire sand.

Sensitivity – Fault Threshold Pressure

The fault threshold pressure is defined as the amount of buoyant pressure each fault can hold prior to overcoming the entry pressure. The approach used to vary the threshold pressure uses a range of contact angles between CO_2 and brine. Contact angle measurements on a Vedder core sample show a range of 35 – 44 degrees. The range used for the variation of the contact angle is 30 – 50 degrees with the base case using 40 degrees. **Figure 54** shows the AoR sensitivity to variations in the fault threshold pressure.

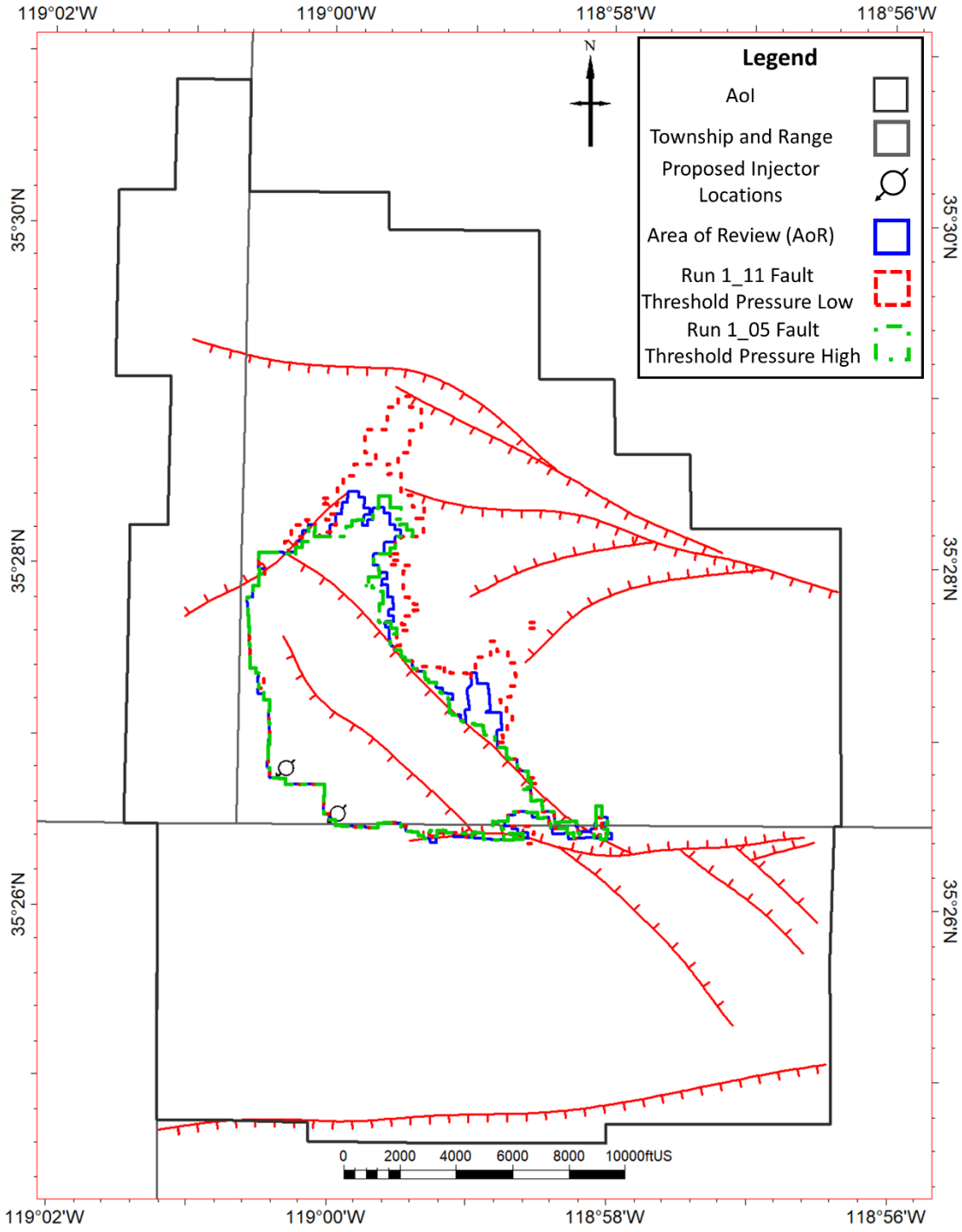

Figure 54. AoR as a sensitivity to variations in fault threshold pressure. Run_1_05 is the result of higher threshold pressures and Run_1_11 is the result of lower threshold pressures.

Sensitivity – Fault Transmissibility

The fault transmissibility multipliers are calculated with the fault thickness & permeability and then further validated with pressure transient analysis within the Vedder Sand within the AoI. The validation derives an additional multiplier of 0.025 applied to all faults. The sensitivity analysis tests two cases. The more transmissive case (Run_1_12) doubles that value to 0.050 which breaks the validation with transient analysis. The more sealing case (Run_1_06) reduces the additional multiplier to 0.005 which matches validation with the transient analysis. **Figure 55** shows the results of these two sensitivities.

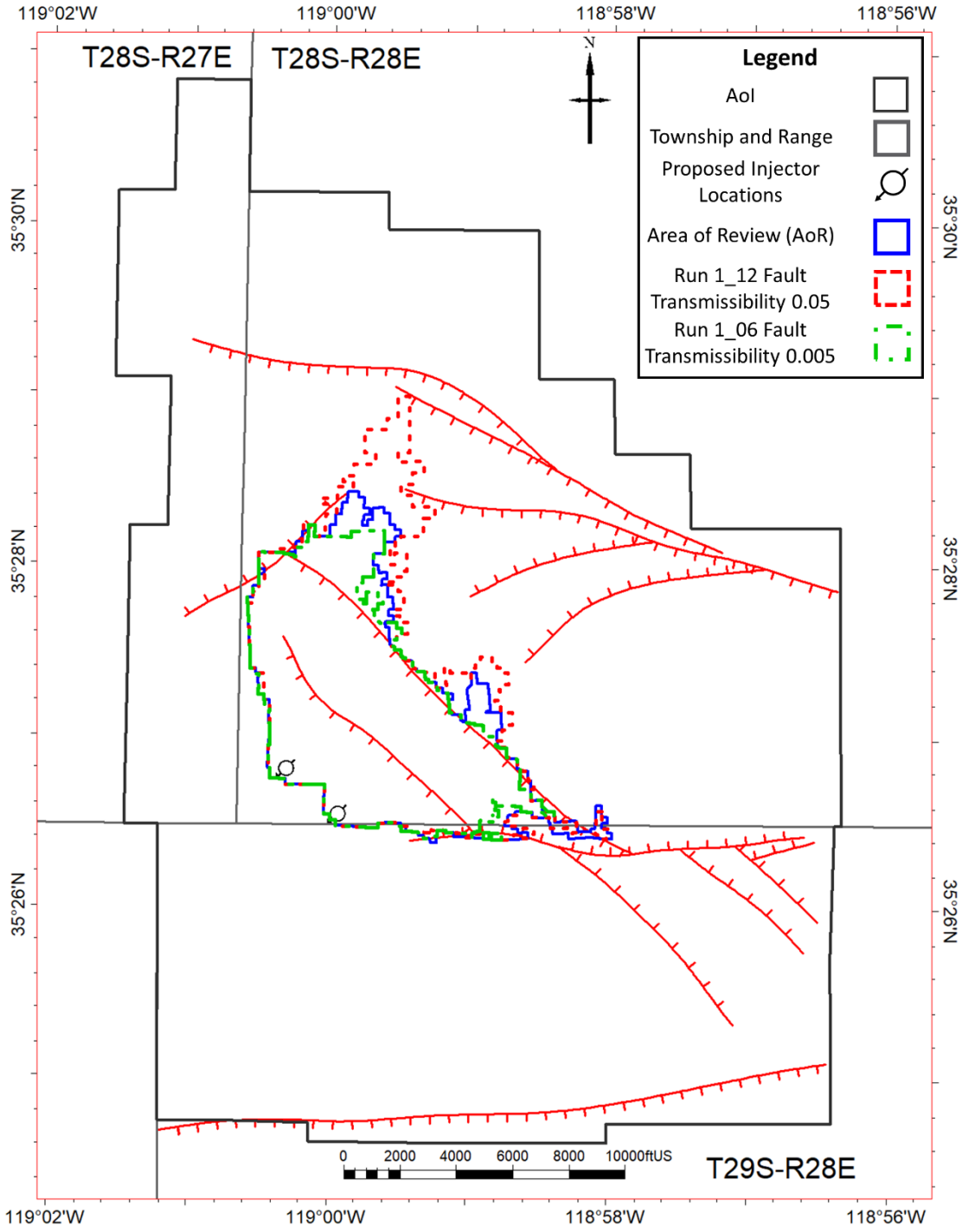

Figure 55. AoR as a sensitivity to fault transmissibility multiplier. Run_1_12 is a more transmissive fault whereas Run_1_06 is a more sealing fault.

Sensitivity – Summary

Figure 56 and **Figure 57** summarize the impact of the sensitivity analysis on AoR with the first, **Figure 56**, showing the cases that result in an expanded AoR and the second, **Figure 57**, showing the cases that result in a reduced the AoR.

Chevron carefully considered these sensitivities in designing the Testing and Monitoring Plan. Monitoring well placement is shown with AoR in **Figure 22**. With the selected monitoring technologies, data collection frequencies, and well placement described in detail in the Testing and Monitoring Plan, Chevron will be able to accurately monitor the development of the CO_2 and pressure response in the reservoir. This data will be analyzed and incorporated into periodic AoR Reevaluations as described in the AoR Reevaluation Cycle and Triggers for AoR Reevaluations Prior to the Next Scheduled Reevaluation sections of this document.

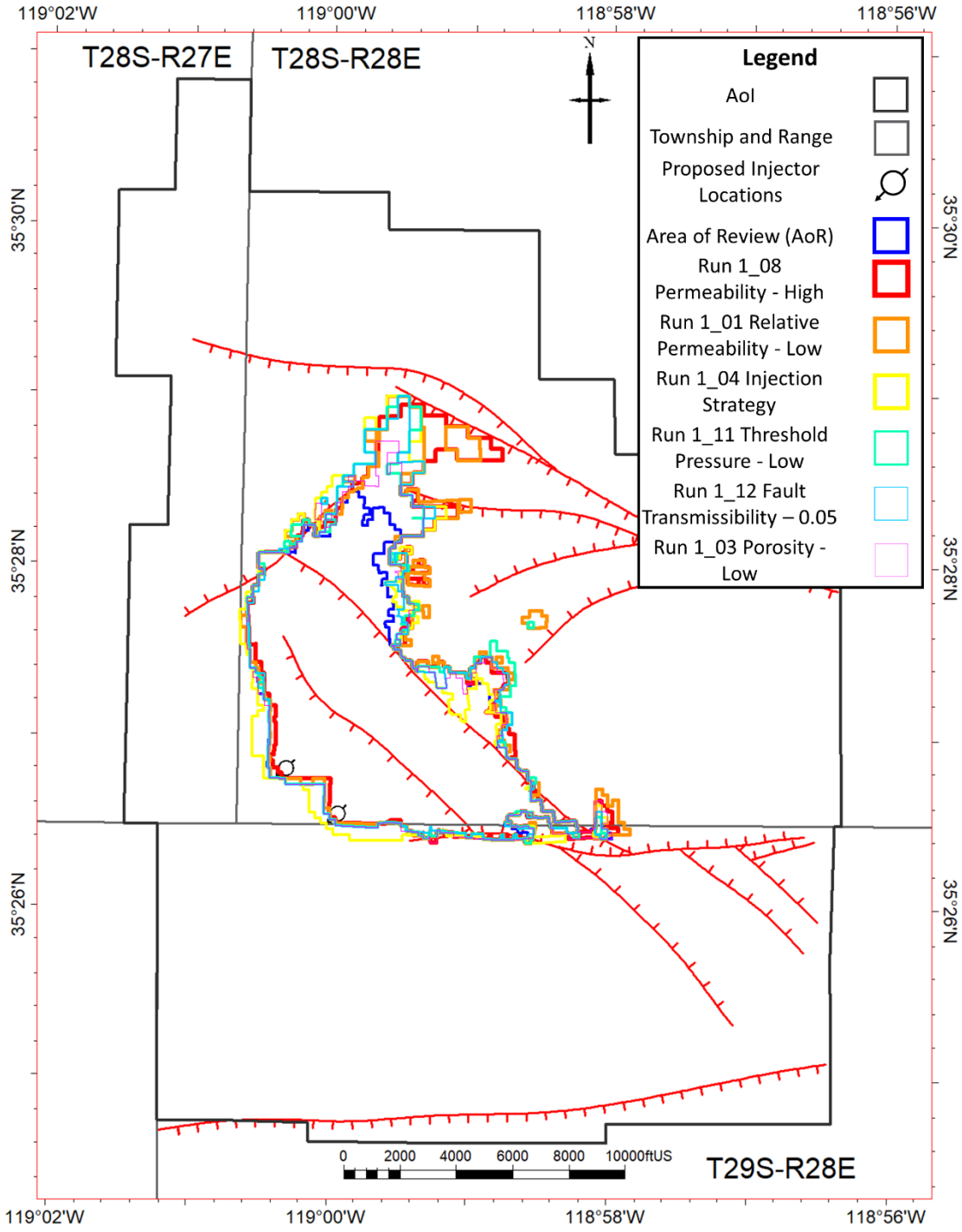

Figure 56. Sensitivity analysis summary showing the cases that result in an expanded AoR.

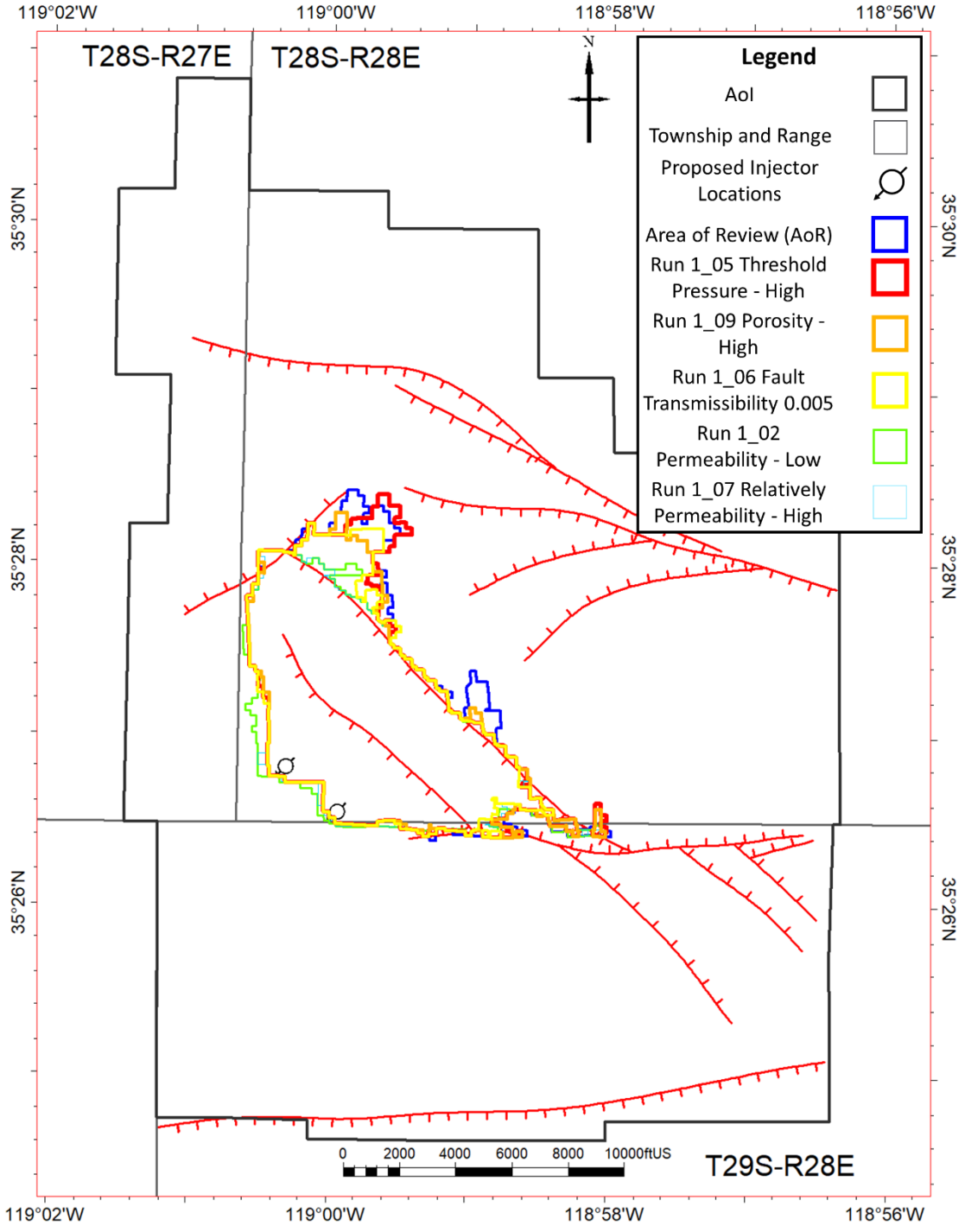

Figure 57. Sensitivity analysis summary showing the cases that result in a reduction of the AoR.

Corrective Action

Tabulation of Wells within the AoR

Wells within the AoR

There are 6,011 wells located within the AoR, though all but 15 of these wells have a total depth that terminates above the confining Freeman-Jewett Silt. The full well list, shown in **Appendix 1**, was populated by combining Chevron's internal system of record, developed over multiple decades of ownership and operatorship within the field, and with California Geologic Energy Management Division's well records. Statuses and well type reflect California Geologic Energy Management Division's records as of September 28, 2023. **Appendix 1** shows AoR maps for this well list and all other features required for consideration by the program director.

Wells Penetrating the Confining Zone

Of the total 6,011 wells within the AoR, 15 penetrate the confining zone above the Vedder Sand known as the Freeman-Jewett Silt. **Table 17** summarizes the status and type of the wells penetrating the confining zone within the AoR. Current wellbore diagrams indicating well conditions for all 15 penetrations can be found in **Appendix 2**. All but HF_0004 penetrate the Vedder Sand. Depths for these penetrations were obtained from surveying tools available at the time of drilling. These wells are shown in map view relative to the AoR in **Figure 22**.

Table 17. Summary of Wells in the AoR Penetrating the Confining Layer by Status & Type

Status	Count
Active Class II Disposal Plugged Back to Shallower Zone	2
Idle Class II Disposal	1
Plugged and Abandoned	12
Total	15

Under current operational conditions, there are no integrity concerns for these wells. With proposed CO_2 injection, Chevron plans to conduct work to support proactive zonal isolation for three specific wells within the AoR (FEC0074, API# 040292411200; GWA0145, API# 040292697300; and OM_0044, API# 040290009800). With proposed CO_2 injection, Chevron also plans to abandon KA_0053X (API# 040296990300), the single idle Class II Disposal well. A general procedure for all proposed well work is provided below. This general procedure will be refined with well specific details in preparation for execution. The proposed well work for these four wells will be executed prior to CO_2 injection.

General Procedures for Well Work

1. Locate well.
2. Prep location for rig and/or coil tubing unit.
3. Excavate location as necessary to expose cemented casing stub and metal plate with API numbers on top.
4. Move in rig and/or coil tubing unit and rig up.
5. If necessary, pull the completion equipment.
6. Re-enter well and drill out/clean out well to total depth (TD).
7. Use a rig and/or a coil tubing unit to perform the following operations:
    a. If required, perf and squeeze any un-cemented annuli that exist across markers and require isolation.
    b. Spot CO_2 resistant cement plugs from TD to surface in stages utilizing balanced plugs. After spotting the balanced plug, pull above the top of the cement and circulate the hole clean.
    c. Wait for the cement to set. After the cement has set, run in the hole, and tag the top of the cement plug to verify the depth and hardness of the plug before initiating the next cement plug.
    d. Repeat steps b and c until cement is placed at the surface.
8. Cut the wellhead and casing at a minimum of 5' below grade and weld a permanent steel plate with well identifying information onto the casing stub.
9. Backfill hole above the casing stub to original grade.

Plan for Site Access

Chevron owns and operates 100% of the surface and mineral rights directly surrounding FEC0074, GWA0145, OM_0044, and KA_0053X and therefore anticipates no issues in accessing these wells to execute proposed well work.

Proactive Zonal Isolation Execution Schedule

Chevron plans to execute well work to support proactive zonal isolation for FEC0074 (API# 040292411200), GWA0145 (API# 040292697300), OM_0044 (API# 040290009800), and KA_0053X (API# 040296990300) prior to CO_2 injection.

Reevaluation Schedule and Criteria

AoR Reevaluation Cycle

Chevron will reevaluate the above described AoR every 5 years during the injection and post-injection phases, as required by 40 CFR 146.84 (e).

Every 5 years, operating and monitoring data will be compiled and analyzed in comparison with computation simulation results. Specifically, data to be gathered and analyzed includes:

- Pressure data from monitoring wells to constrain and define the development of the AoR

- Monitoring data from both the monitoring wells and injectors. This includes cased hole logging and seismic surveys.

- Injection rates, injection pressures, and injection volumes to constrain computational model parameters and inputs.

- As applicable, production rates, production pressures, and production volumes to constrain computational model parameters and inputs.

- Fluid samples and corresponding reports analyzing the formation water collected from monitoring wells in dissipation zones to evaluate unexpected migration into shallower formations.

Every 5 years, or as necessary based on triggers described below, Chevron will reevaluate the AoR and will generate and submit to EPA a report comparing computation results and recently obtained field data. If needed, Chevron will describe specific actions to be taken to mitigate discrepancies between monitoring data and computational simulation results.

The collection of operating and monitoring data through the project life may be used to refine static and dynamic models that may prove to inadequately represent the subsurface. At each AoR reevaluation, Chevron will evaluate model inputs based on operating and monitoring data and adjust as needed. In the event of model changes, Chevron will submit a report to EPA listing the changes and providing proper justification.

Note: AoR reevaluation frequency during the post-injection phase may be adjusted in the future, pursuant to EPA approval, based on regulatory changes allowing for a decreased frequency.

Triggers for AoR Reevaluations Prior to the Next Scheduled Reevaluation

The occurrence of any of the following events would trigger a collection of data and AoR reevaluation:

- Significant deviations between the computational modeling and observed AoR development. Specifically,
    - Unexpected significant changes from baseline in groundwater chemistry within the Olcese Sand or Santa Margarita Sandstone related to CO_2 injection
    - Unexpected significant changes in pressure increase at monitoring wells within the Vedder Sand with a greater than 25% deviation from the forecast range (after accounting for actual injection and withdrawal rates)
- Seismic monitoring anomalies within two miles of the injection zone with a magnitude greater than M2.7.

Chevron will discuss any such events with the UIC Program Director to determine if an AoR reevaluation is required. If an unscheduled reevaluation is triggered, Chevron will perform the steps described at the beginning of this section of this Plan within six months of the triggering event.

References

Abeid, J. and Knauer, L., 2014, Fault Play Wells In A 115 Year Old Heavy Oil Field, Kern River Field, Bakersfield, California, USA. Pacific Section AAPG, SPE, and SEPM Joint Technical Conference, Bakersfield, CA.

Amaefule, J.O., Altunbay, M., Tiab, D., Kernsey, D.G., and Keelan, D.K., 1993, Enhanced reservoir description: using core and log data to identify hydraulic (flow) units and predict permeability in uncored intervals/wells: Society of Petroleum Engineers Journal SPE26436, p. 205-220.

Bajsarowicz, C.J., 1992, Core alteration and preservation: part 3, well site methods, *in* Morton-Thompson, D., and Woods, A.M., eds., American Association of Petroleum Geologists, Methods in Exploration v. 10, Development Geology Reference Manual, p. 127-130.

Baker, S.E., Joshuah K. Stolaroff, George Peridas, Simon H. Pang, Hannah M. Goldstein, Felicia R. Lucci, Wenqin Li, Eric W. Slessarev, Jennifer Pett-Ridge, Frederick J. Ryerson, Jeff L. Wagoner, Whitney Kirkendall, Roger D. Aines, Daniel L. Sanchez, Bodie Cabiyo, Joffre Baker, Sean McCoy, Sam Uden, Ron Runnebaum, Jennifer Wilcox, Peter C. Psarras, Hélène Pilorgé, Noah McQueen, Daniel Maynard, Colin McCormick, 2020, Getting to Neutral: Options for Negative Carbon Emissions in California, January 2020, Lawrence Livermore National Laboratory, LLNL-TR-796100. https://www-gs.llnl.gov/content/assets/docs/energy/Getting_to_Neutral.pdf

Bartow, J.A., and Nilsen, T., 1990, Review of the Great Valley sequence, eastern Diablo Range and northern San Joaquin Valley, central California, *in* Kuespert, J.G., and Reid, S.A., Structure, Stratigraphy and Hydrocarbon Occurrences of the San Joaquin Basin, California, Pacific Section American Association of Petroleum Geologists, p. 253-265.

Bretan, P., Yielding, G., and Jones, H., 2003, Using calibrated shale gouge ratio to estimate hydrocarbon column heights. AAPG Bulletin, v. 87, No. 3, pp. 397-413.

Calabrese C. et al., 2019, Extension of Vibrating-Wire Viscometry to Electrically Conducting Fluids and Measurements of Viscosity and Density of Brines with Dissolved CO_2 at Reservoir Conditions, Journal of Chemical Engineering Data.

California Department of Conservation, 2023, Maps: Mines and Mineral Resources. Department of Conservation Map Server (ca.gov). Accessed September 22, 2023.

California Department of Fish and Wildlife, 2023, CDFW Open Data Home: California Streams. California Streams | California Streams | CDFW Open Data Portal (arcgis.com), Accessed September 22, 2023.

California Department of Toxic Substances Control, 2023, Envirostor. https://www.envirostor.dtsc.ca.gov/public/. Accessed September, 19, 2023.

California Department of Water Resources, 2023, Well Completion Reports. https://water.ca.gov/Programs/Groundwater-Management/Wells/Well-Completion-Reports. Accessed October 3, 2023.

California Division of Oil, Gas and Geothermal Resources, 1998, California Oil and Gas Fields, Volume–I - Central California: California Department of Conservation.

California Resources Corporation, 2019, Kern Front Vedder UIC Application, Appendix 3D. https://geotracker.waterboards.ca.gov/uic_project_tracking_report. Accessed October 4, 2023.

California Water Boards, 2023, GeoTracker. https://geotracker.waterboards.ca.gov/map/?CMD=runreport&myaddress=kern+county. Accessed September 19, 2023.

California Water Boards, 2023, Ground Water Ambient Monitoring and Assessment Program (GAMA). Groundwater Information System. https://www.waterboards.ca.gov/water_issues/programs/gama/. Accessed October 3, 2023.

Coburn, M.G., and J.M. Gillespie, 2002 A hydrogeologic study to optimize stream flood performance in a giant oilfield: Kern River Field, California: American Association of Petroleum Geologists Bulletin, v. 86, n. 8, p. 1489-1505.

Jairam Kamath, Frank Nakagawa, Josephina Schembre, Tom Fate, Ed deZabala, Padmakar Ayyalasomayajula, Chevron, CORE BASED PERSPECTIVE ON UNCERTAINTY IN RELATIVE PERMEABILITY, International Symposium of the Society of Core Analysts, Toronto, Canada, 21-25 August 2005.

Jerauld, G.R., 1997, General Three-Phase Relative Permeability Model for Prudhoe Bay, Society of Petroleum Engineers.

Jerauld, G.R, and Rathmell, J.J., 1997, Wettability and relative permeability of Prudhoe Bay: A case study in mixed-wet reservoirs. United States: N., p., Web. doi:10.2118/28576-PA.

Kamath, J., Nakagawa, F., Schembre, J., Fate, T., deZabala, E., Ayyalasomayajula, P., 2005, Core Based Perspective on Uncertainty in Relative Permeability, International Symposium of the Society of Core Analysts, Toronto, Canada.Killough, J.E., 1976, Reservoir Simulation With History-Dependent Saturation Functions, Society of Petroleum Engineers Journal.

Land, C.S., 1968, Calculation of Imbibition Relative Permeability for Two- and Three-Phase Flow From Rock Properties, Society of Petroleum Engineers.

Manzocchi, T., Walsh, J.J., Nell, P., and Yielding, G., 1999, Fault transmissibility multipliers for flow simulation models: Petroleum Geoscience, v. 5, p. 53-63.

McBride-Wright, M., Maitland, G..C, Trusler, J.P.M., 2015, Viscosity and Density of Aqueous Solutions of Carbon Dioxide at Temperatures from (274 to 449) K and at Pressures up to 100 MPa, Journal of Chemical Engineering Data.

McCutcheon, S.C., Martin, J.L., Barnwell, T.O, Jr., 1993, Water Quality, Maidment, D.R. (Editor), Handbook of Hydrology, McGraw-Hill, New York, N. Chapter 11.

Nicot, J.P., Oldenburg, C.M., Bryant, S.L., & Hovorka, S.D., 2008, Pressure perturbation from geologic carbon sequestration: Area-of-review boundaries and borehole leakage driving forces, Energy Procedia.

Saleeby, J., Saleeby, Z., and Le Pourhiet, L., 2013, Epeirogenic transients related to mantle lithosphere removal in the southern Sierra Nevada region: Part II. Implications of rock uplift and basin subsidence relations: Geosphere, doi:10.1130/GES00816.1.

Saleeby, J., Saleeby, Z., and Le Pourhiet, L., 2013a, Epeirogenic transients related to mantle lithosphere removal in the southern Sierra Nevada region, California, Part II: Implications of rock uplift and basin subsidence relations: Geosphere, v. 9, n. 3, p. 394–425, doi.org/10.1130/GES00816.1.

Saleeby, J., Saleeby, Z., and Sousa, F., 2013b, From deep to modern time along the western Sierra Nevada Foothills of California, San Joaquin to Kern River drainages, *in* Putirka, K., ed., Geologic Excursions from Fresno, California, and the Central Valley: Geological Society of America Field Guide 32, p. 37–62, doi.org/10.1130/2013.0032(03).

Schloss, J., Long, W., and Van Grinsven, M., 2019. Water Well Capture Radius Analysis Update, Kern River Aquifer Exemption: Water Wells and Completion Information. Division of Oil, Gas, and Geothermal Resources (DOGGR) Memorandum.

Sheehan, J.R., 1986, Tectonic evolution of the Bakersfield Arch, Kern County, California, *in* Bell, P., ed., Southeast San Joaquin Valley Field Trip, Kern County, California Part II: Structure and Stratigraphy, Pacific Section American Association of Petroleum Geologists, p. 10-17.Wagner, W., and Pruß, A., 2002, The IAPWS Formulation 1995 for

the Thermodynamic Properties of Ordinary Water Substance for General and Scientific Use, Journal of Physical Chemistry Reference Data, Vol. 31, No. 2.

Yang, A.P., Eacmen, J.C., 2003, Fault Identification and Modeling for Production Enhancement. SPE-83495-MS. https://doi.org/10.2118/83495-MS.

Z. Ziabakhsh-Ganji, H. Kooi, 2012, An Equation of State for thermodynamic equilibrium of gas mixtures and brines to allow simulation of the effects of impurities in subsurface CO2 storage, International Journal of Greenhouse Gas Control, Volume 11, Supplement, Pages S21-S34, ISSN 1750-5836, https://doi.org/10.1016/j.ijggc.2012.07.025.

Appendix 1: AoR Maps and Well Lists

Chevron performed a comprehensive search of the AoR to identify and map the features required for consideration by the program director within and directly adjacent to the AoR. A search of the California Department of Conservation's "Mines Online" map showed that there are no active or abandoned mines or quarries in our AoR (California Department of Conservation, 2023). A review of California's EnviroStor and GeoTracker databases indicated that there are no state or federal subsurface cleanup sites in our AoR (California Department of Toxic Substances Control, 2023, California Water Boards, 2023a). There are no state, tribal, or territorial boundaries within the AoR. Bodies of water are shown in **Figure 58** below (California Department of Fish and Wildlife, 2023). There are no springs within the AoR.

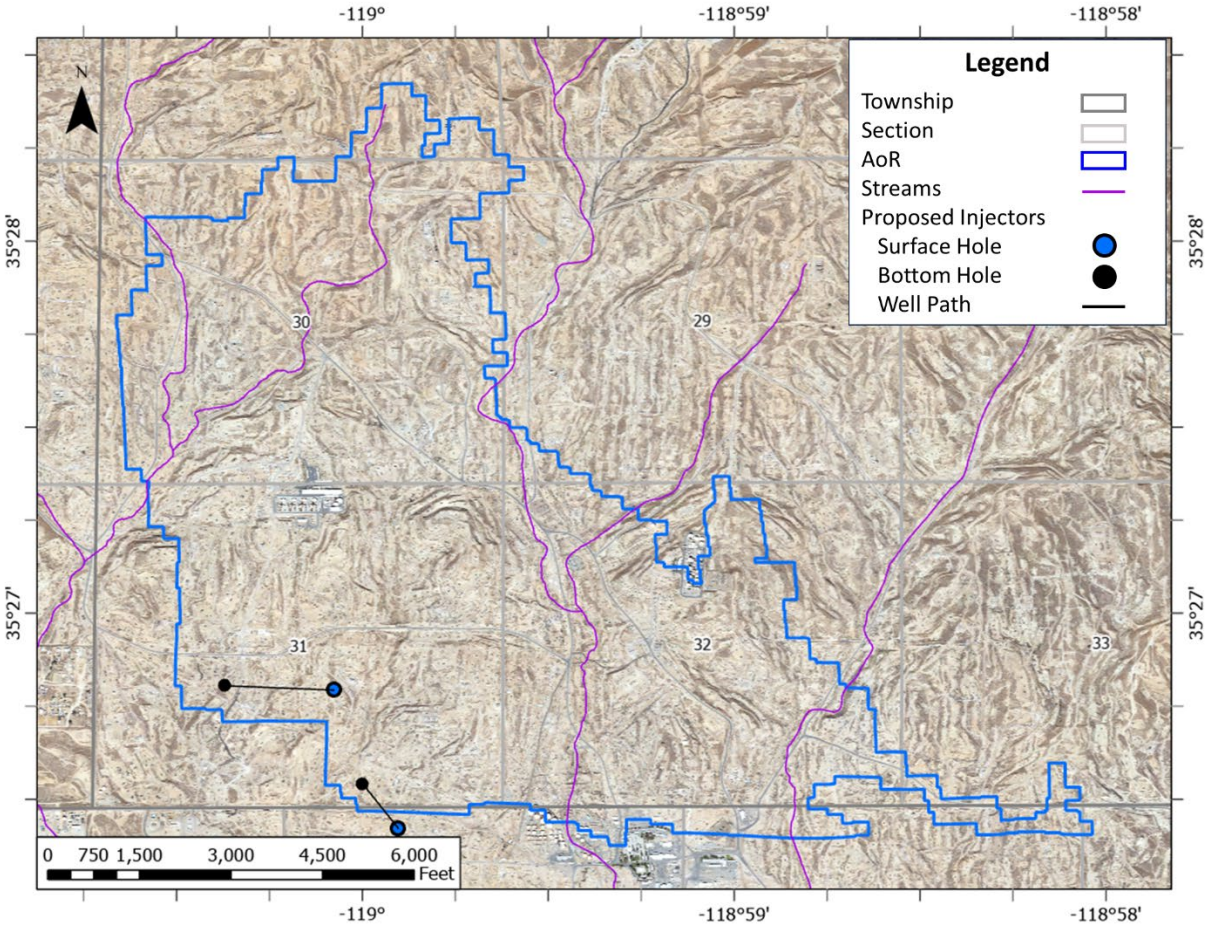

Figure 58: Bodies of water within and adjacent to the AoR (California Department of Fish and Wildlife, 2023).

Structures for human occupancy are shown in **Figure 59** and roads are mapped in **Figure 60**. The roads in the Kern River Oil Field are private and access is controlled by gates at all entrances.

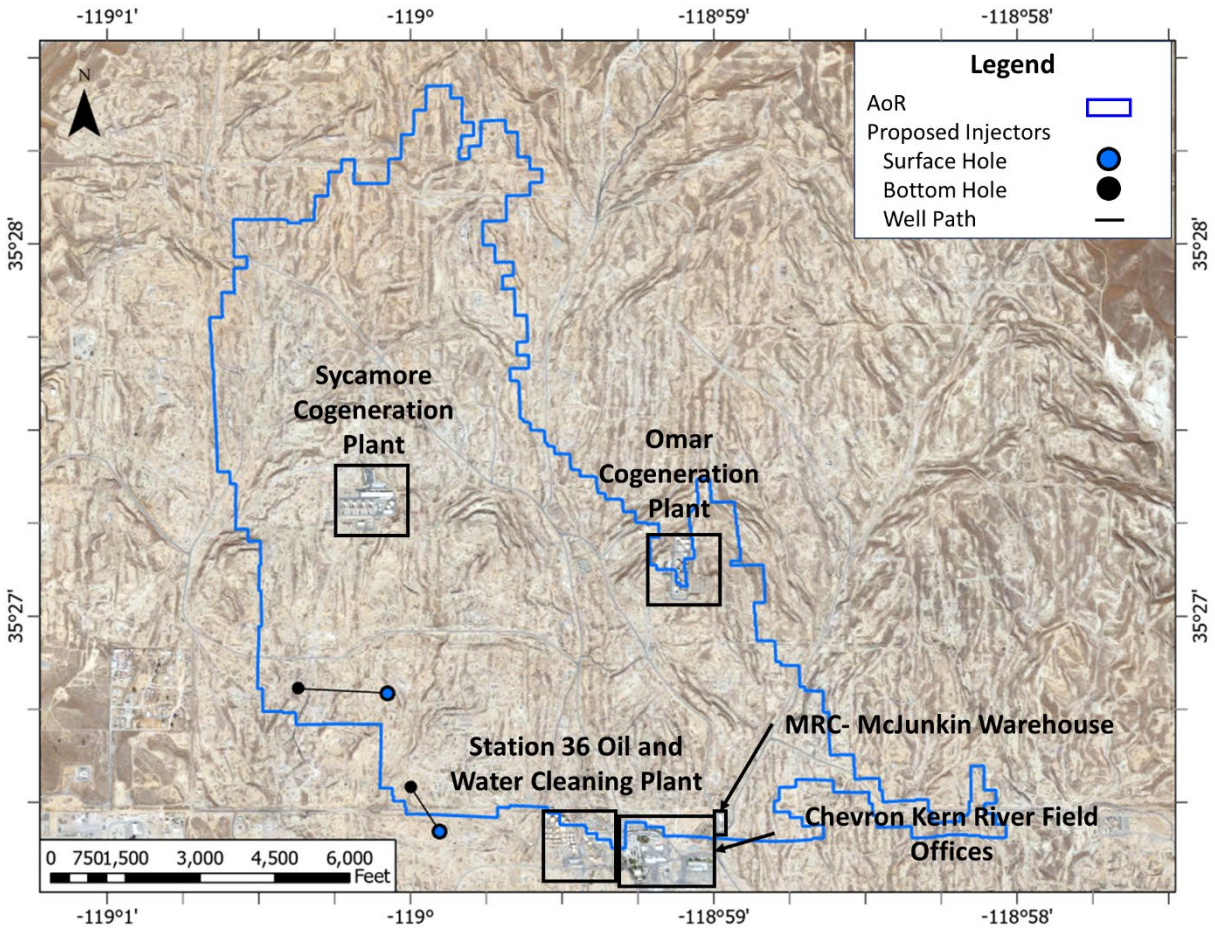

Figure 59. Structures for Human Occupancy in the AoR

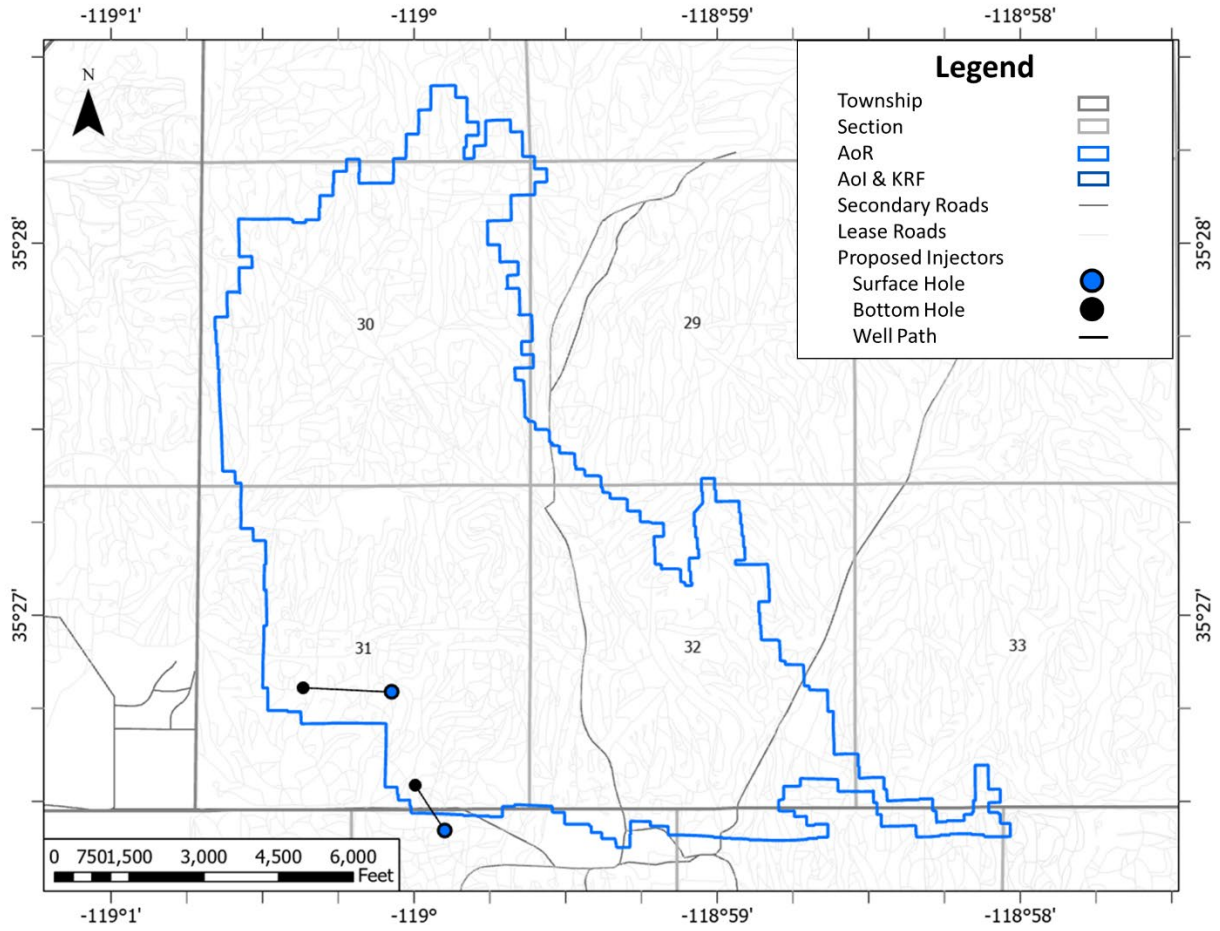

Figure 60. Roads in the AoR. All roads in the AoR are private with controlled gated entrances to the Kern River Field.

Water wells were evaluated using the California Department of Geologic and Geothermal Resources Memorandum of December 18, 2018 identifying all active water wells in the Kern River field as a baseline (Schloss et al., 2019). The list was then compared against the databases of the California Department of Water Resources (DWR) and the California Water Boards Groundwater Ambient Monitoring and Assessment (GAMA) Program (California Department of Water Resource, 2023; California Water Boards, 2023b). There are no active water source wells within the AoR. The nearest active groundwater wells and destroyed wells from DWR are presented in **Figure 61.** The destroyed wells from the DWR are listed in **Table 18**. Many of the destroyed wells in DWR's database are only located to the center of the nearest section. The deepest active water well recorded in the vicinity of the AoR is only ~800 ft deep and the deepest destroyed well in or near the AoR is ~1,900 ft deep, significantly shallower than the target injection zone and primary confining layer.

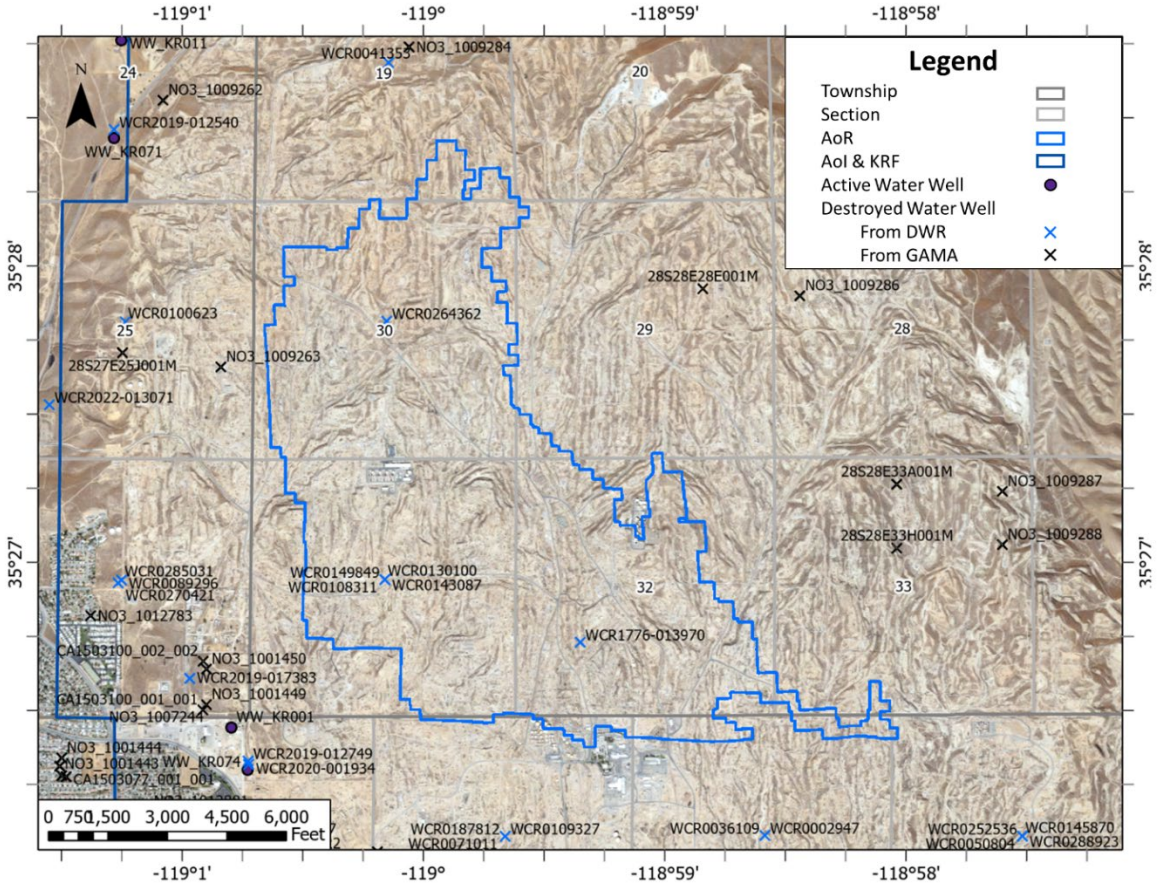

Figure 61. Destroyed water source wells within the AoR and nearest active water source wells outside the AoR. (Data are from Schloss et al., 2019; California Department of Water Resources, 2023; California Water Boards, 2023b)

Table 18. California Department of Water Resources data on destroyed wells that are or potentially within the AoR. Locations for many of the wells are only known to the center of the Section they are in, so we included all wells posted at the center of any section the AoR entered (California Department of Water Resources, 2023).

DWR ID Number	Legacy Well ID	Permit Number	Well Purpose	Status	Latitude	Longitude	Location Accuracy	Township and Range	Section	APN	Work Completion Date	Total Completion (ft md)	Top Perf. (ft md)	Base Perf. (ft md)	Data Source
WCR0130100	NN	None	Unknown	Presumed Destroyed	35.44852	-119.00268	Centroid of Section	28S 28E	31	--	--	800	0	0	DWR
WCR1776-013970	E0371580	None	Cathodic Protection	Presumed Destroyed	35.444992	-118.989179		28S 28E	32	--	--	0	0	0	DWR
WCR0002947	75148	None	Water Supply Industrial	Presumed Destroyed	35.43412	-118.97642	Centroid of Section	29S 28E	4	--	3/29/1979	50	20	50	DWR
WCR0036109	75147	None	Water Supply Industrial	Presumed Destroyed	35.43412	-118.97642	Centroid of Section	29S 28E	4	--	3/21/1979	80	20	80	DWR
WCR0089297	115339	None	Water Supply Industrial	Presumed Destroyed	35.44852	-119.00268	Centroid of Section	28S 28E	31	--	11/4/1965	756	546	756	DWR
WCR0143087	906644	WP 11404	Cathodic Protection	Presumed Destroyed	35.44852	-119.00268	Centroid of Section	28S 28E	31	436-030-001	12/22/2008	400	0	0	DWR
WCR0149849	500135	EH-135-97	Unknown	Destroyed	35.44852	-119.00268	Centroid of Section	28S 28E	31	093-210-037	6/4/1997	730	421	730	DWR
WCR0108311	78692	None	Water Supply Industrial	Presumed Destroyed	35.44852	-119.00268	Centroid of Section	28S 28E	31	--	9/13/1963	800	340	800	DWR
WCR0248793	500134	EH-136-97	Unknown	Presumed Destroyed	35.44852	-119.00268	Centroid of Section	28S 28E	31	093-210-031	6/4/1997	756	546	756	DWR
WCR0232829	500136	EH-134-97	Unknown	Destroyed	35.44852	-119.00268	Centroid of Section	28S 28E	31	093-210-037	6/4/1997	804	340	804	DWR
WCR0109327	706431	EH-590	Unknown	Destroyed	35.43407	-118.99437	Centroid of Section	29S 28E	5	436-030-002	10/25/2000	0	0	0	DWR
WCR0071011	219157	A450	Water Supply Domestic	Presumed Destroyed	35.43407	-118.99437	Centroid of Section	29S 28E	5	--	2/3/1985	800	500	800	DWR
WCR0041353	63701	None	Water Supply Industrial	Presumed Destroyed	35.4776	-119.00242	Centroid of Section	28S 28E	19	--	10/11/1972	1885	1680	1882	DWR
WCR0234138	115341	None	Water Supply Industrial	Presumed Destroyed	35.44852	-119.00268	Centroid of Section	28S 28E	31	--	12/2/1965	747	327	747	DWR
WCR0264362	NN	None	Unknown	Presumed Destroyed	35.46306	-119.00255	Centroid of Section	28S 28E	30	--	--	0	0	0	DWR
WCR0187812	--	None	Unknown	Presumed Destroyed	35.43407	-118.99437	Centroid of Section	29S 28E	5	--	--	0	0	0	DWR
WCR0145870	559030	EH-057-97	Cathodic Protection	Presumed Destroyed	35.43408	-118.95863	Centroid of Section	29S 28E	3	--	4/9/1997	150	0	150	DWR
WCR0002946	559031	EH-058-97	Cathodic Protection	Presumed Destroyed	35.43408	-118.95863	Centroid of Section	29S 28E	3	--	4/14/1997	150	0	155	DWR
WCR0288923	559038	EH-101-97	Cathodic Protection	Presumed Destroyed	35.43408	-118.95863	Centroid of Section	29S 28E	3	--	5/6/1997	150	0	150	DWR

DWR ID Number	Legacy Well ID	Permit Number	Well Purpose	Status	Latitude	Longitude	Location Accuracy	Township and Range	Section	APN	Work Completion Date	Total Completion (ft md)	Top Perf. (ft md)	Base Perf. (ft md)	Data Source
WCR0252536	559049	EH-137-98	Cathodic Protection	Presumed Destroyed	35.43408	-118.95863	Centroid of Section	29S 28E	3	436-022-007	8/11/1998	160	0	0	DWR
WCR0050804	559033	EH-080-97	Cathodic Protection	Presumed Destroyed	35.43408	-118.95863	Centroid of Section	29S 28E	3	--	4/20/1997	150	0	150	DWR
WCR0304516	559036	EH-091-97	Cathodic Protection	Presumed Destroyed	35.43408	-118.95863	Centroid of Section	29S 28E	3	--	4/29/1997	150	0	150	DWR
WCR0192345	559037	EH-092-97	Cathodic Protection	Presumed Destroyed	35.43408	-118.95863	Centroid of Section	29S 28E	3	--	5/4/1997	150	0	150	DWR
WCR0263409	67470	None	Cathodic Protection	Presumed Destroyed	35.43408	-118.95863	Centroid of Section	29S 28E	3	--	6/4/1972	400	0	0	DWR
WCR0103950	559029	EH-058-97	Cathodic Protection	Presumed Destroyed	35.43408	-118.95863	Centroid of Section	29S 28E	3	--	4/3/1997	150	0	150	DWR
WCR0229334	559035	EH-091-97	Cathodic Protection	Presumed Destroyed	35.43408	-118.95863	Centroid of Section	29S 28E	3	--	4/27/1997	0	0	155	DWR
WCR0313025	906613	WP 10787	Unknown	Destroyed	35.43408	-118.95863	Centroid of Section	29S 28E	3	436-022-001	12/13/2007	0	0	0	DWR
WCR0050805	559039	EH-102-97	Cathodic Protection	Presumed Destroyed	35.43408	-118.95863	Centroid of Section	29S 28E	3	--	5/11/1997	150	0	150	DWR

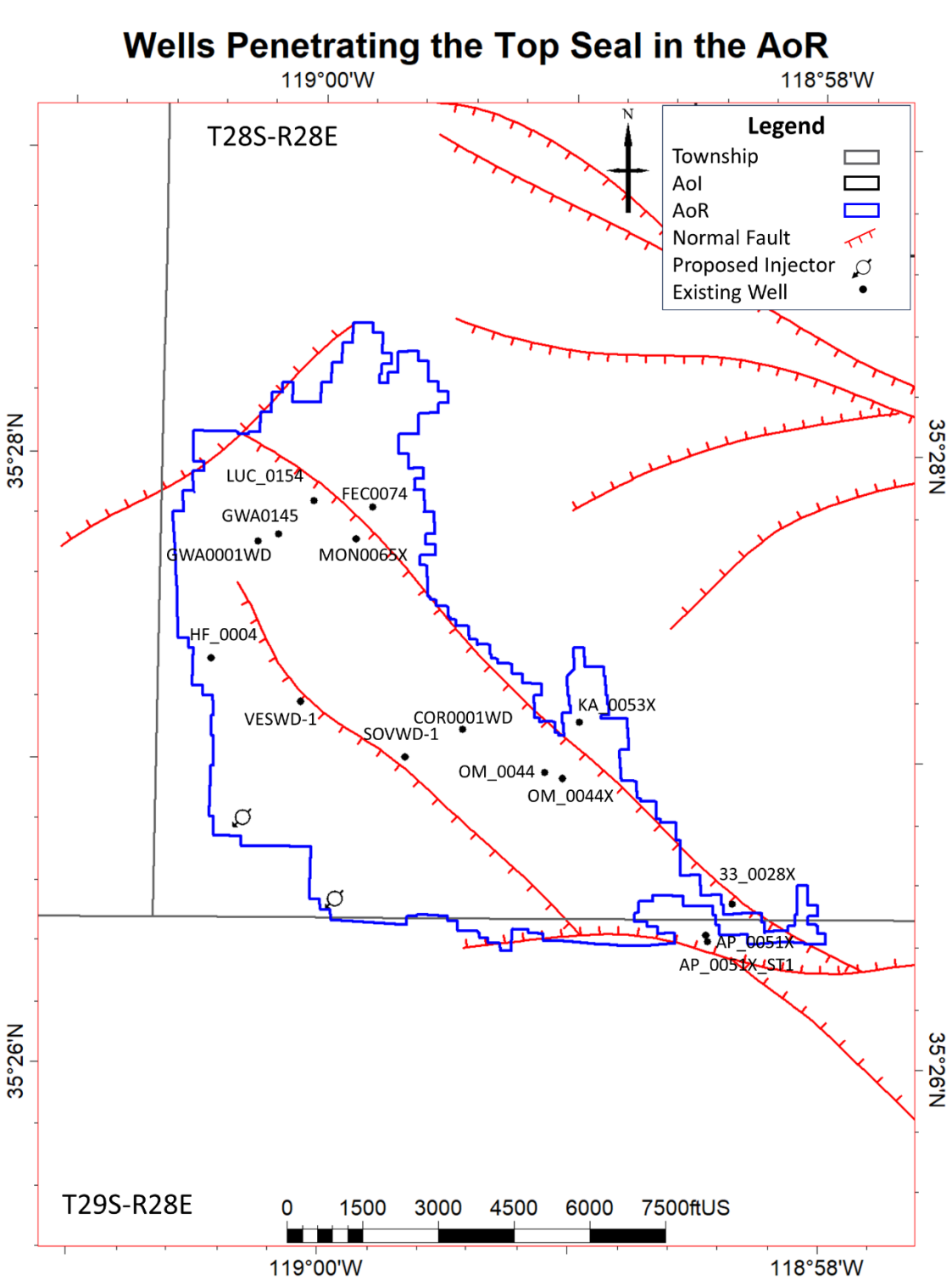

Figure 62. Wells within the AoR that penetrate the top seal (Freeman-Jewett Silt) of the storage complex. Fault intersections are shown at the top of the Vedder Sand.

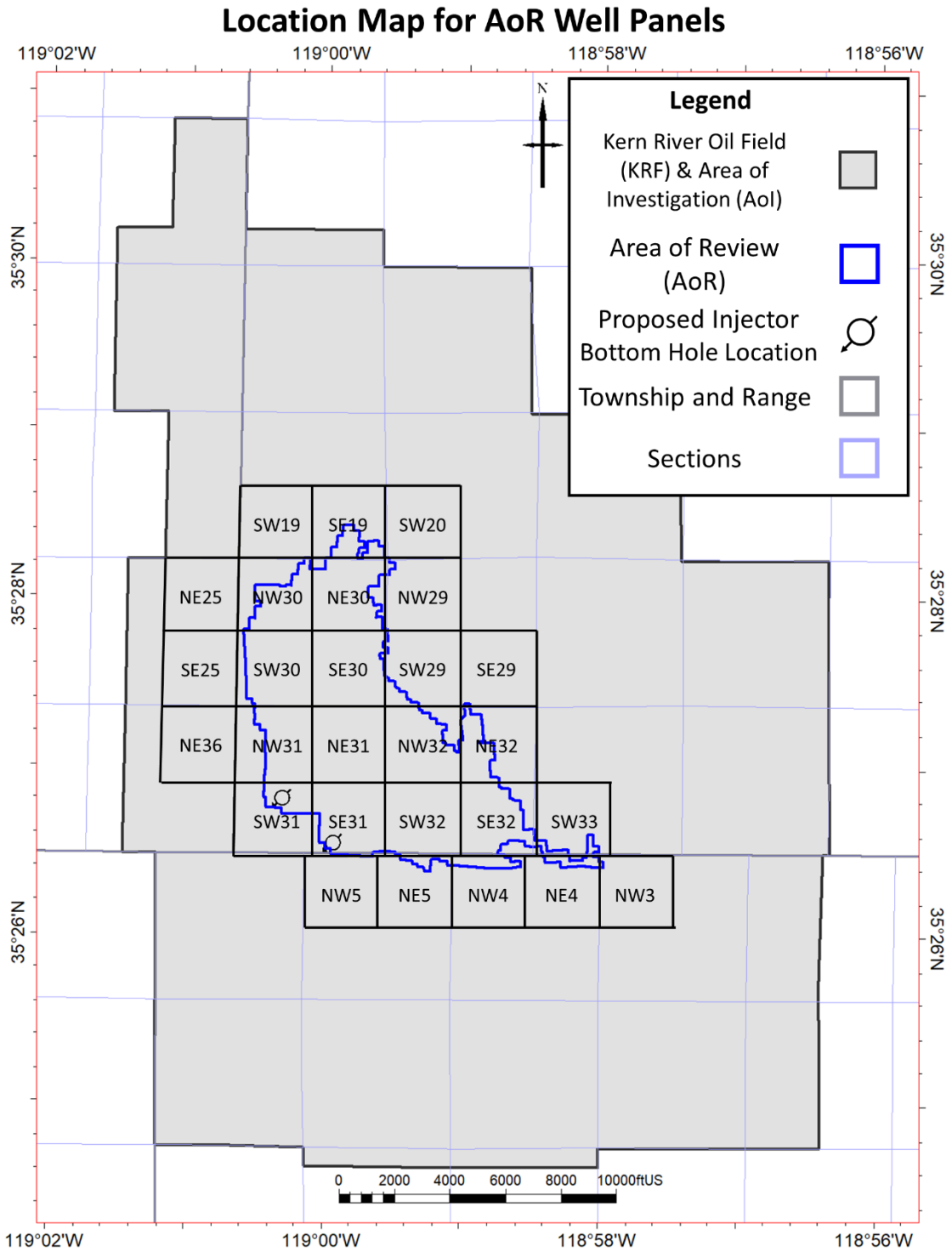

Figure 63. Location map of all quarter section scale maps within and directly adjacent to the AoR (Figures 65-91).

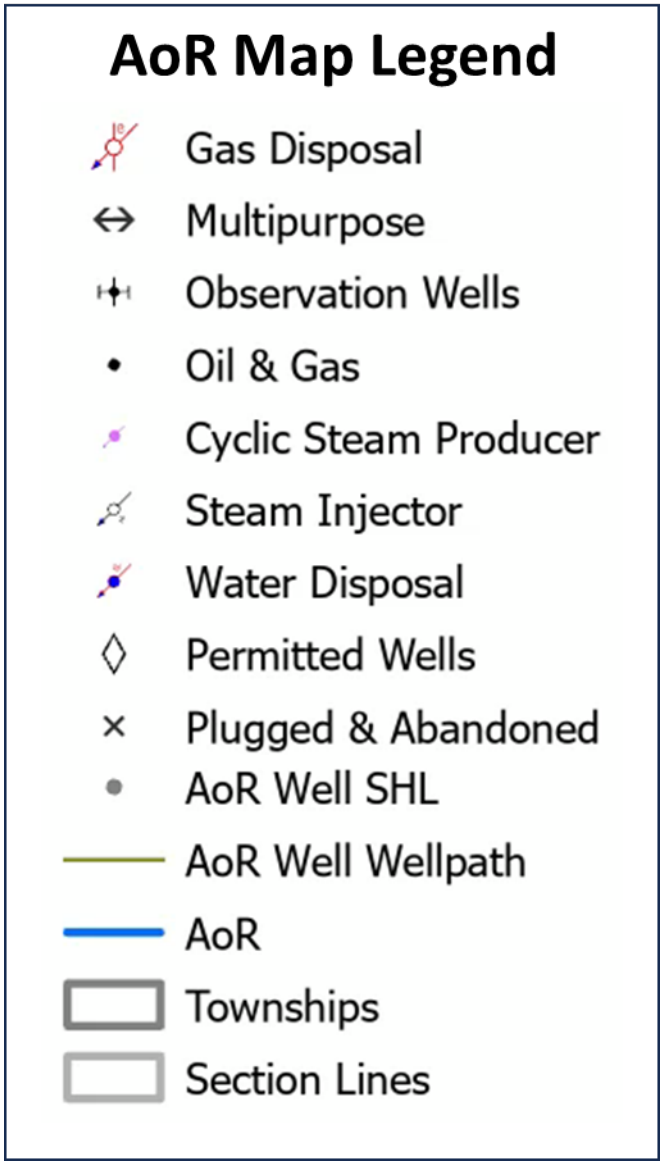

Figure 64. Legend for well types in subsequent **Figure 65** through **Figure 91**.

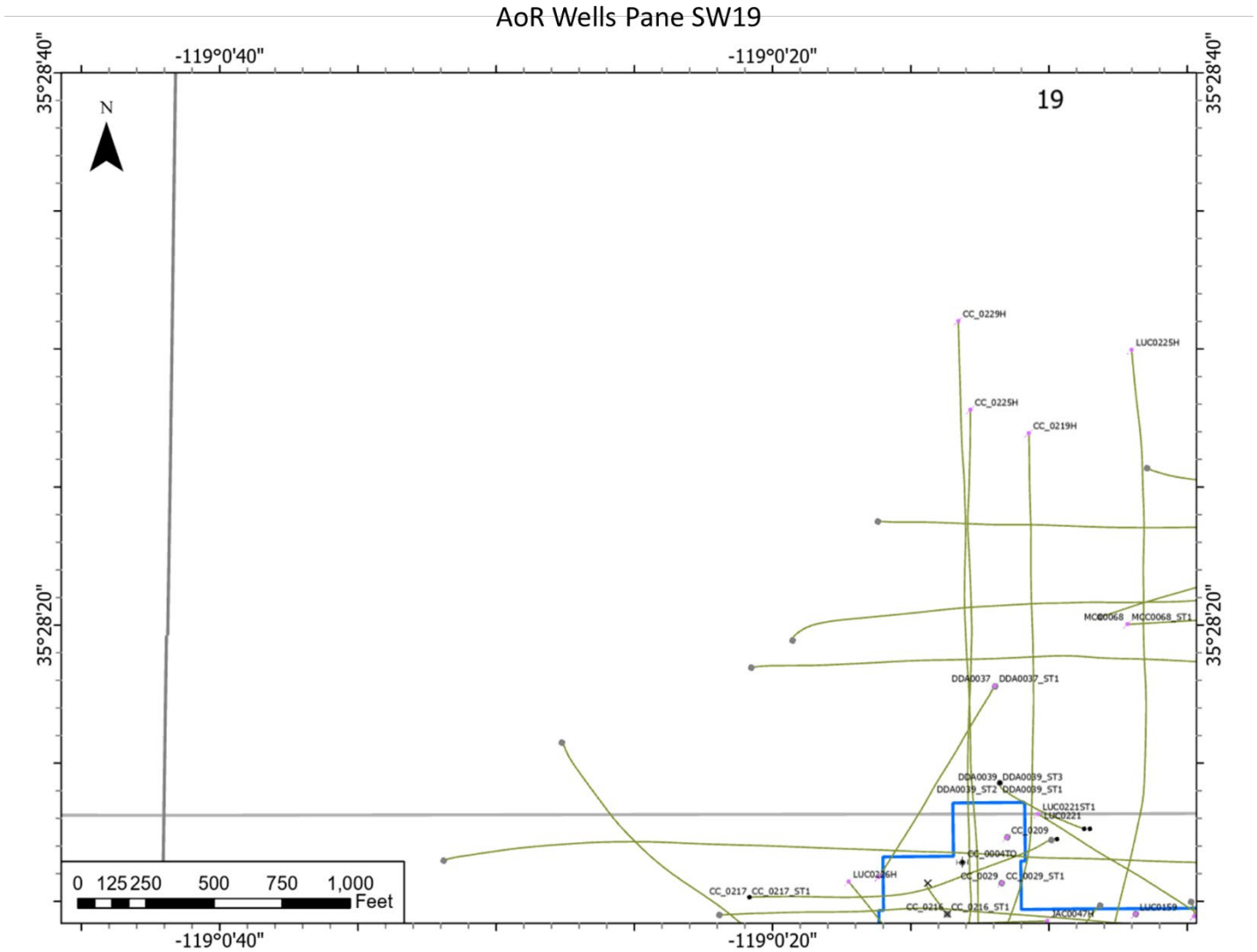

Figure 65. Panel 19SW, showing all wells in the AoR in the southwest quadrant of Section 19. Refer to **Figure 63** for location and **Figure 64** for the legend.

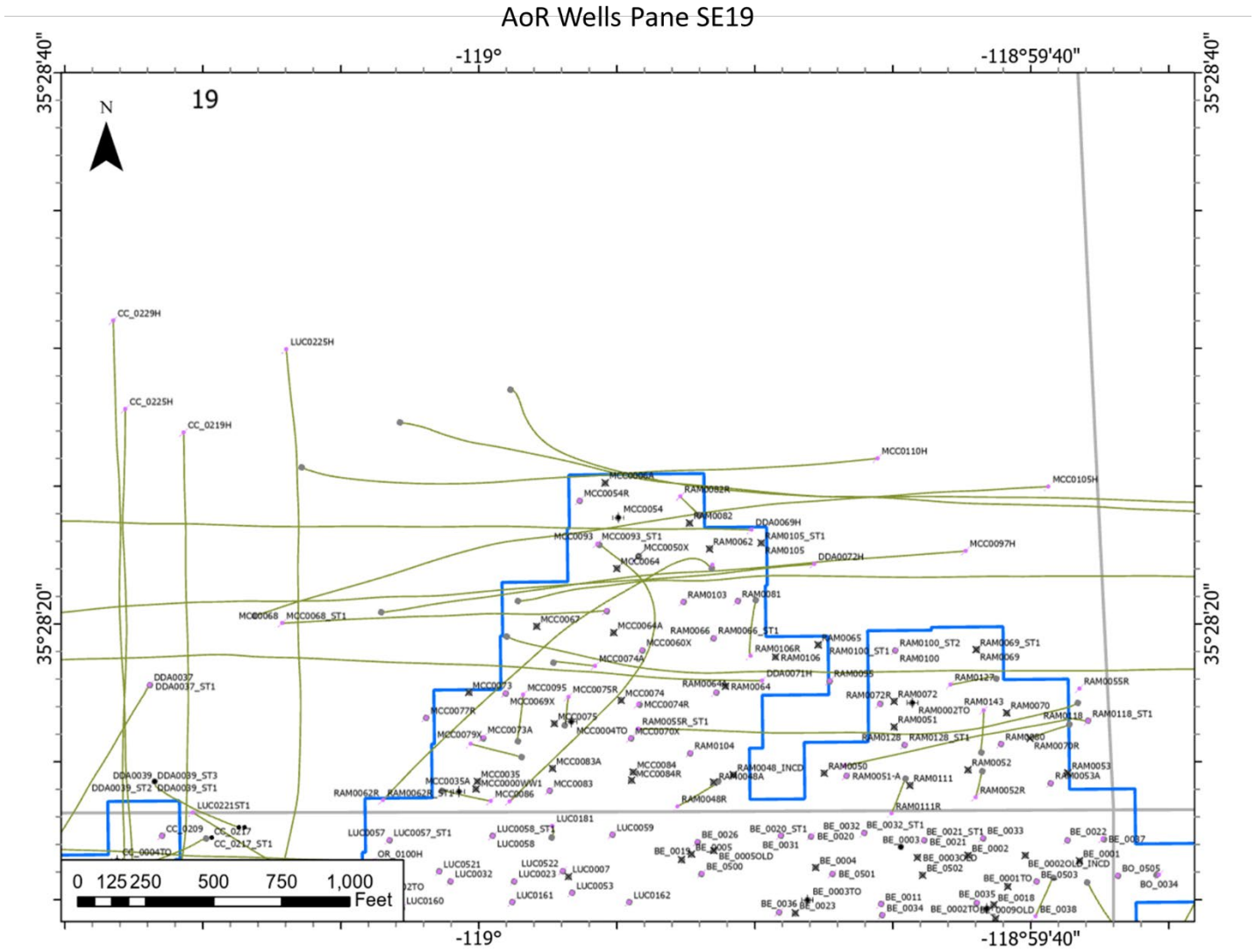

Figure 66. Panel SE20, showing all wells in the AoR in the southeast quadrant of Section 19. Refer to **Figure 63** for location and **Figure 64** for the legend.

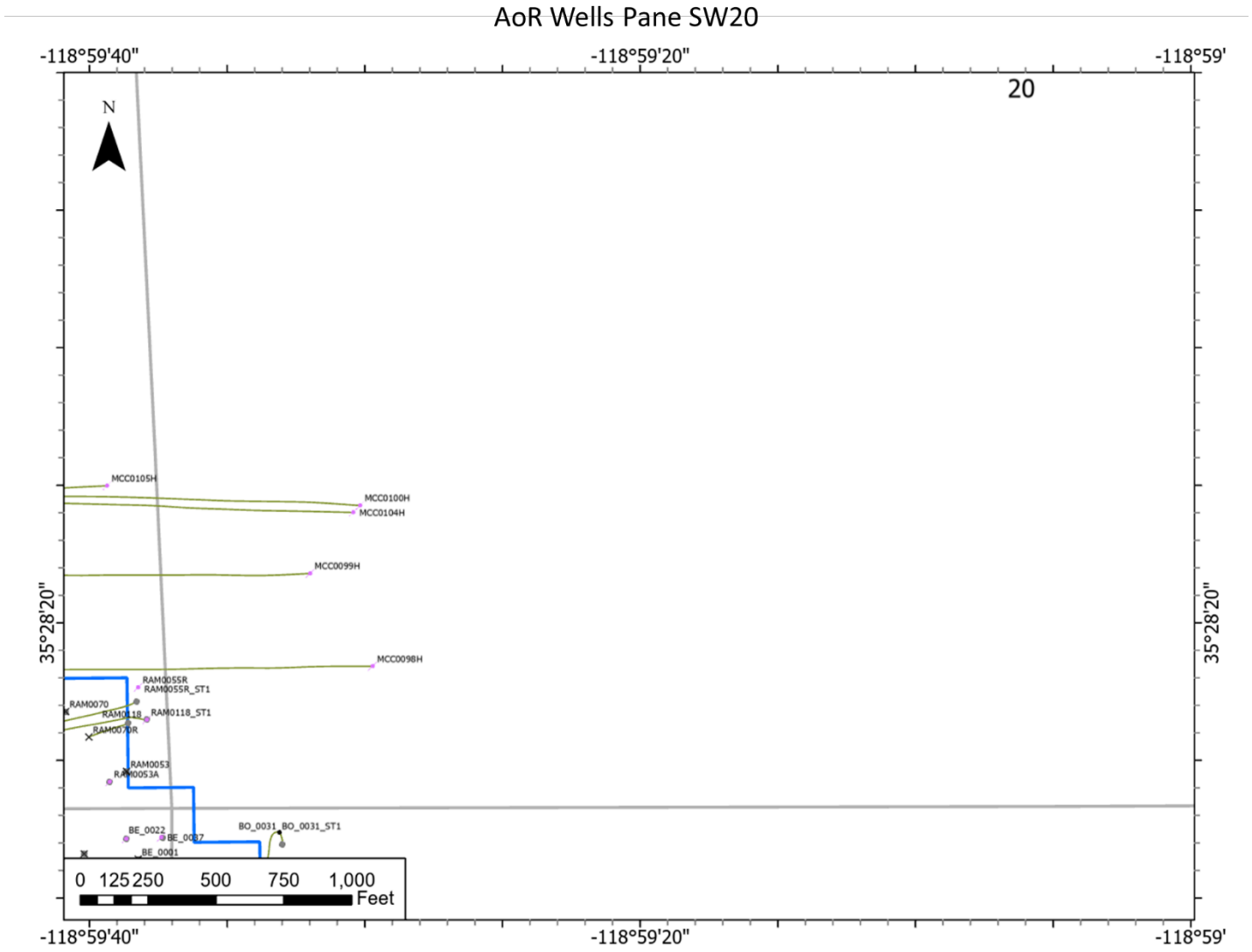

Figure 67. Panel SW20, showing all wells in the AoR in the southwest quadrant of Section 20. Refer to **Figure 63** for location and **Figure 64** for the legend.

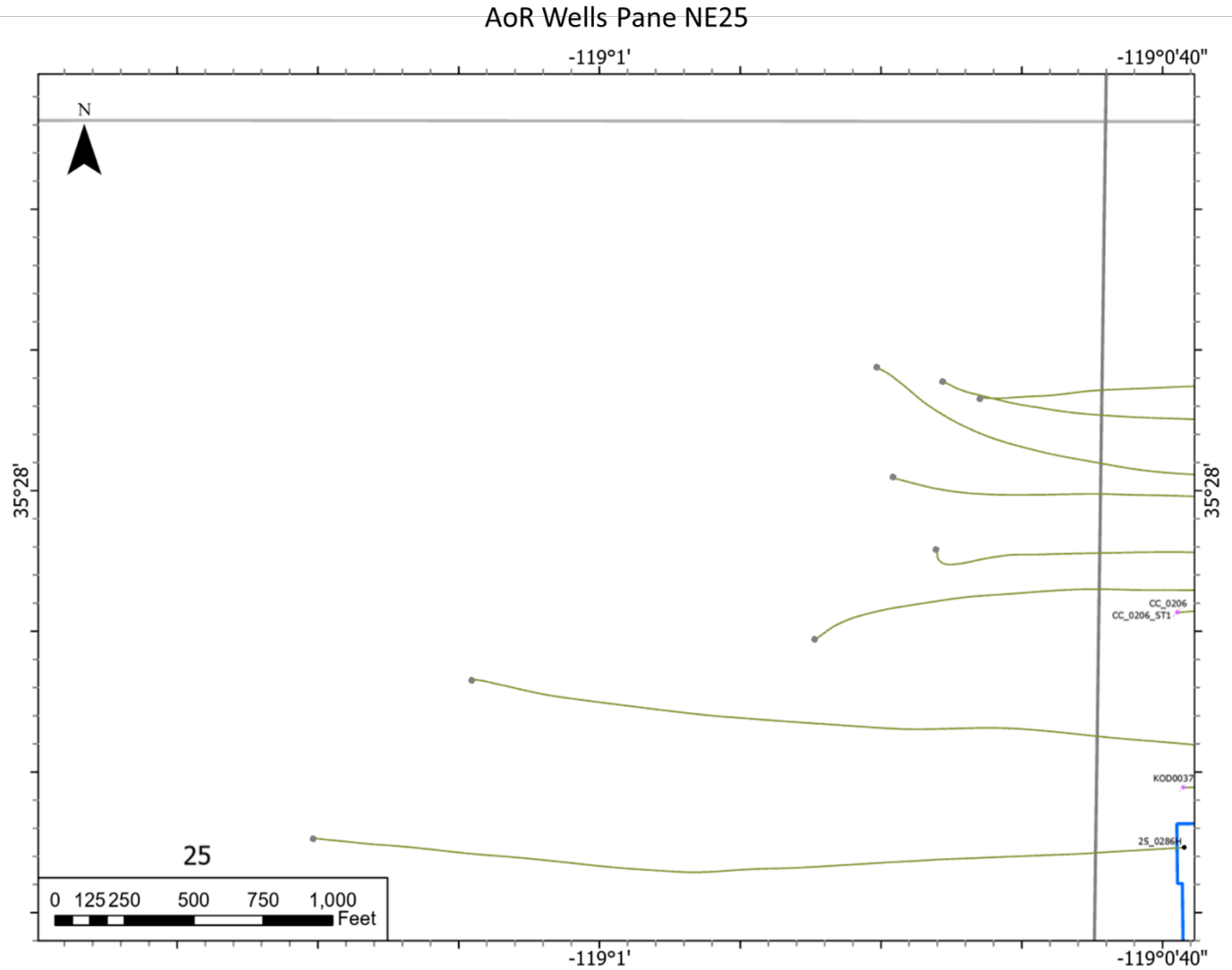

Figure 68. Panel NE25, showing all wells in the AoR in the northwest quadrant of Section 30. Refer to **Figure 63** for location and **Figure 64** for the legend.

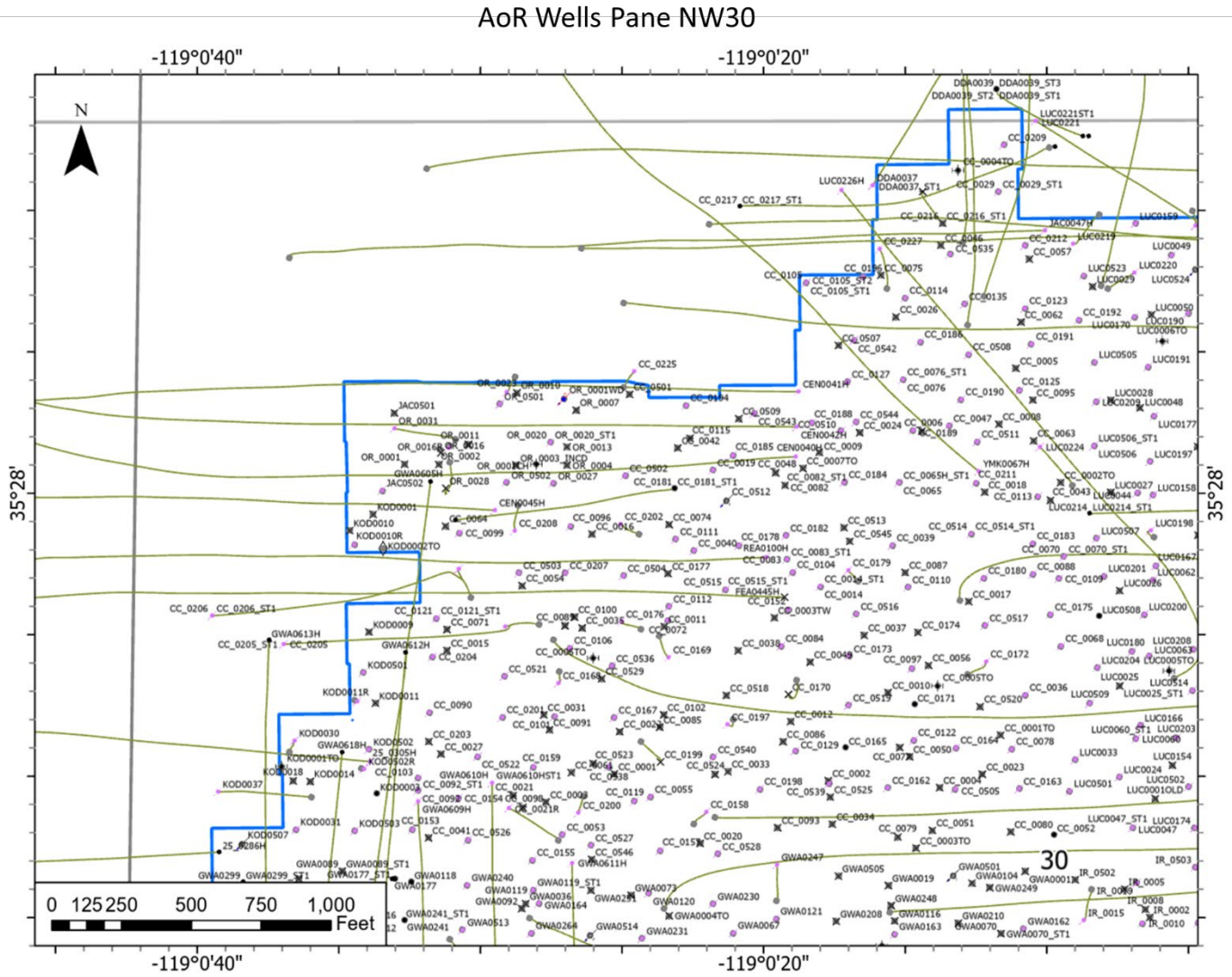

Figure 69. Panel NW30, showing all wells in the AoR in the northwest quadrant of Section 30. Refer to **Figure 63** for location and **Figure 64** for the legend.

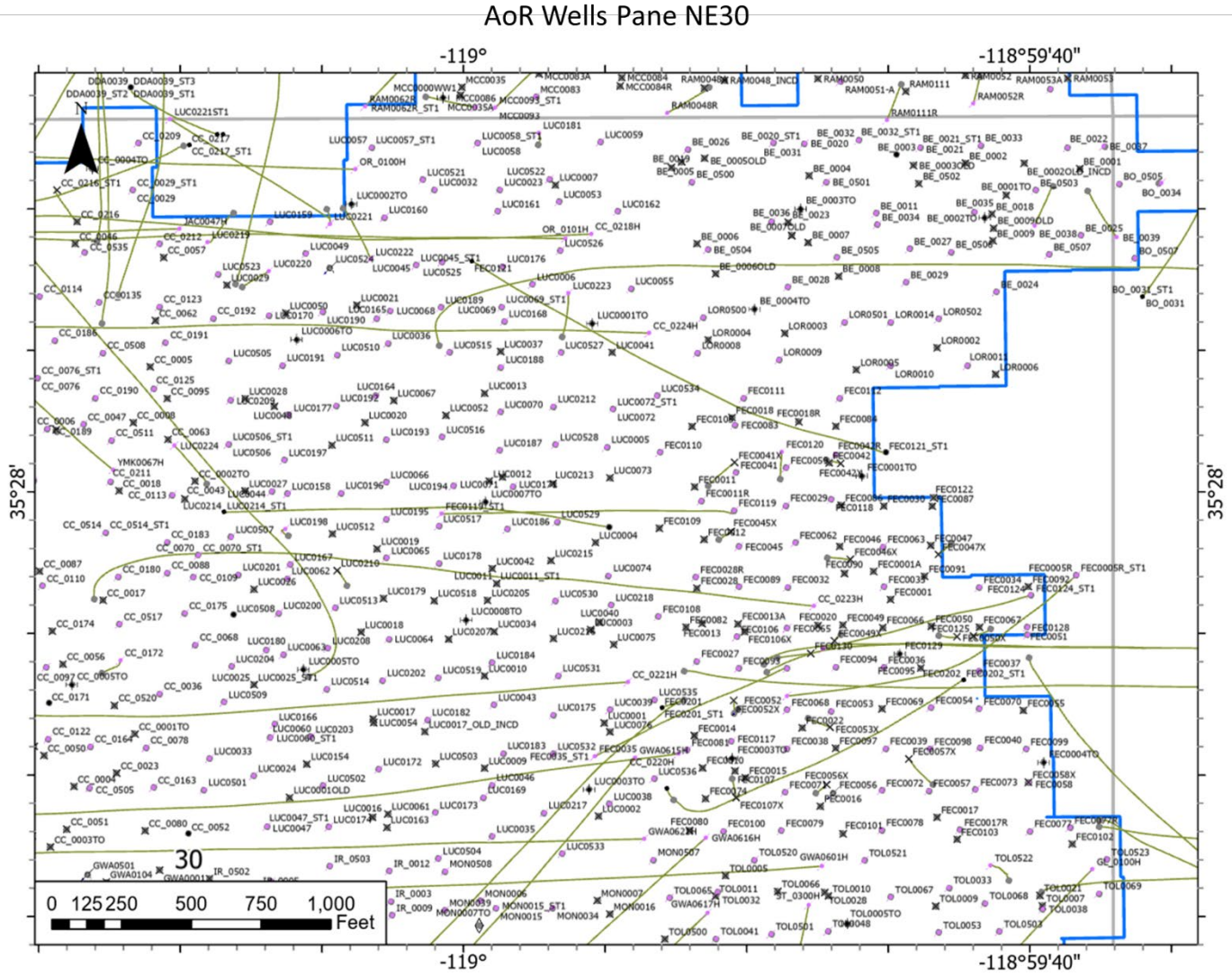

Figure 70. Panel NE30, showing all wells in the AoR in the northeast quadrant of Section 30. Refer to **Figure 63** for location and **Figure 64** for the legend.

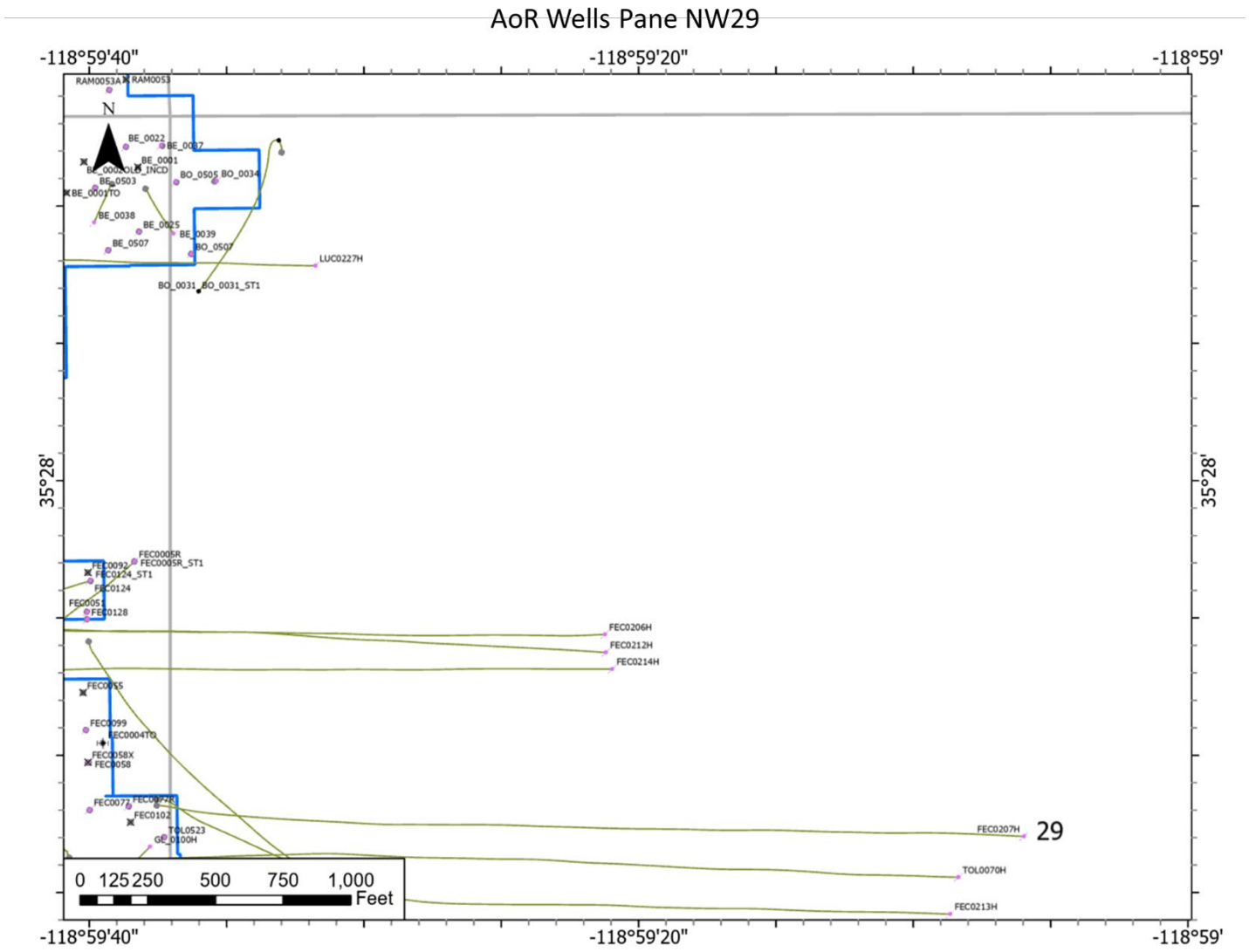

Figure 71. Panel NW29, showing all wells in the AoR in the northwest quadrant of Section 29. Refer to **Figure 63** for location and **Figure 64** for the legend.

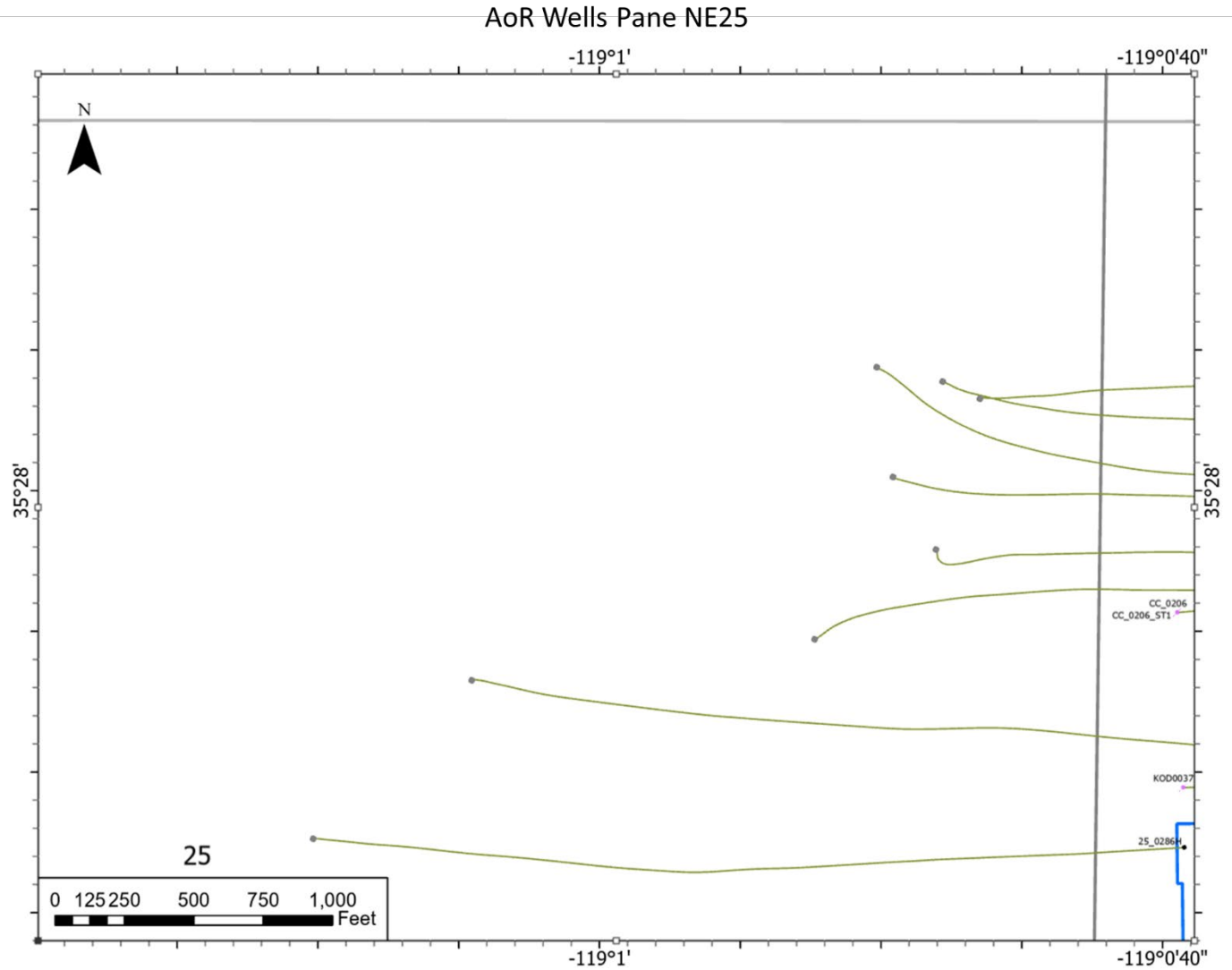

Figure 72. Panel 25NE, showing all wells in the AoR in the northeast quadrant of Section 25. Refer to **Figure 63** for location and **Figure 64** for the legend.

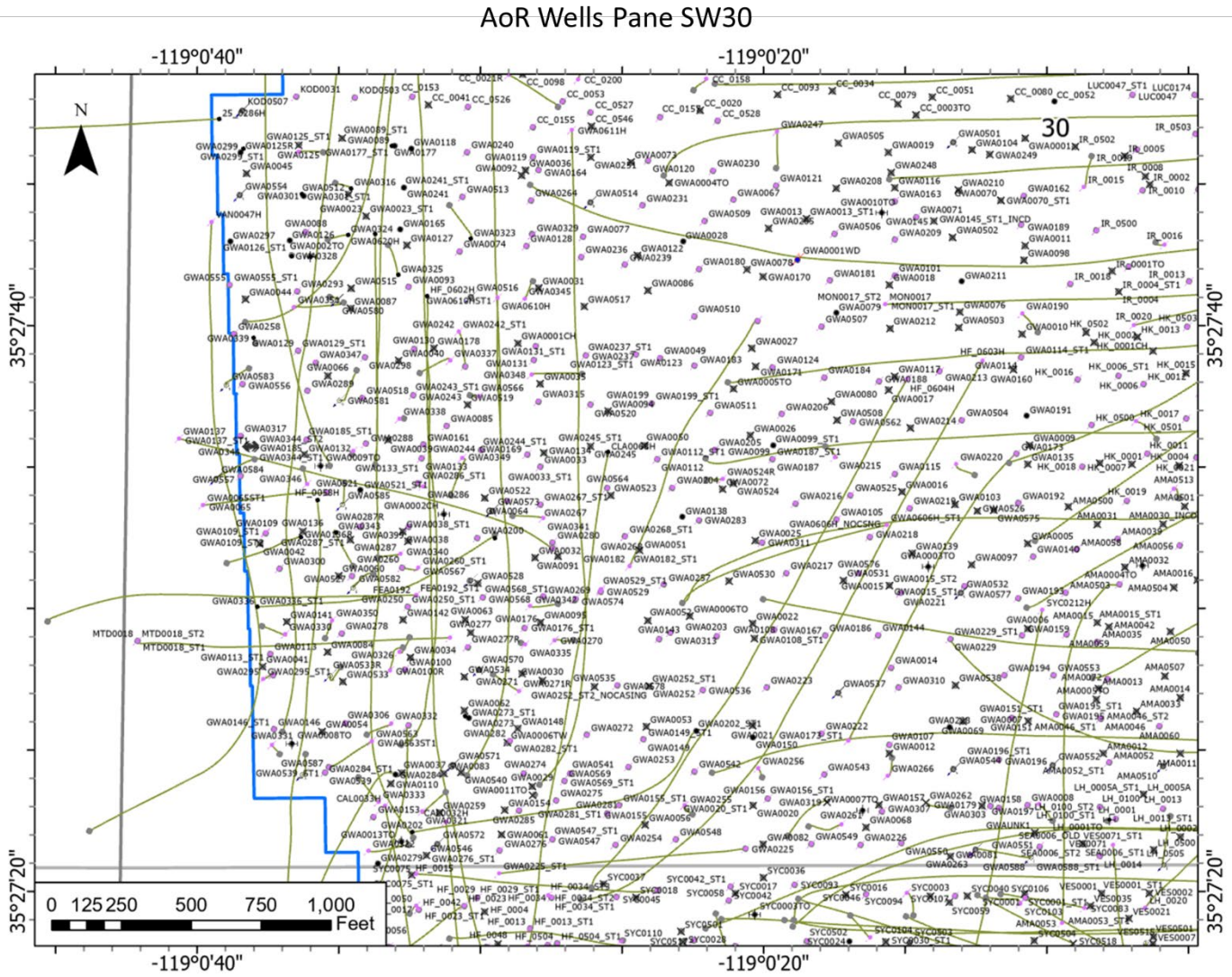

Figure 73. Panel SW30, showing all wells in the AoR in the southwest quadrant of Section 30. Refer to **Figure 63** for location and **Figure 64** for the legend.

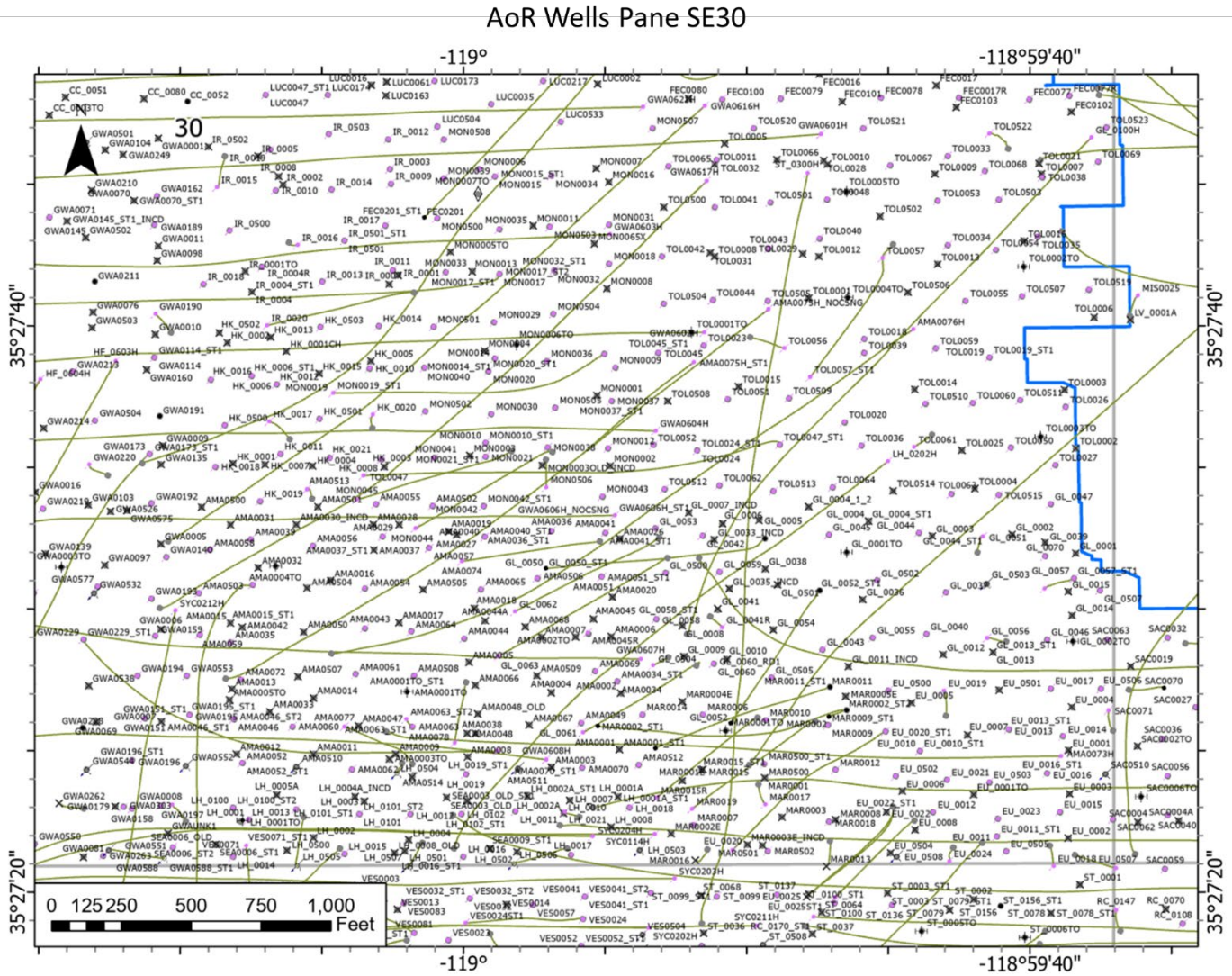

Figure 74. Panel SE30, showing all wells in the AoR in the southeast quadrant of Section 30. Refer to **Figure 63** for location and **Figure 64** for the legend.

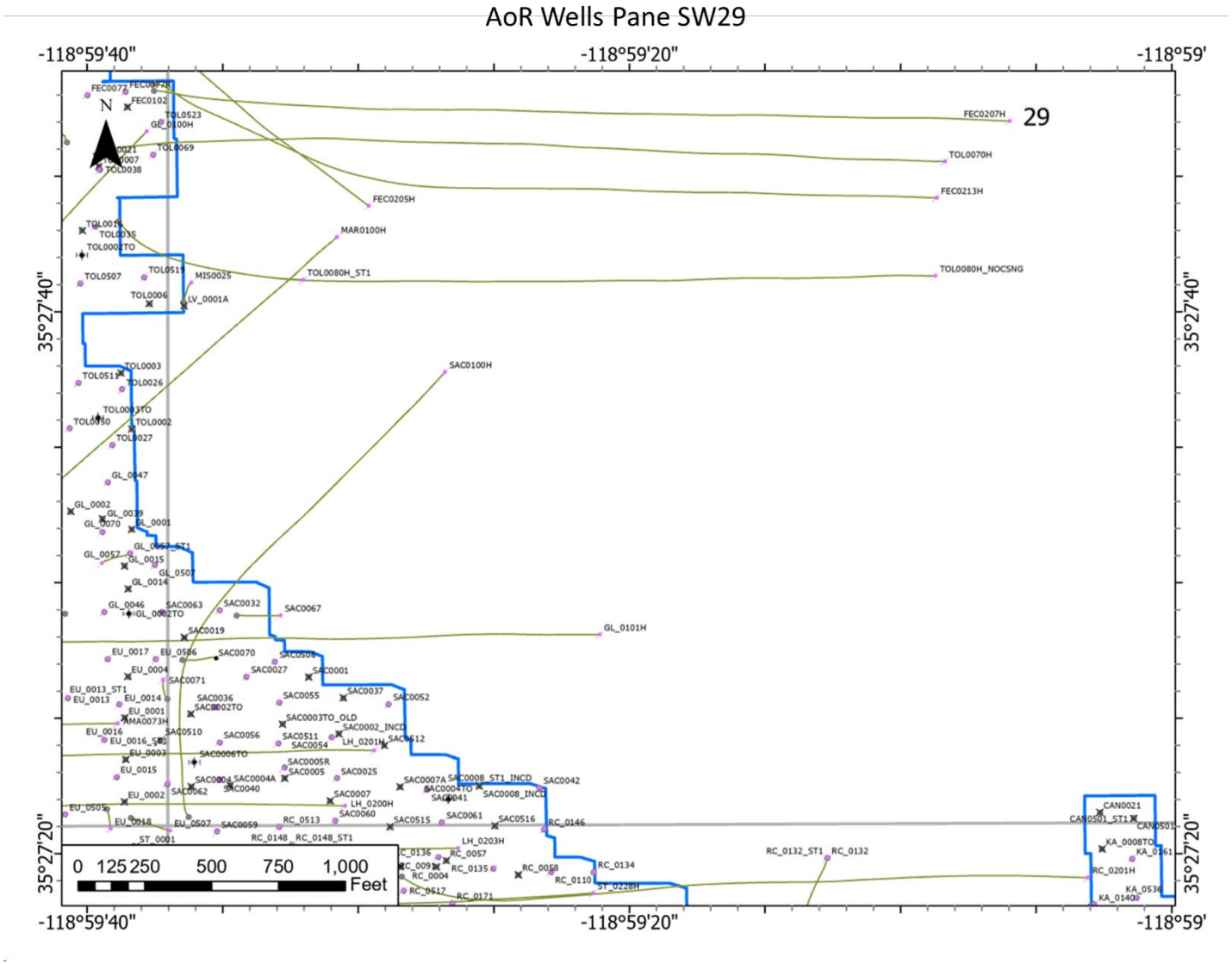

Figure 75. Panel SW29, showing all wells in the AoR in the southwest quadrant of Section 29. Refer to **Figure 63** for location and **Figure 64** for the legend.

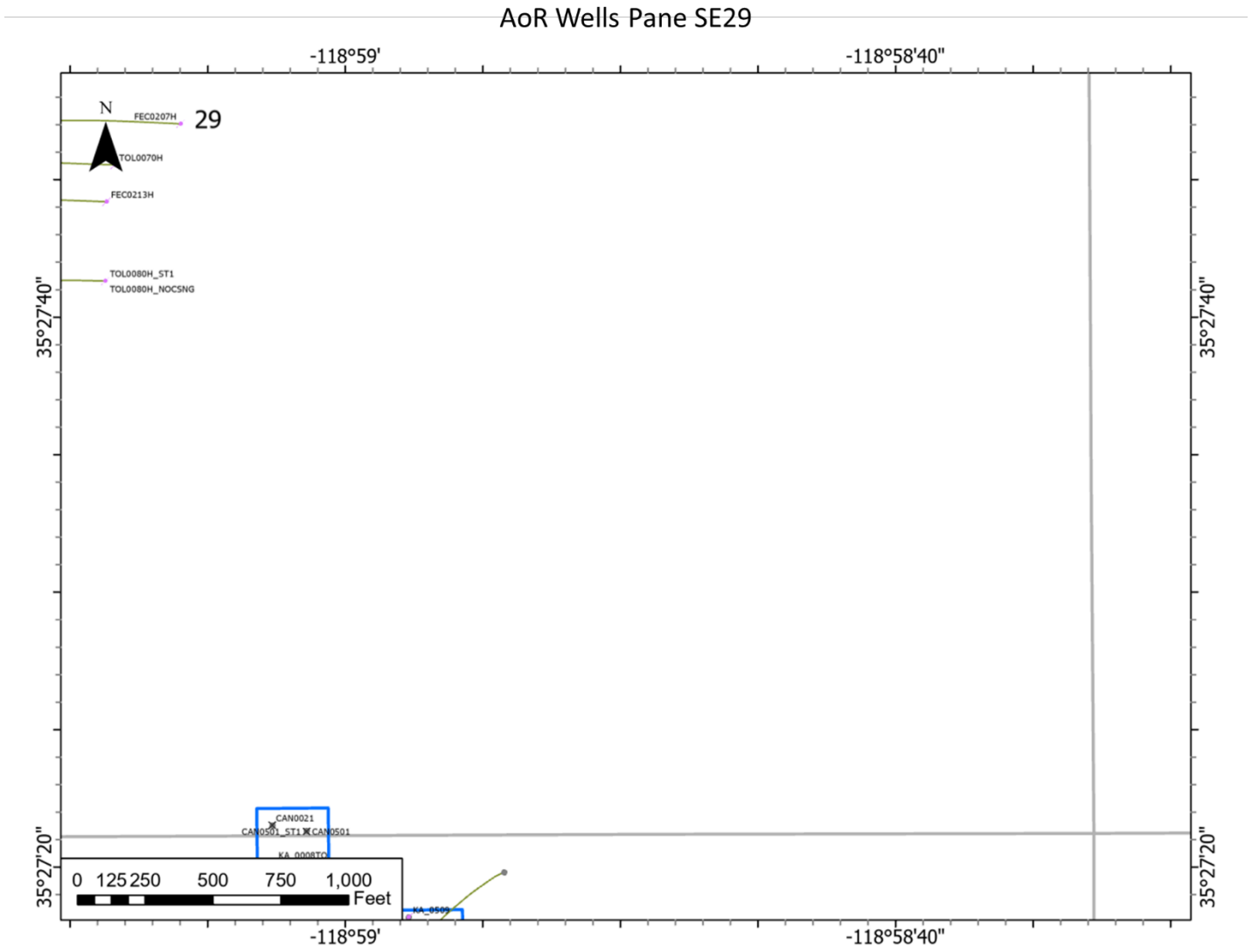

Figure 76. Panel SE29, showing all wells in the AoR in the southeast quadrant of Section 29. Refer to **Figure 63** for location and **Figure 64** for the legend.

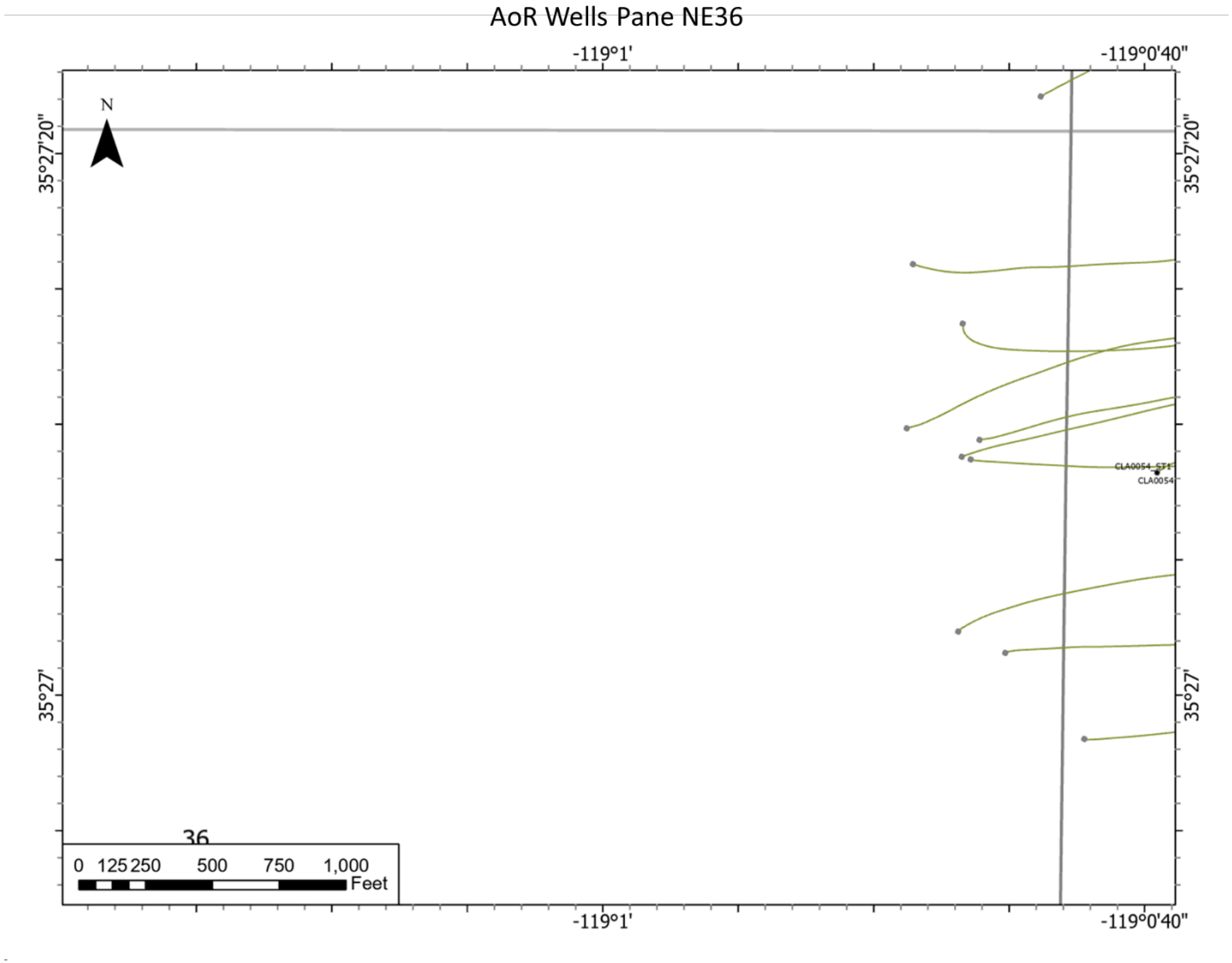

Figure 77. Panel NE36, showing all wells in the AoR in the northeast quadrant of Section 36. Refer to **Figure 63** for location and **Figure 64** for the legend.

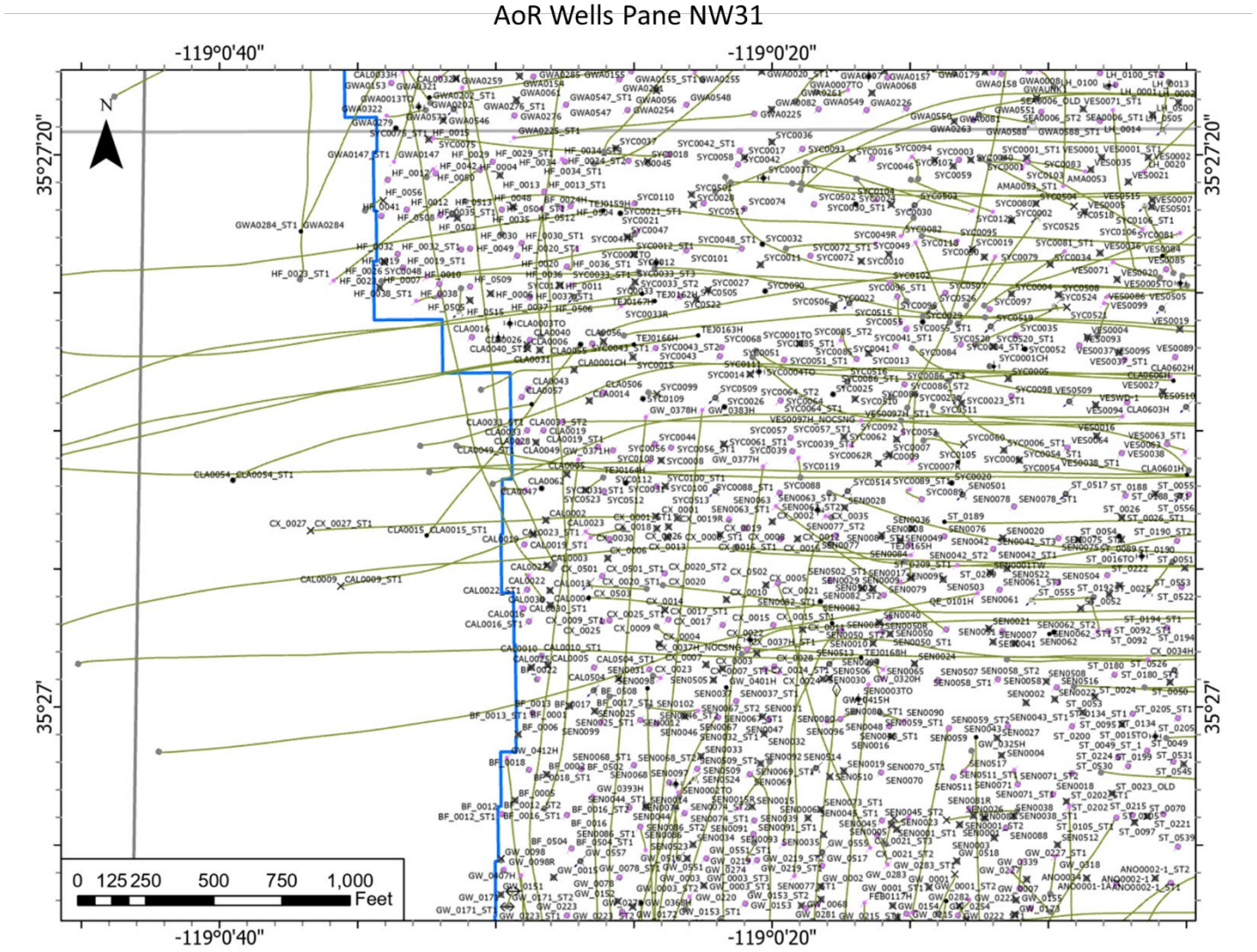

Figure 78. Panel NW31, showing all wells in the AoR in the northwest quadrant of Section 31. Refer to **Figure 63** for location and **Figure 64** for the legend.

Figure 79. Panel NE31, showing all wells in the AoR in the northeast quadrant of Section 31. Refer to **Figure 63** for location and **Figure 64** for the legend.

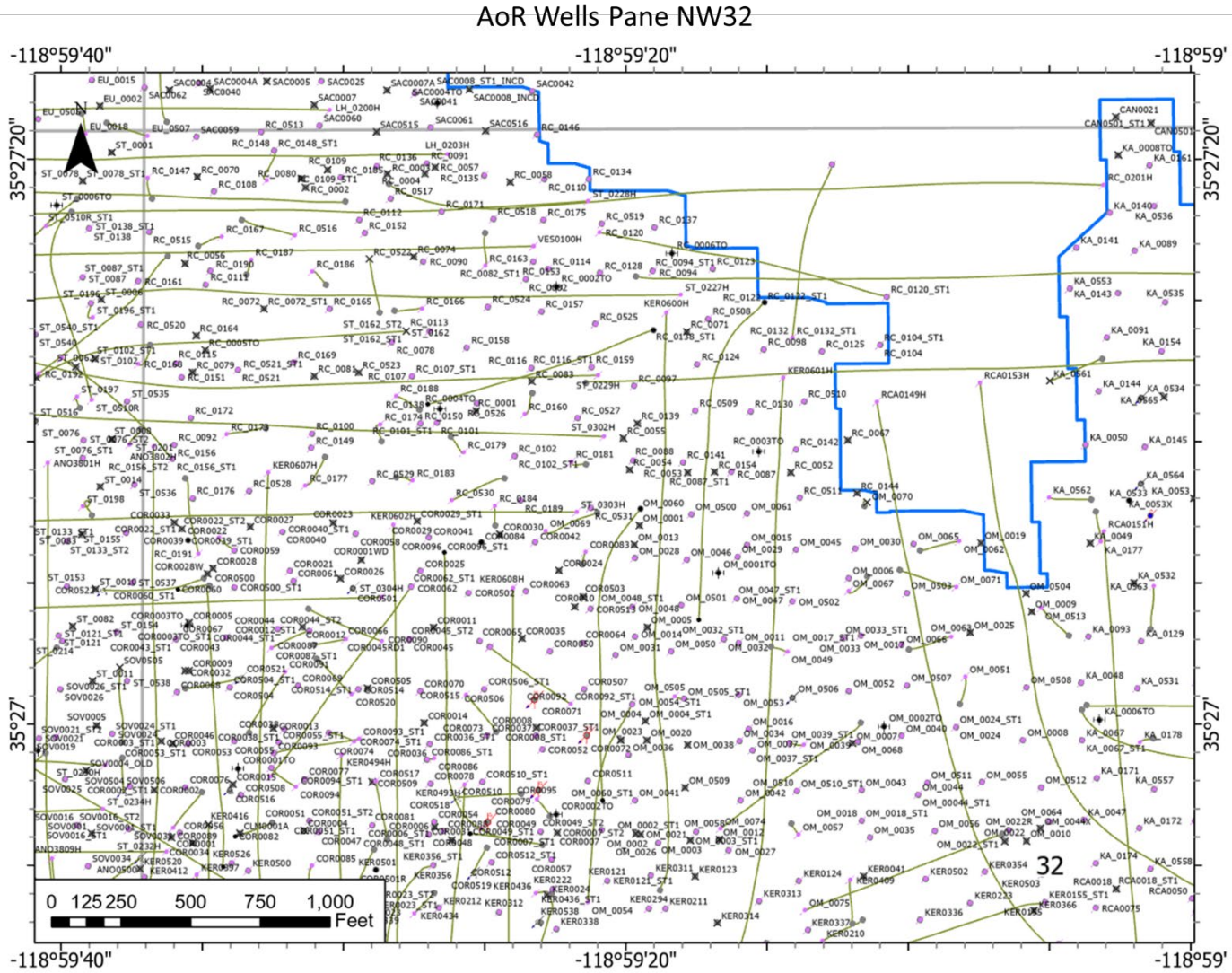

Figure 80. Panel NW32, showing all wells in the AoR in the northwest quadrant of Section 32. Refer to **Figure 63** for location and **Figure 64** for the legend.

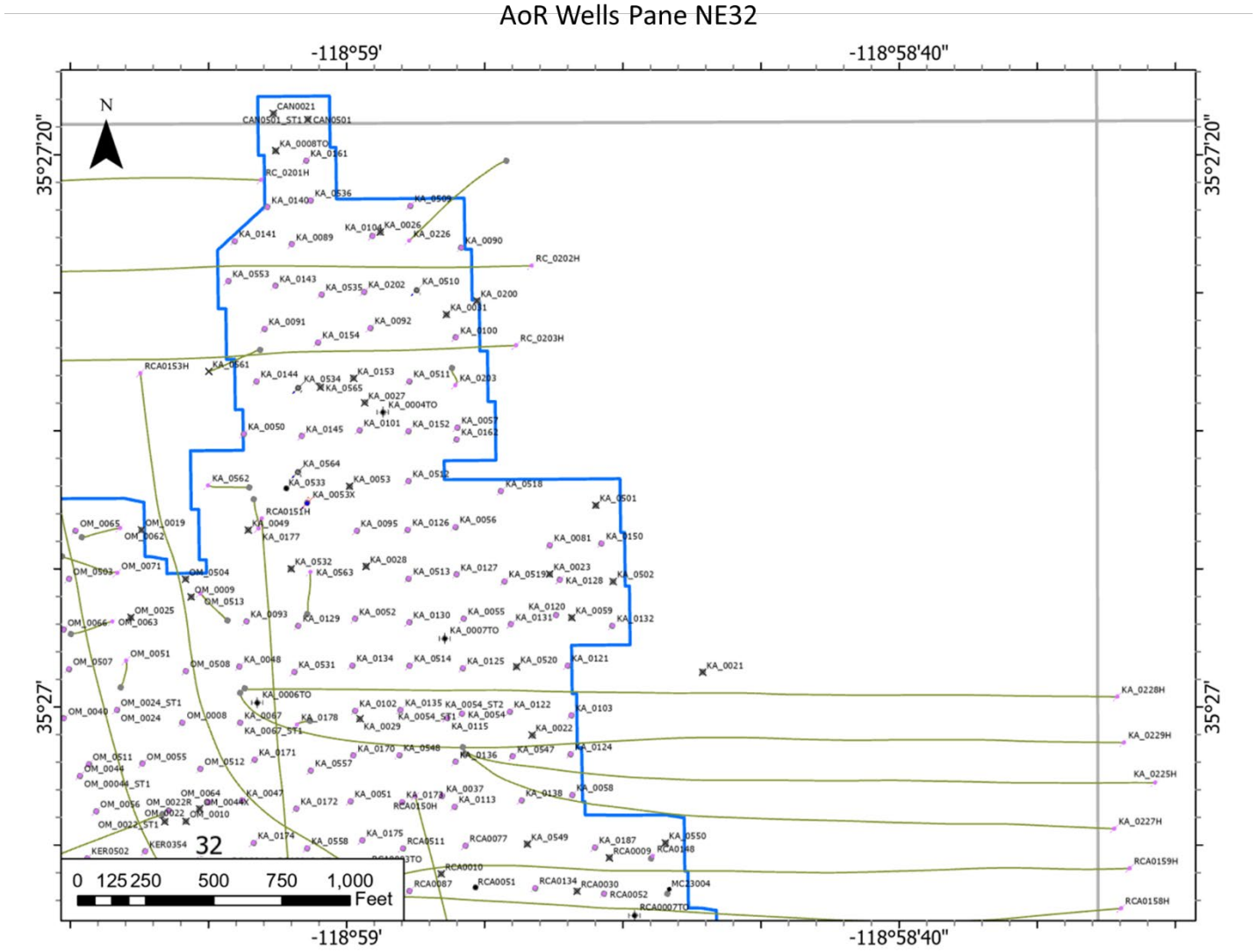

Figure 81. Panel NE32, showing all wells in the AoR in the Northeast quadrant of Section 32. Refer to **Figure 63** for location and **Figure 64** for the legend.

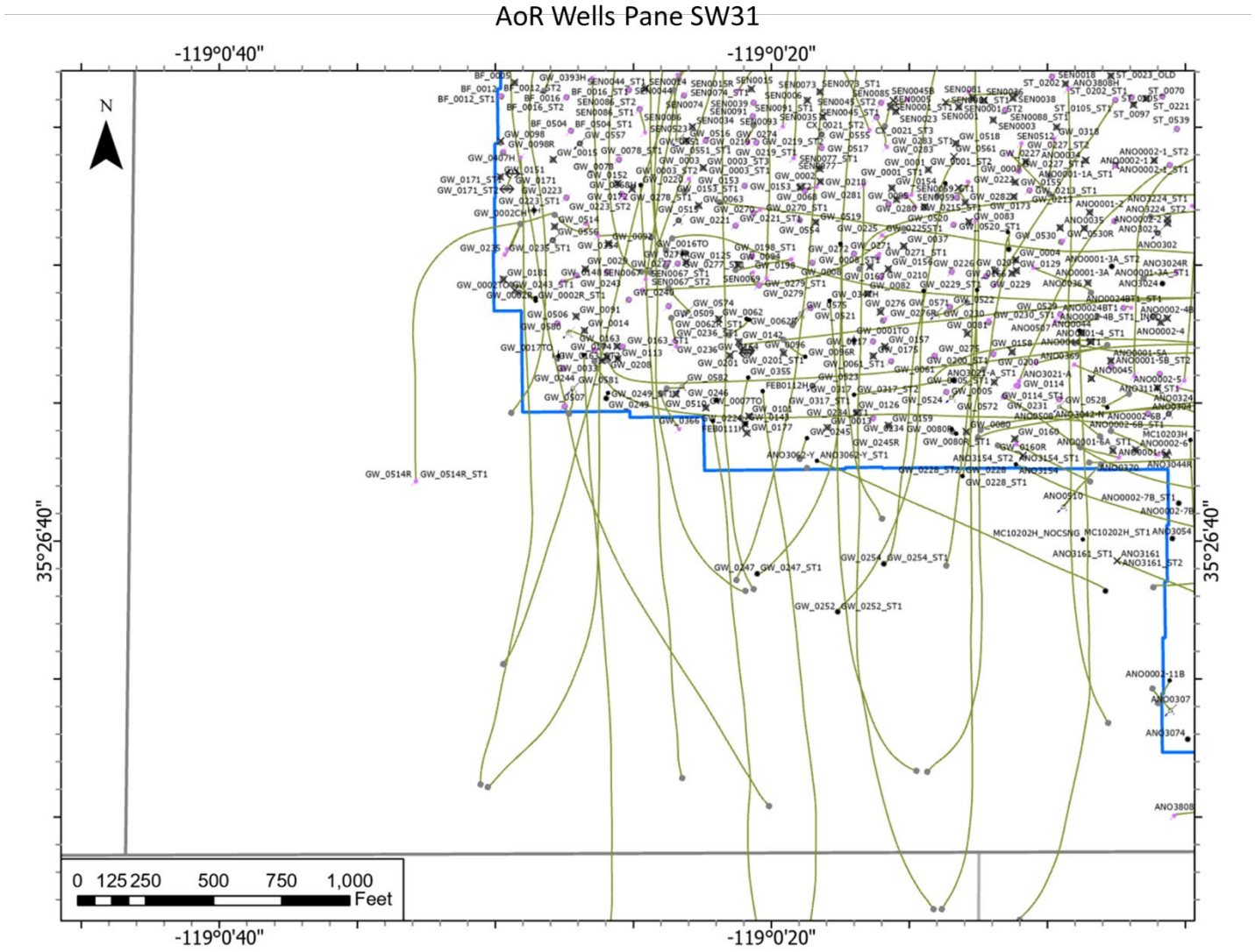

Figure 82. Panel SW31, showing all wells in the AoR in the southwest quadrant of Section 31. Refer to **Figure 63** for location and **Figure 64** for the legend.

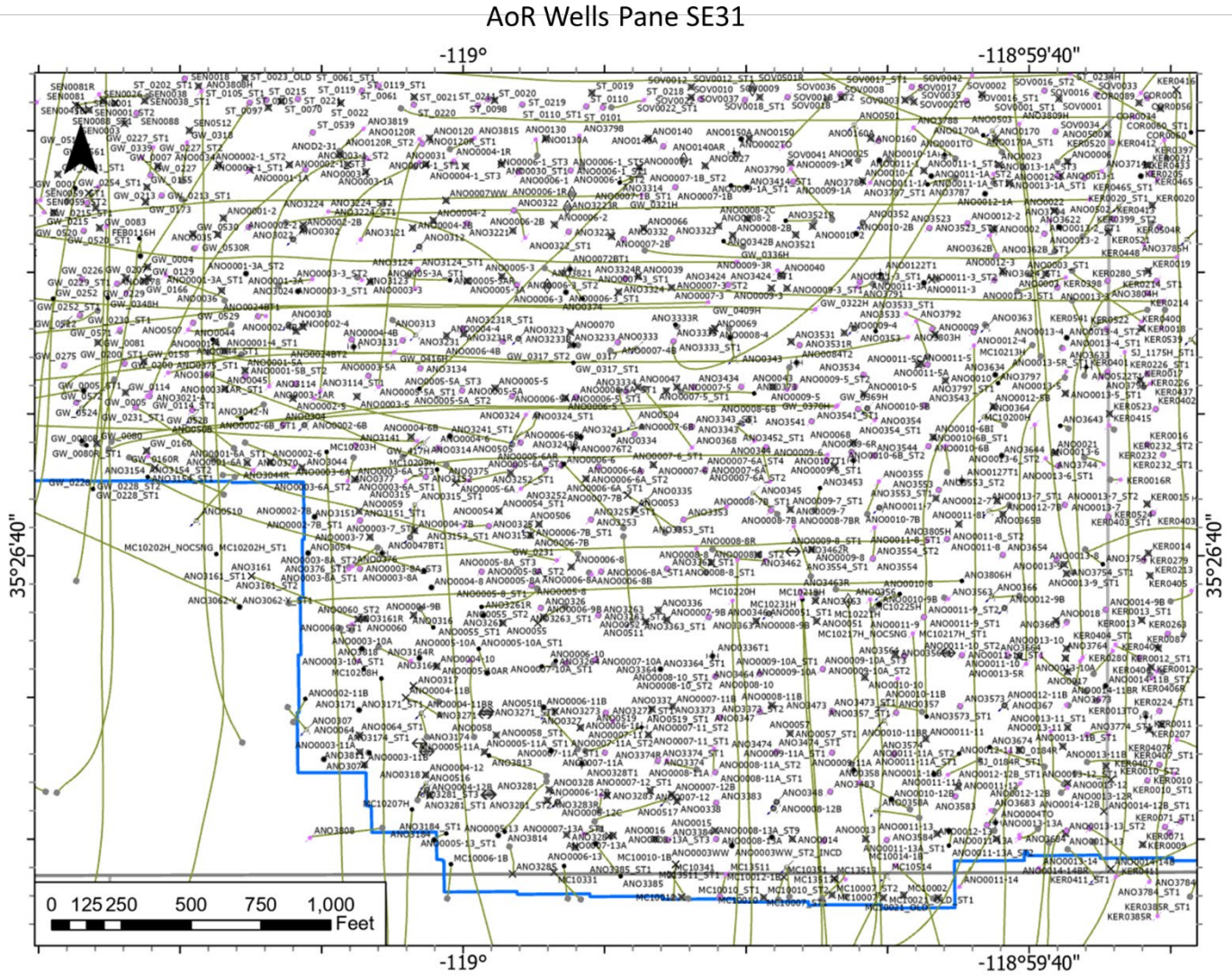

Figure 83. Panel SE31, showing all wells in the AoR in the southeast quadrant of Section 31. Refer to **Figure 63** for location and **Figure 64** for the legend.

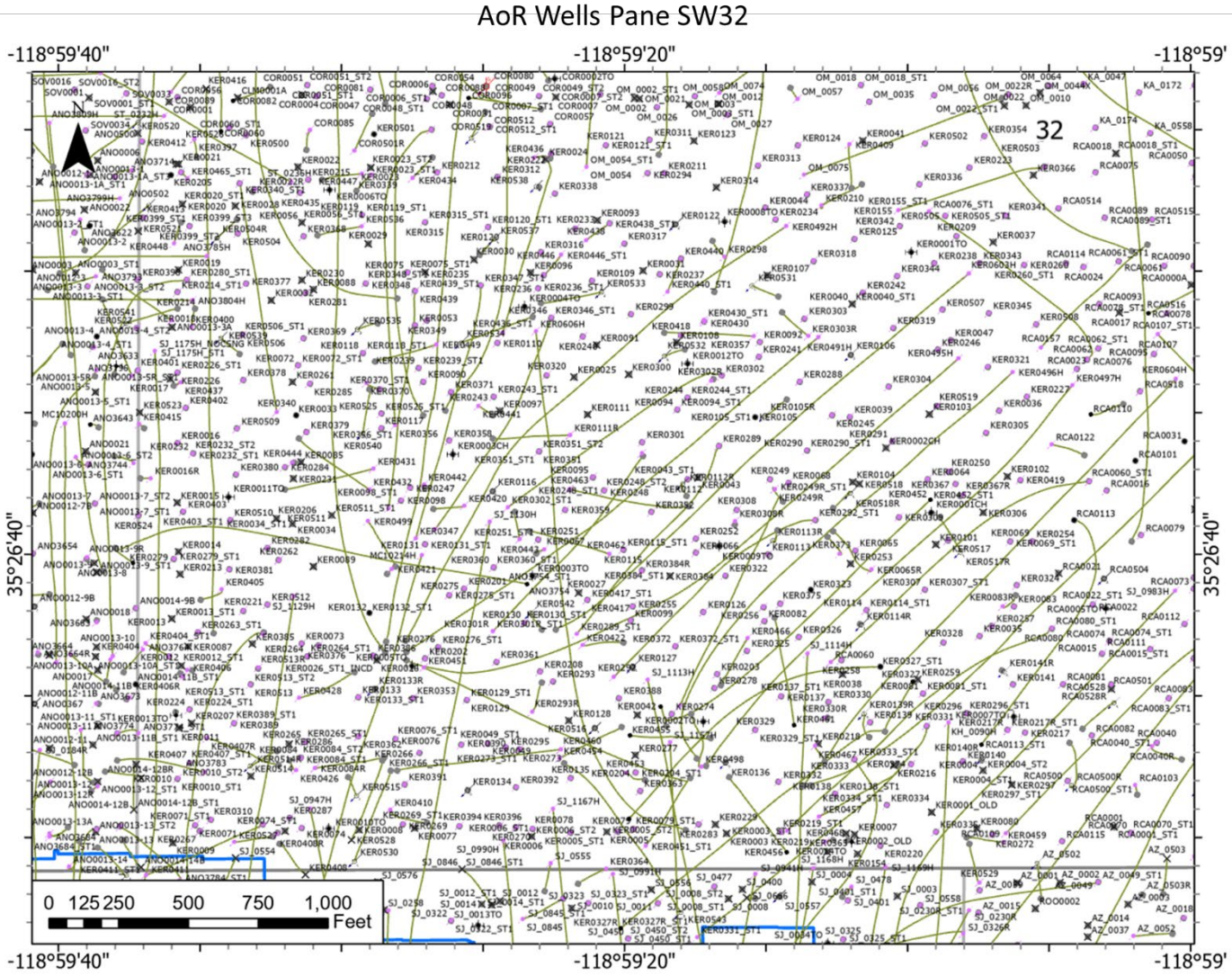

Figure 84. Panel SW32, showing all wells in the AoR in the southwest quadrant of Section 32. Refer to **Figure 63** for location and **Figure 64** for the legend.

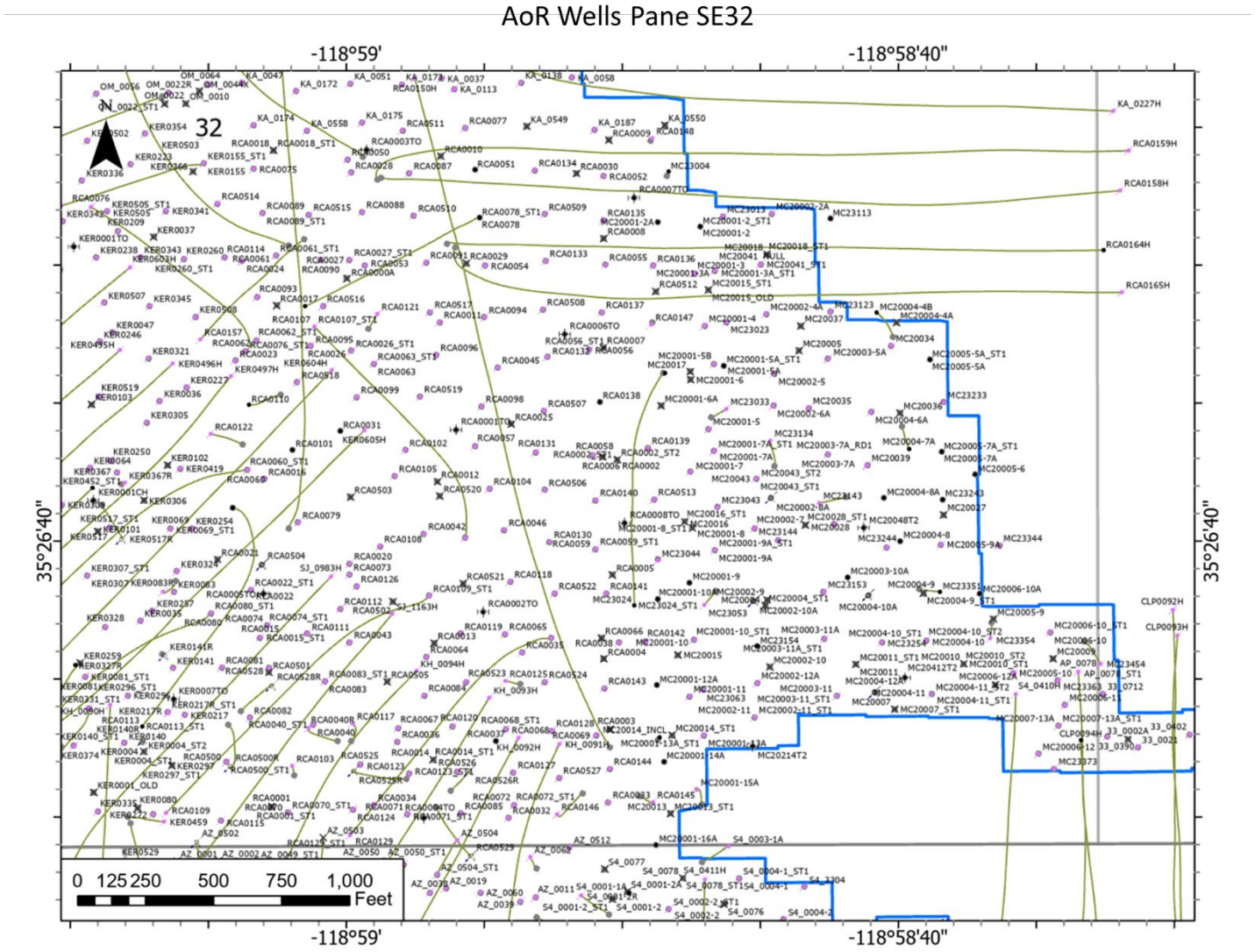

Figure 85. Panel SE32, showing all wells in the AoR in the southeast quadrant of Section 32. Refer to **Figure 63** for location and **Figure 64** for the legend.

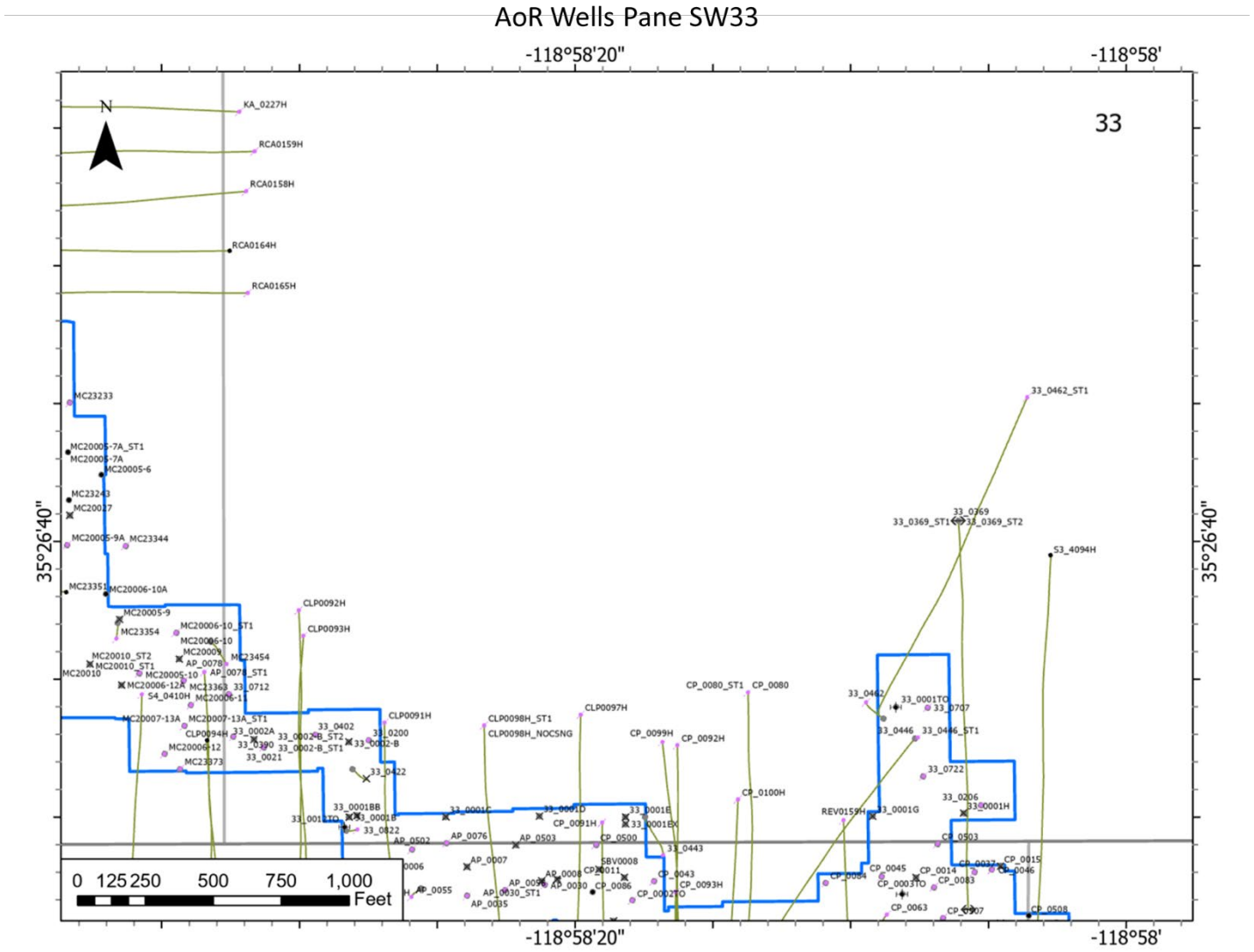

Figure 86. Panel SW33, showing all wells in the AoR in the southwest quadrant of Section 33. Refer to **Figure 63** for location and **Figure 64** for the legend.

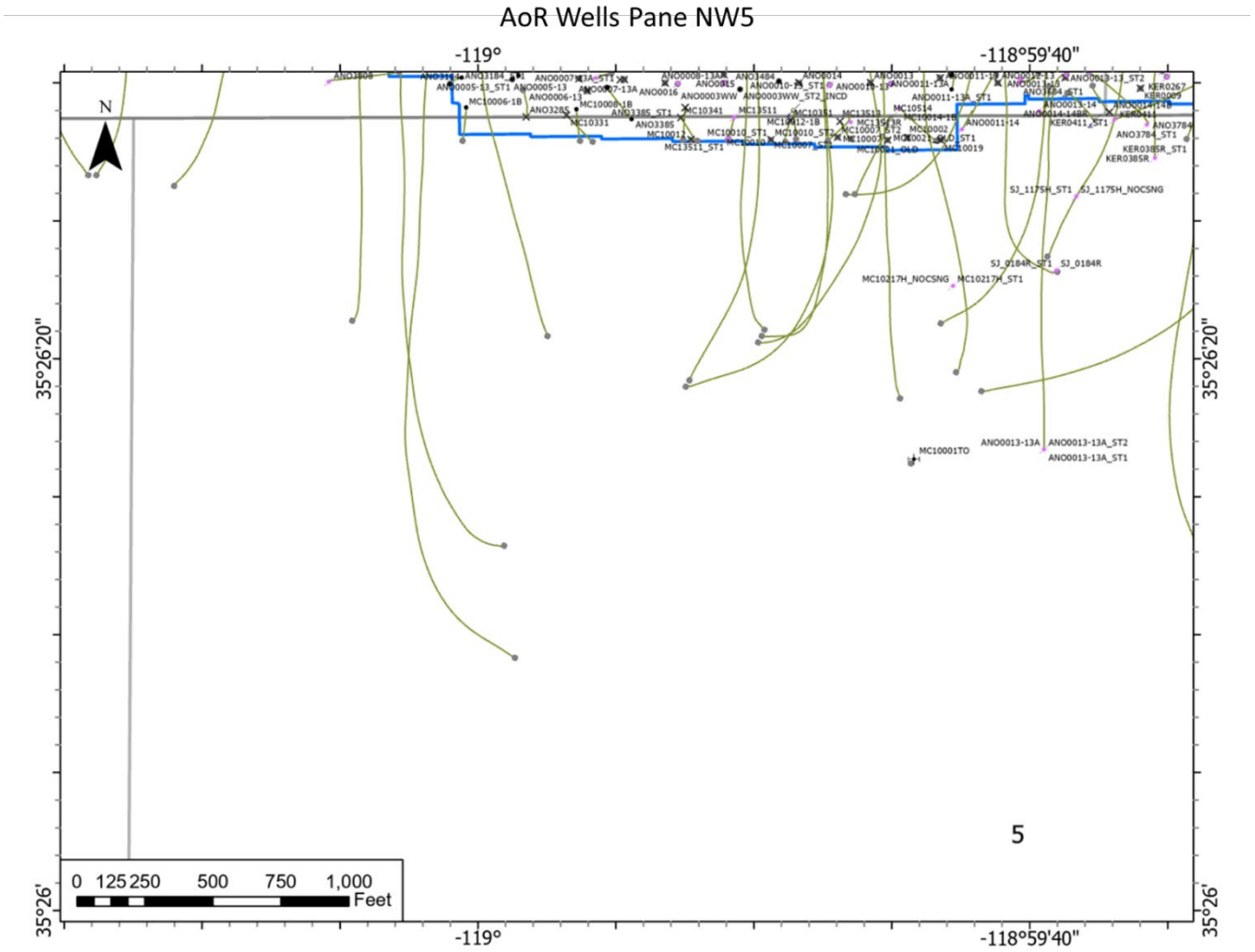

Figure 87. Panel NW5, showing all wells in the AoR in the northwest quadrant of Section 5. Refer to **Figure 63** for location and **Figure 64** for the legend.

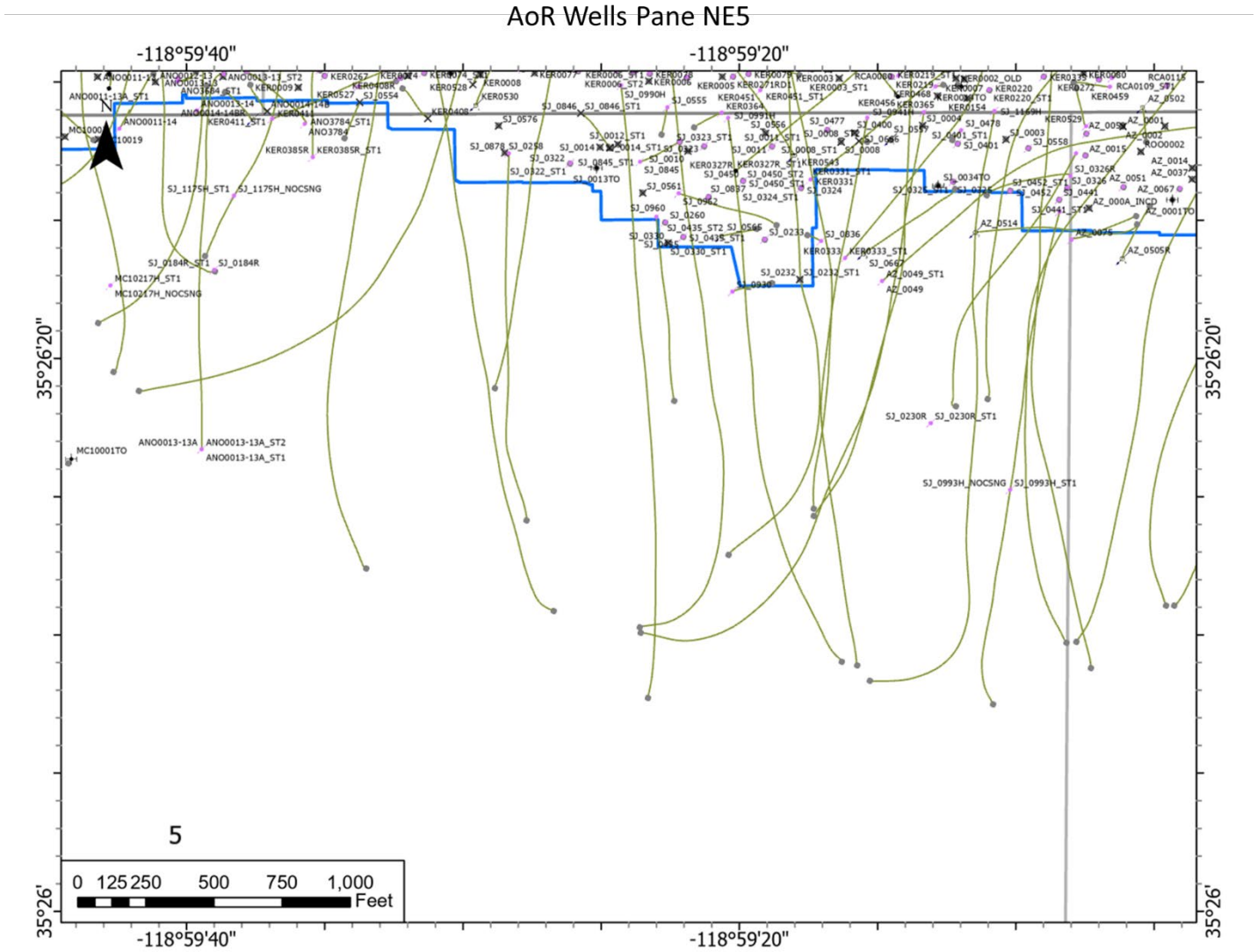

Figure 88. Panel NE5, showing all wells in the AoR in the northeast quadrant of Section 5. Refer to **Figure 63** for location and **Figure 64** for the legend.

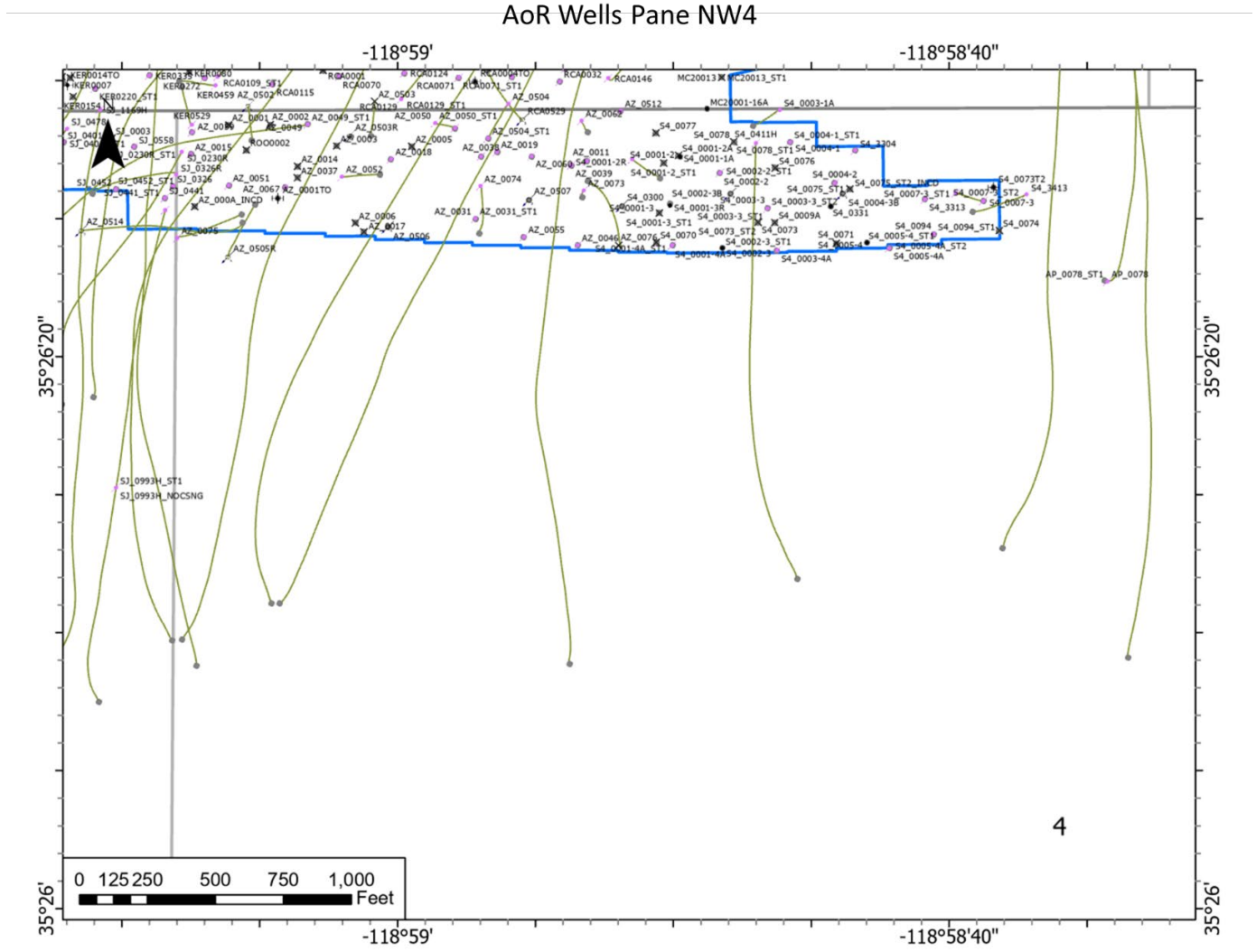

Figure 89. Panel NW4, showing all wells in the AoR in the northwest quadrant of Section 4. Refer to **Figure 63** for location and **Figure 64** for the legend.

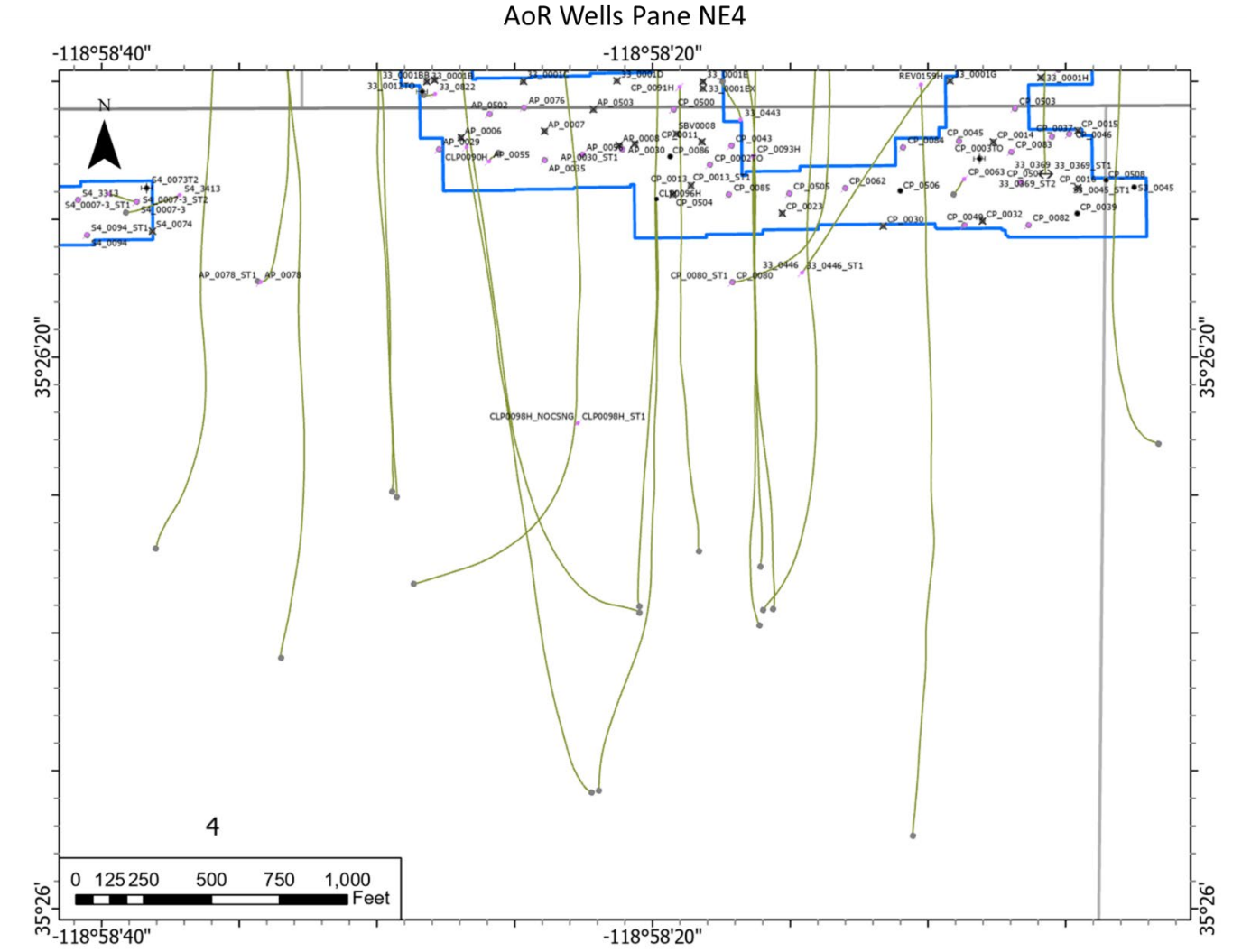

Figure 90. Panel NE4, showing all wells in the AoR in the northeast quadrant of Section 4. Refer to **Figure 63** for location and **Figure 64** for the legend.

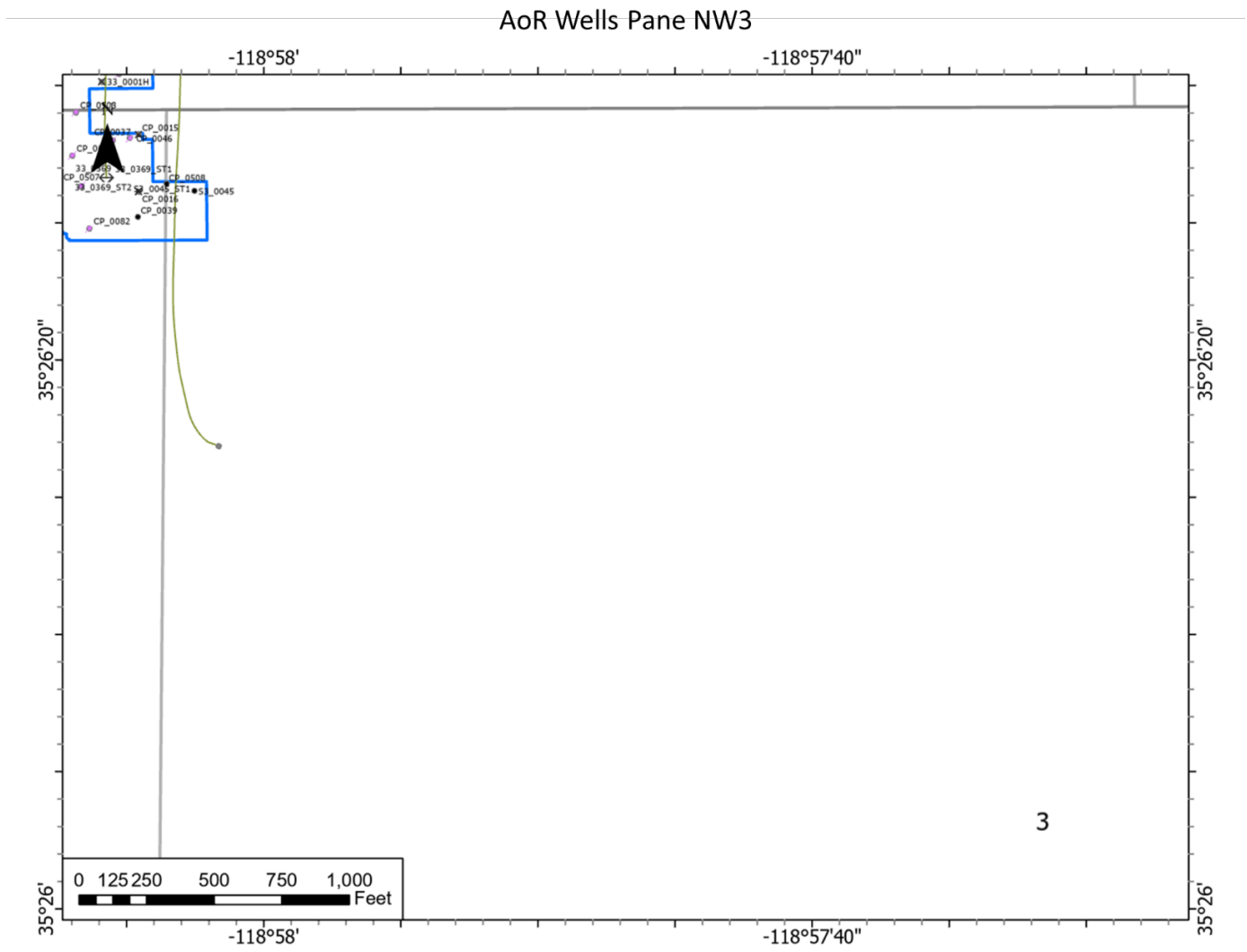

Figure 91. Panel NW3, showing all wells in the AoR in the northwest quadrant of Section 3. Refer to **Figure 63** for location and **Figure 64** for the legend.

Table 19. A list of all wells within the AoR.

Appendix 2: Wellbore Diagrams of Wells Penetrating the Confining Layer within the AoR